UNIVERSIDADE ESTADUAL PAULISTA
"JÚLIO DE MESQUITA FILHO"
School of Engineering of Ilha Solteira - SP
Post-Graduate Program in Electrical Engineering

HÉBER HWANG ARCOLEZI

A Novel Robust and Intelligent Control Based Approach for Human Lower Limb Rehabilitation via Neuromuscular Electrical Stimulation

Nova Abordagem Robusta e Inteligente de Controle para Reabilitação de Membros Inferiores Humanos via Estimulação Elétrica Neuromuscular

Ilha Solteira

2019

HÉBER HWANG ARCOLEZI

A Novel Robust and Intelligent Control Based Approach for Human Lower Limb Rehabilitation via Neuromuscular Electrical Stimulation

Nova Abordagem Robusta e Inteligente de Controle para Reabilitação de Membros Inferiores Humanos via Estimulação Elétrica Neuromuscular

Dissertation presented to the São Paulo State University (UNESP) - School of Engineering - Campus of Ilha Solteira, in fulfillment of one of the requirements for obtaining the Master's degree in Electrical Engineering.
Specialty: Automation.

Prof. Dr. Aparecido Augusto de Carvalho
Advisor

Ilha Solteira

2019

FICHA CATALOGRÁFICA

Desenvolvido pelo Serviço Técnico de Biblioteca e Documentação

UNIVERSIDADE ESTADUAL PAULISTA

Câmpus de Ilha Solteira

CERTIFICADO DE APROVAÇÃO

TÍTULO DA DISSERTAÇÃO: A Novel Robust and Intelligent Control Based Approach for Human Lower Limb Rehabilitation via Neuromuscular Electrical Stimulation

AUTOR: HÉBER HWANG ARCOLEZI
ORIENTADOR: APARECIDO AUGUSTO DE CARVALHO

Aprovado como parte das exigências para obtenção do Título de Mestre em ENGENHARIA ELÉTRICA, área: Automação pela Comissão Examinadora:

Prof. Dr. APARECIDO AUGUSTO DE CARVALHO
Departamento de Engenharia Elétrica / Faculdade de Engenharia de Ilha Solteira

Prof. Dr. MARCELO AUGUSTO ASSUNÇÃO SANCHES
Departamento de Engenharia Elétrica / Faculdade de Engenharia de Ilha Solteira

Dr. RAPHAËL COUTURIER
Computer Science / Université Burgogne Franche-Comté (UBFC) - França

Ilha Solteira, 19 de agosto de 2019

ACKNOWLEDGMENTS

Primarily, I am thankful to the unique God, that by love, compassion and a lot of mercy, provided me with life, health, a family and people to help me during this journey. For my family, my beloved parents and brothers, my greatest thank for each of you, that have been supporting and taking care of me during my entire life. From each of you, a different type of love has been demonstrated as the years pass by, and with pleasure, I consider and retribute it with all the love I can provide for all of you.

I thank my advisor, Aparecido Augusto de Carvalho, for accepting me at the Laboratório de Instrumentação e Engenharia Biomédica. I thank him for trusting and guiding me through this work; even more for supporting me on decision-making and opportunities that I searched for. I also thank professor Marcelo Teixeira, for his trust and a lot of advice on professional and research subjects, whose the last he does it with passion.

I am grateful for meeting the most special person to me, thank you, Selene, for being this person. I admire Selene for her great willing for helping and sharing with others. I learned a lot with her, both technically and life experience, which essentially helped me during this research.

I am thankful for all colleagues at the research laboratory, especially Rafael and Willian who directly contributed to this work in both theoretical and practical questions. To Willian, I have a lot to thank about and he knows it, it is inspiring his willing to research and to contribute, as well as his patience for helping.

I am also grateful for each person that accepted to volunteer to this research, even more for those with spinal cord injury, that with locomotion limitation disposed themselves to come at the research laboratory to contribute with this study.

I thank professors Rubén Lázaro, Rodrigo Cardim, Jean Marcos, and Sérgio Kurokawa, in no strict order, for supporting and helping me in the decisions taken during this master's degree. I am also grateful to Christophe Guyeux, Raphaël Couturier, and Jean-François Couchot, professors at the University of Franche-Comté, for their welcome and support in the AND team.

RESUMO

Nos últimos anos, vários estudos foram realizados mostrando que a estimulação elétrica neuro-muscular (EENM) pode produzir bons resultados terapêuticos em pacientes com lesão medular (LM). Esta pesquisa introduz uma nova metodologia robusta e inteligente baseada em controle para a reabilitação de membros inferiores humanos via EENM usando uma técnica de controle de tempo contínuo chamada robust integral of the sign of the error (RISE). Embora na literatura o controlador RISE tem demonstrado bons resultados sem qualquer método de ajuste fino, uma abordagem de tentativa e erro poderia levar rapidamente à fadiga muscular em pacientes com LM. Portanto, foi mostrado nesse estudo que o desempenho do controle para rastrear com robustez um sinal de referência pode ser melhorado através da abordagem proposta, fornecendo um ajuste inteligente para cada voluntário. Resultados de simulação com um modelo matemático e oito sujeitos identificados da literatura são fornecidos, e experimentos reais são feitos com sete indivíduos saudáveis e dois paraplégicos. Além disso, esta pesquisa introduz a aplicação de redes neurais profundas e dinâmicas, especificamente o perceptron multicamadas, uma rede neural recorrente simples e a arquitetura Long Short-Term Memory, para identificar a relação não-linear e variante no tempo entre a EENM fornecida e a posição angular alcançada. Os resultados de identificação indicam boa adaptação aos dados e erro quadrático médio muito baixo usando poucos dados para treinamento, provando ser métodos muito prospectivos para propor modelos orientados ao controle.

Palavras-chave: Estimulação elétrica neuromuscular. Controle da articulação do joelho. Controlador RISE. Algoritmo genético melhorado. Redes neurais recorrentes.

ABSTRACT

In the last few years, several studies have been carried out showing that neuromuscular electrical stimulation (NMES) can produce good therapeutic results in patients with spinal cord injury (SCI). This research introduces a new robust and intelligent control-based methodology for human lower limb rehabilitation via NMES using a continuous-time control technique named robust integral of the sign of the error (RISE). Although in the literature the RISE controller has shown good results without any fine-tuning method, a trial and error approach would quickly lead to muscle fatigue in SCI patients. Therefore, it was shown in this study that the control performance for robustly tracking a reference signal can be improved through the proposed approach by providing an intelligent tuning for each voluntary. Simulation results with a mathematical model and eight identified subjects from the literature are provided, and real experiments are performed with seven healthy and two paraplegic subjects. Besides, this research introduces the application of deep and dynamic neural networks namely the multilayer perceptron, a simple recurrent neural network, and the Long Short-Term memory architecture, to identify the nonlinear and time-varying relationship between the supplied NMES and achieved angular position. Identification results indicate good fitting to data and very low mean square error using few data for training, proving to be very prospective methods for proposing control-oriented models.

Keywords: Neuromuscular electrical stimulation. Knee joint control. RISE controller. Improved genetic algorithm. Recurrent neural networks.

LIST OF FIGURES

LIST OF TABLES

LIST OF ABBREVIATIONS & ACRONYMS

CGA	Complete Genetic Algorithm
FES	Functional Electrical Stimulation
FGA	Fast Genetic Algorithm
GA	Genetic Algorithm
GRASP	Greedy Randomized Adaptive Search Procedure
IGA	Improved Genetic Algorithm
LSTM	Long Short-Term Memory
MLP	Multilayer Perceptron
NMES	Neuromuscular Electrical Stimulation
NN	Neural Network
PW	Pulse Width
RIP	Real Initial Population
RISE	Robust Integral of the Sign of the Error
RMSE	Root Mean Squared Error
RNN	Recurrent Neural Network
SCI	Spinal Cord Injury

LIST OF SYMBOLS

$\mathbb{R}^+$ Set of Real numbers

$\mathbb{U}$ Input space

$\mathbb{Y}$ Output space

$\mathbb{F}$ Functional space

$\otimes$ Element-wise multiplication

tanh   Hyperbolic tangent

$sgn(\cdot)$ Signum function

TABLE OF CONTENTS

1 INTRODUCTION

1.1 CONTEXT OF THE PROBLEM

In the last few years, several studies have been carried out showing that neuromuscular electrical stimulation (NMES) and functional electrical stimulation (FES) can produce good results in rehabilitation treatments of spinal cord injured patients. On the one hand, damages to the spinal cord may be occasioned by traumatic causes like a road accident, sports injuries, and violence, or, nontraumatic ones such as diseases that destroy the neurological tissues and tumors. Notwithstanding, the problem itself, spinal cord injury (SCI), is often irreversible and it can cause some issues like the inability to complete daily activities or occupational ones; loss of sensation and function of muscles; difficulties related to sexual functions; total or partial paralysis; and a lot of pain to the individual. However, the main consequences depend on several factors, such as the personal condition of the patient itself, the extent of the damage, availability of time and resources, and socioeconomic factors, e.g., in low-income countries the SCI normally lead to death in contrast with high-income ones where patients enjoy a better and more productive life.

The application of NMES/FES for SCI rehabilitation is one of the most frequent methods, which provides many health and social benefits for its patients, such as the maintenance and recovery of muscles strength; prevention of flaccidity and hypotrophy, which are classic signs of muscle inactivity; offering higher expectation and quality of life; and by allowing social reinsertion. NMES/FES are techniques based on the use of equipment that generates electrical current for muscle stimulation at the motor level, aiming to generate a muscle contraction via surface or intramuscular electrodes. On the use of electrical stimulation, the strength of muscle contraction is controlled by manipulating pulse frequency, amplitude or duration, given stimulation being delivered as a waveform of electrical current pulses (HO et al., 2014; LAW; SHIELDS, 2007; LYNCH; POPOVIC, 2008).

Efforts have been made motivated by the promising therapeutic treatment and beneficial results of NMES to increase the efficacy of motor rehabilitation on accomplishing functional tasks (e.g., grasping, walking, standing, cycling and sitting pivot transfers) (KAPADIA; ZIVANOVIC; POPOVIC, 2013; JAIME; MATJACIC; HUNT, 2002; FONSECA et al., 2017) where it is named as FES. However, there are numerous challenges to be faced in designing automatic stimulation strategies, e.g., the system must run in real-time and safely even in face of bodily uncertainties such as the muscle response to the electrical stimulus, pH, body fat, hydration level, body temperature, inter and intra-subject variability in muscle properties. A

particular problem of variability in muscle properties is the difficulty of predicting the exact contraction force exerted by the muscle, which generates an unknown mapping between the stimulus parameters and the generated muscle force. To overcome some of these problems, better control procedures using feedback and/or feedforward techniques has been developed (FERRARIN et al., 2001; PREVIDI; CARPANZANO, 2003; JEZERNIK; WASSINK; KELLER, 2004; LYNCH; GRAHAM; POPOVIC, 2011; NUNES et al., 2018; LYNCH; POPOVIC, 2012; SANCHES et al., 2014; SHARMA et al., 2009; OLIVEIRA et al., 2017; CHENG et al., 2016; STEGATH et al., 2007, 2008) to benefit of acquired information about the controlled system, i.e., the movements measured in real-time with sensors, are used by the control system to adjust the control operation in a closed-loop design.

1.2 MOTIVATIONS

Even though there are several investigations on closed-loop control of FES/NMES for lower limb rehabilitation, these systems are hardly put into production. Alternatively, there exist commercial stimulators normally available on open-loop designs and with pre-programmed electrical stimulus, which are not enough to deal with the nonlinear and time-varying nature of muscles. Thus, the main reason to continue investigating on this field is that real-world NMES/FES applications to rehabilitate SCI patients require control strategies that compensate for modeling errors on the plant, system's faults, individual's muscles behavior, external disturbances, nonideal muscle conditions (fatigue, tremor, and spasms) and many other factors (LYNCH; GRAHAM; POPOVIC, 2011; MOHAMMED et al., 2012; LEW et al., 2016; PECKHAM; KNUTSON, 2005).

The present study investigated the continuous and robust control technique for uncertain nonlinear systems that have been reported in the literature as robust integral of the sign of the error (RISE) (XIAN et al., 2003; XIAN; QUEIROZ; DAWSON, 2004). In the literature one can find Stegath et al. (2007, 2008) and Sharma et al. (2009) as pioneers authors on developing the RISE controller for the lower limb tracking control. Afterward, Sharma et al. (2012) presented an improvement of the RISE control method for the same application using an NN feedforward term. Downey, Cheng and Dixon (2013) and Downey et al. (2015b), developed a RISE controller for asynchronous stimulation to the lower limb. Kawai et al. (2014) simulated the tracking control performance of a RISE-based controller to a model to the co-contraction control of the human lower limb. Lastly, Kushima et al. (2015) modeled an FES knee bending and stretching system and developed a RISE-based controller to stimulate the quadriceps and hamstrings muscle groups.

The RISE method was chosen to perform this study by some intrinsic characteristics, such as it considers disturbances that were not previously modeled and it also has implicit learning characteristics, which are important in performing rehabilitation experiments. However,

adjusting the parameters of the controller is the main component to guarantee high-quality performance, i.e., the method can only guarantee good responses selecting appropriately the gain constants.

Considering the stability analysis and the gains sufficient condition initially provided by Sharma et al. (2009) for an uncertain nonlinear muscle model, it is difficult to reach expected control effects in practice just adjusting empirically the gain parameters in the extremely large search space $\mathbb{R}^+$. In daily routines of NMES/FES application to SCI patient rehabilitation exist several problems like muscle fatigue, due to incomplete tetanus and even from the electrical stimulus application itself, which would be increased by applying a "trial and error" method to tune the controller.

Although the literature indicates good lower limb tracking performance using the RISE controller, the motivation of this research emerges from the lack of intelligent techniques to adjust the RISE controller parameters, wherein the aforementioned researches authors did not inform how they tuned the controller or that was used an empiric approach (pretrial tests) to define gain parameters before conducting the real experiments. Besides, those controllers were tested only on healthy patients, and as well-known, muscles of SCI patients do not have the same strength as a healthy one, and the brain may have lost the regular way of communication given certain damage in the spinal cord tissue. Table 1 presents information on the number of patients and the tuning procedure used by the aforementioned researches.

Table 1 - RISE controller for lower limb tracking control.

Authors and years	Validation	Tuning
Stegath et al. (2007, 2008)	2 healthy subjects	Not informed
Sharma et al. (2009, 2012)	5 and 9 healthy subjects	Not informed
Kawai et al. (2014)	Simulation	Adjusted by simulation
Kushima et al. (2015)	7 healthy subjects	Not informed
Downey et al. (2015b)	4 healthy subjects	Pretrial tests

Source: Developed by the author

1.3 OBJECTIVES AND HYPOTHESES

To overcome the aforementioned problems, this paper proposes a novel robust and intelligent control-based methodology to human lower limb rehabilitation via NMES/FES, aiming to overcome the empiric tuning procedure to the RISE controller observed in the literature. Moreover, this study proposes to extend the analysis of the RISE controller to paraplegic individuals who present not ideal conditions as healthy ones. This methodology includes an identification step based on neural networks black-box models where the novelty is the use of past identification and control data for each patient, the RISE control method (or fundamentally similar

control laws) to guarantee the system's stability and an offline controller optimizer.

Specific objectives of this research are:

- Propose an improved genetic algorithm (IGA) as an offline RISE controller optimizer to the problem of nonlinear lower limb tracking via NMES/FES;

- Validate the proposed methodology with simulation results, considering healthy and paraplegic identified subjects from Ferrarin and Pedotti (2000) on ideal and nonideal muscle conditions (including fatigue, spasms, and tremor) using a mathematical muscle model;

- Substantiate the proposed methodology with experimental results, considering healthy and paraplegic subjects identified via neural networks black-box models;

- Analyze the effectiveness of using past identification and control data on the construction of NNs black-box models for each subject;

- Investigate the performance of deep and dynamic neural networks namely the multilayer perceptron, a simple recurrent neural network, and the Long Short-Term Memory architecture in the specific task of identifying the knee joint angular position under electrical stimulation.

On the one hand, the first hypothesis for this research is that by using an empirical approach to clinical procedures, it would present a large number of poor performances, while a more adequate tuning with a more representative identified model can provide better tracking control of the lower limb. And, the second hypothesis is that by using past rehabilitation data for identifying a patient, this model will improve the description of the relationship between angular position and the delivered electrical stimulus, where fatigue and other problems as tremors are already implicit in the data.

1.4 MASTER THESIS OUTLINE

The following chapters are structured as follow.

- Chapter 2 introduces the proposed control-based methodology for the human lower limb rehabilitation with NMES/FES and its theoretical background. It proposes the improved genetic algorithm (IGA), which aims to better-acquire the RISE controller parameters. It provides the basic principles of the RISE control design. Lastly, it describes system identification and modeling via neural networks.

- Chapter 3 presents simulation results for five healthy and three paraplegic subjects identified by Ferrarin and Pedotti (2000) using a mathematical model. It mathematically describes the dynamic lower limb model and the reproduction of the "non-idealities" block (modeling of fatigue, tremors, and spams) from Lynch, Graham and Popovic (2011). It defines the metrics used to evaluate the control performance and presents the materials and methods. Simulation results are presented and discussed to isotonic and isometric contractions on ideal and nonideal conditions using an empiric and an IGA tuning approaches.

- Chapter 4 presents experimental results made with seven healthy subjects and two paraplegic ones. It describes the instrumentation apparatus, analyzed individuals, and the experimental procedure used in stimulation sessions. It defines the metrics used to evaluate the control and identification performances. Results are presented and discussed to both isotonic and isometric contractions using an empiric and an IGA tuning approach.

- Chapter 5 introduces the investigation of deep and dynamic neural networks for identifying the knee angular position under NMES/FES. It briefly describes the MLP, a simple RNN, and the LSTM architecture. It presents how data were structured and the selection of each model and its hyperparameters. Results are presented using data acquired in Chapter 4 comparing the effectiveness of each NN model.

- Finally, in Chapter 6 the general conclusions of this research and future works are presented.

2   PROPOSED METHODOLOGY AND THEORETICAL BACKGROUND

In the literature, it is shown that an empirical tuning approach to the RISE controller can also guarantee stability if gains inequalities are respected given the stability proof analysis proposed by Sharma et al. (2009). However, once gains selections are immense it is likely to one choose combinations that would not guarantee the best performance and accuracy during the rehabilitation of SCI patients.

Hence, Figure 1 illustrates the proposed methodology, where at the first session a patient has no data and a stimulation session is made on the attempt to acquire information on the relationship between delivered electric stimulus and reached angular position. The acquired data is appropriately treated to pass through an identification step via neural network black-box models. Therefore, assuming that this relationship is efficiently mapped, a simulation process making use of a global and fast search optimization algorithm that tests numerous gain combinations evaluating a well-defined control task is made to efficiently tune the RISE controller for this patient. At final, the rehabilitation procedure is retaken with fine-tuned gains for a better control-stimulation session, aiming to prevent premature fatigue and other problems of SCI patients that would be present by not choosing an appropriate gains combination.

In future sessions, all data (control and identification) from previous rehabilitation sessions are used for training a neural network model in an offline scheme, where before each next section, all data from a patient is combined to a single dataset and used to better map its relationship with electrical stimulus. Thus, the same optimization process using the trained model provides fine-tuned gain parameters to be afterward applied to the rehabilitation procedure. In Section 4.3 the methodology is experimentally implemented, where it is explained more comprehensively.

The use of neural networks is motivated by the advantages of these methods for the nonlinear system identification problem and by a high power for computation and storage of data encountered nowadays. However, as one can see in Chapter 3 and its preliminary results in Arcolezi et al. (2019), our proposal is not limited to black-box modeling, where a mathematical model and identified parameters of five subjects and three SCI patients are used to provide simulation results.

To the identification step, the novelty of the proposal is motivated by the use of past rehabilitation data. The primary purpose is to build up a dataset for each patient, where the number of data will increase during rehabilitation sessions, and the identified model will improve with more data and details about the nonlinear muscular behavior. As highlighted in the literature, muscular behavior is very susceptible to parametric variation between one day to another, and

Figure 1 - The proposed robust and intelligent control-based methodology.
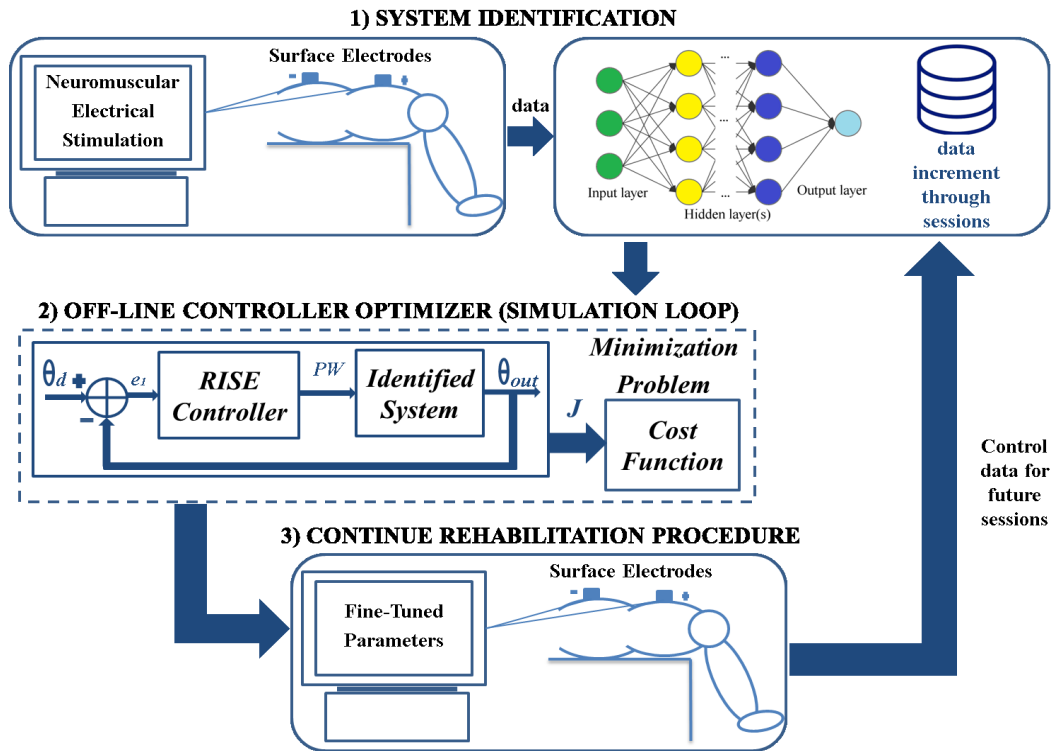
Source: Developed by the author

for instance, evolution and gain of strength due to previous rehabilitation sessions.

Moreover, one of the primary advantages of performing simulations for an NMES-base knee extension is the liberty of studying this problem from different perspectives and divergent levels of abstraction with the acquired data. Different to quite of human limitations to NMES applications, that restrict the number of experiments, simulation provides uncountable executions to better study feasibility and practicality of the designed system, and it supplies continue feedback to maintain improving the system (JEZERNIK; WASSINK; KELLER, 2004; DURIEZ; BRUNTON; NOACK, 2017; LYNCH; GRAHAM; POPOVIC, 2011).

The following sections of this chapter describe each component of the methodology, the RISE control method, an improved genetic algorithm (IGA) for the optimization procedure, and system identification via neural networks black-box models.

2.1 RISE CONTROL DEVELOPMENT

The RISE control technique has been proposed as a continuous-time and high gain feedback control approach for uncertain nonlinear systems, which even in spite of bounded smooth external disturbances and bounded modeling uncertainties, the control law can guarantee asymptotic

tracking (XIAN et al., 2003; XIAN; QUEIROZ; DAWSON, 2004). To achieve the stated control objective, i.e., to enable the lower limb to track a desired angular trajectory even in spite of external disturbances and modeling uncertainties, a position tracking error denoted by $e_1(t) \in \mathbb{R}$, is defined as

$$e_1(t) = \theta_d(t) - \theta(t), \tag{1}$$

where $\theta_d(t)$ is the desired angular trajectory assumed to have bounded continuous time derivatives, and $\theta(t)$ the actual position. Additionally, filtered tracking errors $e_2(t) \in \mathbb{R}$ and $r(t) \in \mathbb{R}$ are defined as

$$e_2(t) = \dot{e}_1(t) + \alpha_1 e_1(t), \tag{2}$$

$$r(t) = \dot{e}_2(t) + \alpha_2 e_2(t), \tag{3}$$

where $\alpha_1, \alpha_2 \in \mathbb{R}$ denote positive and adjustable control gains. Authors in Sharma et al. (2009), Stegath et al. (2008), proved semi-global asymptotic stability for an uncertain nonlinear muscle model with the RISE control law defined as

$$u(t) = (k_s + 1)e_2(t) - (k_s + 1)e_2(0) + \int [(k_s + 1)\alpha_2 e_2(\tau) + \beta sgn(e_2(\tau))]d\tau, \tag{4}$$

where $k_s, \beta \in \mathbb{R}$ are also positive and adjustable control gains, and $sgn(\cdot)$ denotes the standard signum function. As highlighted in the literature, a recommended differentiator for simulations, and used in this work, is mathematically described as

$$H(s) = \frac{Y(s)}{U(s)} = \frac{s}{\tau s + 1}, \tag{5}$$

being composed by the low pass filter $1/(\tau s+1)$; where $Y(s)$ and $U(s)$ are the input signal and its filtered derivative, respectively; and τ is a time constant.

2.2 IMPROVED GENETIC ALGORITHM

Genetic algorithms (GAs) are global search algorithms, which solves mathematical optimization problems based on mechanisms of natural selection. GAs are a class of evolutionary algorithms used to identify and optimize parameters of input-output relationships, in which evolutionary algorithms are an important category of machine learning techniques for optimization. Every generation of a GA, a set of individuals named population, compete at a well-defined

task, and a new set of individuals are created using certain genetic operations. Generally, the initial population of a GA is randomly generated, and every individual is evaluated concerning an objective function. Individuals with lower costs (minimization problem) are more likely to advance to the next generation when passing by a selection method. Afterward, the whole procedure evolves certain genetic operations, such as elitism where the best individuals advance directly to the next generation; replication where individuals also advance directly to the next generation, but with a probability rate related to the cost function; crossover, in which two individuals are selected to interchange parameters; and mutation where a small random change is made in an individual. Fig 2 illustrates an iteration of a standard GA with the respective genetic operations (DURIEZ; BRUNTON; NOACK, 2017; FLEMING; PURSHOUSE, 2002).

Figure 2 - Genetic operations to advance one generation to the next.
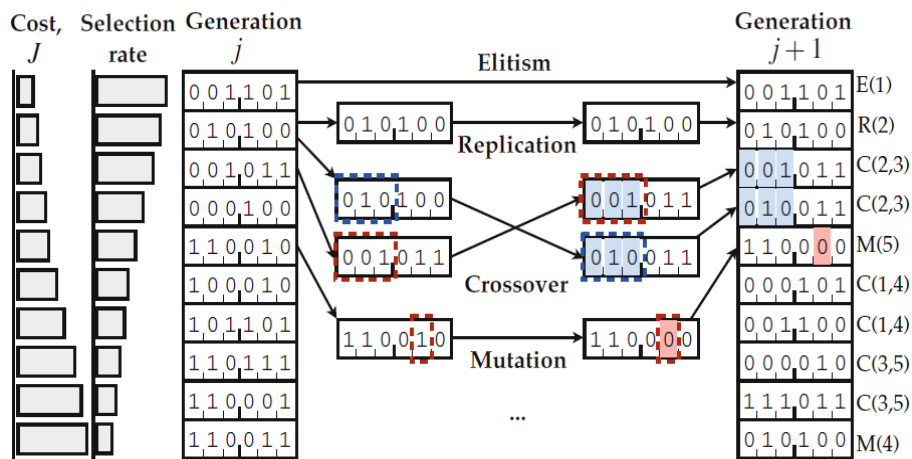
Source: (DURIEZ; BRUNTON; NOACK, 2017)

In this research an improved genetic algorithm (IGA) is proposed to better optimize gains parameters of the RISE controller, which is partially inspired on the standard methodology of the greedy randomized adaptive search procedure (GRASP) proposed by Feo and Resende (1995), running with GA instead of using hybridization of a simple heuristic algorithm and a simple local search procedure. We took advantage of the basic idea of GRASP, which runs in a multistart framework and has the subsequent steps. Firstly, it is implemented a preprocessing step to identify convergence patterns and initiate the process efficiently bounding gain limits. In the construction phase, we used a simple fast genetic algorithm (FGA) to generate a good set of solutions named the real initial population (RIP) to finally run a local search procedure based on a complete genetic algorithm (CGA). Both fast and complete GAs are very similar and related to general approaches of GAs they are different in some aspects as encoding, mutation algorithm to fit our problem and replacement of individuals in the current population. Description of the whole improved genetic algorithm procedures is detailed below.

- A solution to our problem is a chromosome consisting of four real and positive numbers representing the gains parameters of the RISE controller. As shown in Fig 3, every solution representing $\alpha_1, \alpha_2, k_s, \beta \in \mathbb{R}^+$ respectively, concerning gain conditions stated in Sharma et al. (2009) is valid.

Figure 3 - Real and positive coded genes of a chromosome.
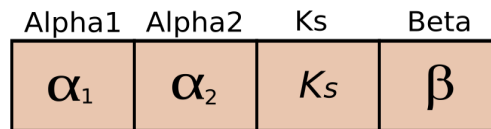
Source: Developed by the author

- At this stage, a selection procedure is made to determine the best chromosomes, according to fitness values. The tournament selection was chosen for many benefits that it provides, such as it is easy to code, efficient and fast (FLEMING; PURSHOUSE, 2002). The idea of this process is described below and illustrated in Figure 4.

  i. Provide n (size of population) games, in which j (2 for this study) individuals are chosen randomly from the present population and the individual with best fitness win each game;

  ii. Finally, the two best individuals, i.e., that won more games during the tournament, are chosen as parents.

Figure 4 - Tournament selection.
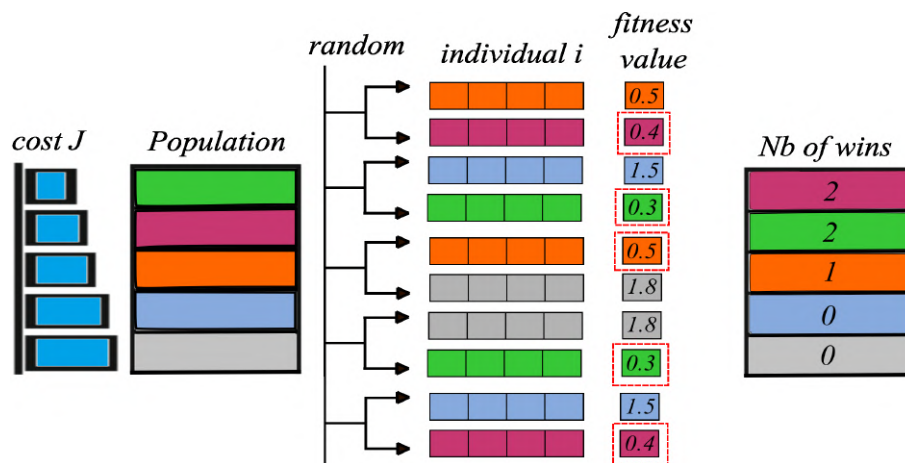
Source: Developed by the author

- The two individuals chosen in the tournament selection process as parents are submitted to the crossover algorithm. This operator generally combines features of two parents to

form two offspring. In this research, the commonly single-point crossover operator is used in the middle of the chromosome.

- The mutation algorithm is designed to expand the search space to regions that may not be close to the actual population, i.e., to increase diversity and avoid premature convergence (DURIEZ; BRUNTON; NOACK, 2017; FLEMING; PURSHOUSE, 2002). It has the following characteristic: Select one point of the chromosome randomly each stage (concerning to a mutation rate), and add or subtract small or medium value to this point according to the preprocessing step, and take its absolute value (e.g., α_1, α_2 accept small variations and k_s, β accept medium variations).

- Further, as the purpose of our nonlinear lower limb tracking problem via NMES/FES is to optimally stimulate the knee angle to track a desired reference, a minimization problem is defined as

$$\min : J(\alpha_1, \alpha_2, k_s, \beta) = RMSE + penalty, \tag{6}$$

$$RMSE = \int_0^T \sqrt{E((\theta_d - \theta)^2)}, \tag{7}$$

$$penalty = \int_0^{TR} \sqrt{E((\theta_d - \theta)^2)}. \tag{8}$$

where T is the whole period and TR is the transient response. In other words, the main objective is to minimize the metric root mean squared error (RMSE) of the actual and desired knee angle, penalizing poor transient response aiming to obtain fast responses with low overshoot.

- Construction phase: the RIP set is generated in an efficient and simple way using the FGA, described in the following steps

  i. Preprocess the problem to identify convergence patterns;

  ii. Define the following initial parameters: size of population (small), number of generations, rate of crossover and mutation operators;

  iii. Generate the initial population randomly and evaluate the fitness function;

  iv. Select two parents using tournament selection;

  v. Perform the single-point crossover and the mutation algorithm;

  vi. Substitute only these two offspring in place of the two worst individual in the current population;

vii. Evaluate and select the best individual of this small population to be a member of the RIP;

viii. Repeat steps (iii) to (vii) until the algorithm reach the predefined number of generations.

Note that, the number of generations is equal to the RIP set size and when the FGA stops, provides the RIP set of individuals also evaluated about their fitness function. Figure 5 shows a generation of the FGA, where the best solution of this new population is selected to be part of the RIP.

Figure 5 - Fast genetic algorithm operators to perform one generation and select the best individual.
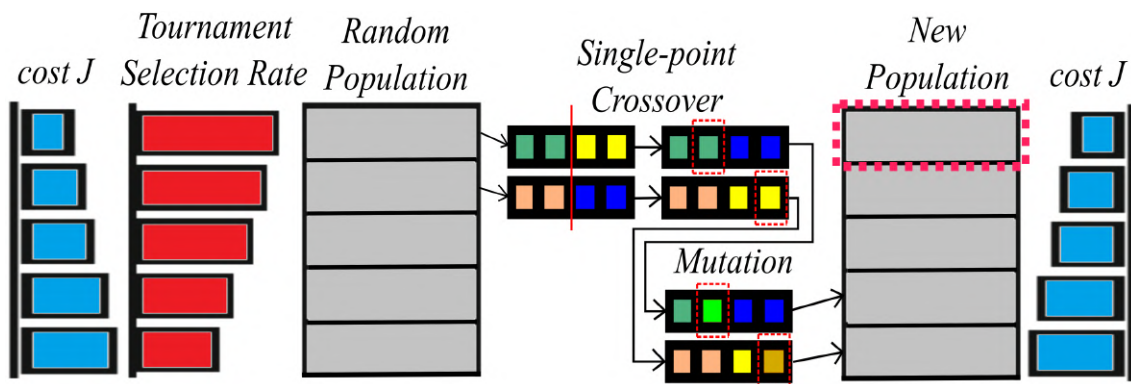
Source: Developed by the author

- Local search phase: the local search procedure is performed with the CGA describe below

  i. Evaluate if there are any repeated individuals in the RIP, and if positive excludes them from population;

  ii. Define the following initial parameters: number of generations, rate of crossover and mutation operators;

  iii. Select two parents using tournament selection;

  iv. Perform the single-point crossover and the mutation algorithm;

  v. Evaluate if the two new individuals are able to replace others from population. The individual is accepted if, and only if it is not equal to another one in the population, and if it performs better than the worst individual in the current population;

  vi. Repeat steps (iii) to (v) until the algorithm reach the predefined number of generations.

Note that the CGA is very similar to the FGA, and when the algorithm reaches the predefined number of generations, it is expected to have a whole final set of different great

solutions. If one chooses a multistart framework of k iterations, the whole process starts again with the FGA to construct the RIP set, passing to the local search with CGA until complete the predetermined number of iterations, presenting the best final set as solution. One is instructed to balance between the multistart framework and the total time of execution.

2.3   SYSTEM IDENTIFICATION VIA NEURAL NETWORKS

Nonlinear systems identification and modeling have been applied in most areas of science to predict the future behavior of dynamic systems. It has been fomented fields in control theory, and it is an essentially important way to explore, study and understand the world by a formal description of events as a model.

On the one hand, there are mathematical models, which are based on the direct description of systems using its physics and mechanics resulting in linear or nonlinear differential equations depending on several parameters. Notwithstanding, there are black-box models, which use no physical insight about the system and will be the approach of this research via NNs. Generally, black-box models are simpler than physical modeling and more appropriate where there is a lack of knowledge of the underlying physiology, or in the case when the physical knowledge is too complex, as it is in this case, where muscular behavior presents time-varying and high nonlinearities properties.

The construction of black-box models is essentially based on the quality of measured data about the system, where the collection of as much relevant data as possible, which cover the whole operating range of interest, is considered the bottom line to achieve success with the developed models. The fundamental concept of this approach is to model the direct input-output relationship, i.e., identifying and modeling just with data, in which the main objective is to find the weights and other coefficients (known as hyperparameters) of the NN (ABLAMEYKO, 2003; WANG, 2017; GONZALEZ; YU, 2018; HAYKIN, 2009).

Moreover, NNs are based on a collection of inter-connected units named neurons. These neurons are structured into three or more layers, input, hidden(s), and output. NNs are in the core of deep learning (several neurons and hidden layers) field and has become a progressively and very popular research topic. Generally, NNs can be divided into two large classes, feedforward NNs and recurrent neural networks (RNNs), where the first has been used for identification and control of simple nonlinear systems and the later for sequences modeling and time-series forecasting (OGUNMOLU et al., 2016)

Fundamentally, an operator F from an input space $\mathbb{U}$ to an output space $\mathbb{Y}$ expresses the model of the system to be identified, where the goal is to find a function $\hat{F}$ that approximates F to a specific requirement. By the Stone-Weierstrass theorem, there exists a continuous and

bounded function F, that can be uniformly approximated as closely as desired by a polynomial function $\hat{F}$. Further, according to the universal approximation theorem, there exists a combination of hyperparameters of an NN that allows it to identify and learn any nonlinear function (HAYKIN, 2009; NARENDRA; PARTHASARATHY, 1990; WANG, 2017).

In the following, a short description of using NNs for identification of discrete dynamic system is provided. Thus, consider a single-input and single-output discrete system structure with only the input and output data available as

$$y(k) = f[y(k-1),...,y(k-n);u(k-1),...,u(k-m)], \tag{9}$$

where $f(\cdot)$ is an unknown nonlinear difference equation that represents the plant dynamics; u and y are measurable scalar input and output respectively; and m and n are the maximum lags for the system output and input, i.e., they are the last values of the input and output respectively. In short, the next value of the dependent output signal $y(k)$ is regressed on previous values of the output and input signals. Extended versions for multi-input and multi-output cases are also possible, but it is not in the scope of this research.

The identification for the discrete-time system in Eq. 9 can be done by following two major types of identification structures presented in the literature as the parallel, and the series-parallel identification model (WANG, 2017; GONZALEZ; YU, 2018; NARENDRA; PARTHASARATHY, 1990). The first structure is formed using past inputs of the system and the outputs of the NN model, which is a more stringent test, and it is only recommended for stable plants. In the second arrangement, both past inputs and system outputs are used (the actual output of the system rather than that of the identification model), which is always recommended for stability reason and motivated by data availability of past system output. Mathematically these models, parallel, and series-parallel are described respectively as

$$\hat{y}(k) = F[\hat{y}(k-1),...,\hat{y}(k-n);u(k-1),...,u(k-m)], \tag{10}$$

$$\hat{y}(k) = F[y(k-1),...,y(k-n);u(k-1),...,u(k-m)], \tag{11}$$

where $\hat{y}$ is the model output, y is the real system output, F is the model structure, m and n are the regression order for the input and output. These last two parameters are chosen before the identification process, which n is the output memory to indicate how many past steps of output will be used in the system identification, and m refers to time-step of input values and it is the longest memory that a model can store. Both parallel and series-parallel identification schemes are shown in Figures 6 and 7 respectively.

Figure 6 - Parallel identification scheme of nonlinear dynamic system.
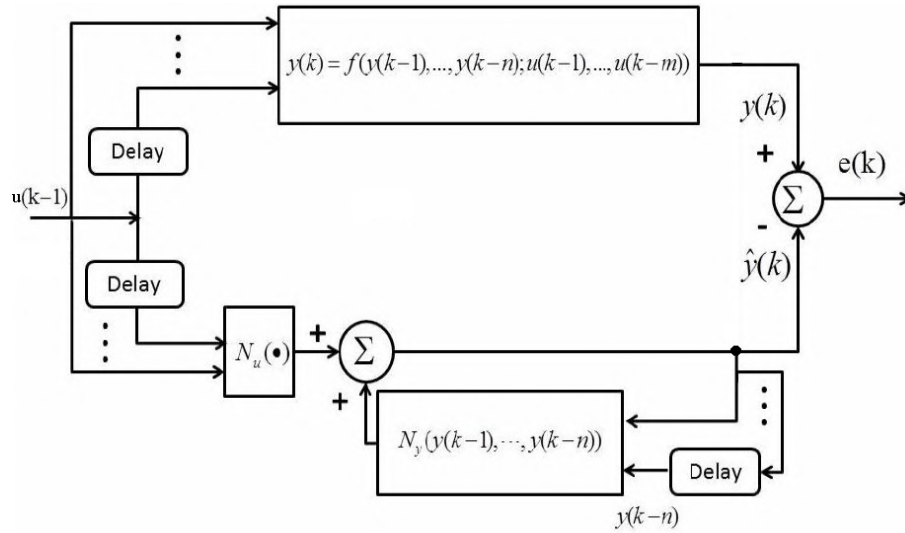
Source: Adapted from Wang (2017)

Figure 7 - Series-parallel identification model of nonlinear dynamic system.
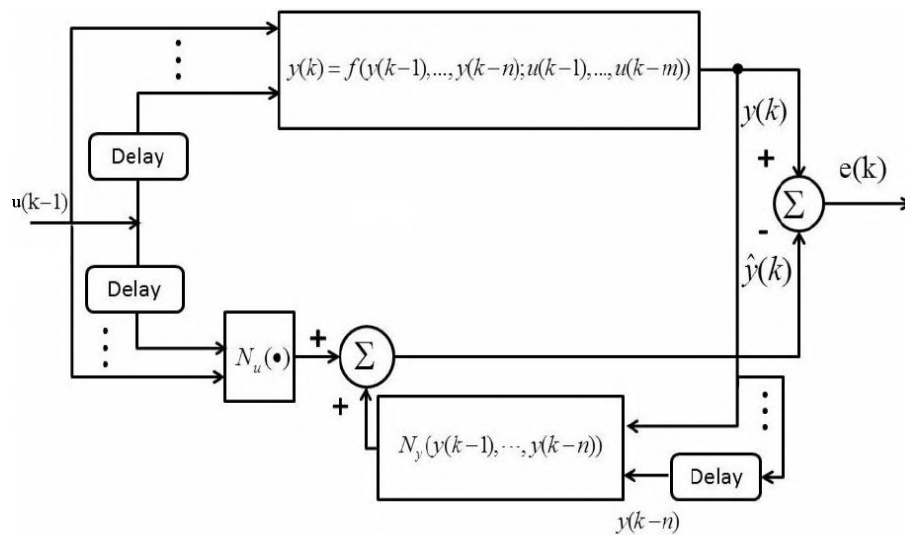
Source: Adapted from Wang (2017)

3 SIMULATION RESULTS WITH A MATHEMATICAL MUSCULAR MODEL

On the attempt to validate the novel approach for lower limb rehabilitation via NMES/FES, simulations results are provided using a mathematical muscle model and parameters for three SCI subjects and five healthy identified from Ferrarin and Pedotti (2000). Besides the new approach, another novelty is reproducing non-idealities (fatigue, spasms, and tremor) encountered on the SCI population based on the work from Lynch, Graham and Popovic (2011) to provide a more realistic scenario for simulating real-world experiments. The following sections of this chapter describe the mathematical muscle model; materials and methods (developed platform, metrics, methodology); results and its discussion.

3.1 HUMAN LOWER LIMB MATHEMATICAL MODEL

Stegath et al. (2007, 2008) and Sharma et al. (2009) developed an uncertain nonlinear muscle model to design and implement the RISE controller to yield an asymptotic stability result even in spite of uncertain nonlinear muscle model and in the presence of additive bounded disturbances. Nevertheless, the muscle model described in this chapter was based on Ferrarin and Pedotti (2000) and on Lynch, Graham and Popovic (2011), which includes muscle fatigue, spasms and tremors being the control of the knee joint made by varying the width of the current pulse.

The lower limb model considers that the individual is seated and the lower leg is freely suspended, as illustrated in Figure 8. Knee flexion is provided by the gravity force and knee extension is given by external electrical stimulus. The knee angular acceleration $\ddot{\theta}(t)$ is expressed as

$$\ddot{\theta}(t) = \frac{1}{J}(-mgl\sin\theta(t) - \tau_{stiffness} - B\dot{\theta}(t) + \upsilon(t)), \tag{12}$$

where J is the moment of inertia of combined shank and foot, $\theta(t)$, $\dot{\theta}(t)$, $\ddot{\theta}(t)$ are the knee angular position, velocity and acceleration respectively, B is the viscous damping coefficient, m is the combined mass of shank and foot, g is the gravity acceleration, and l is the distance between the knee joint and center of mass of shank and foot. The stiffness torque is

$$\tau_{stiffness} = \lambda e^{-E(\theta+\frac{\pi}{2})}(\theta + \frac{\pi}{2} - \omega), \tag{13}$$

where λ, E are exponential term coefficients and ω is the resting elastic knee angle. Additionally, this research simulated muscle fatigue, tremors, and spasms that modify muscle nominal torque in three levels (smooth, moderate and critical). For more information, Lynch, Graham and Popovic (2011) is highly recommended reading and consulting. The mathematical model of this block is

$$\upsilon(t) = (1 + spm(t) + tr(t))\tau_{quad}(t)fat(t), \tag{14}$$

where $\upsilon(t)$ is the output of the "non-idealities" block, $spm(t)$ is a scaled torque resulted from a muscle spasm, $tr(t)$ represents a scaled torque resulted from a muscle tremor, $fat(t)$ indicates a fatigue waveform and $\tau_{quad}(t)$ is the input to the "non-idealities" block, which relates the stimulated Pulse Width (PW) delivered to quadriceps muscle and resulting torque exerted about the knee joint, expressed in the frequency domain as

$$\tau_{quad}(s) = \frac{G}{1 + \eta s}PW_{quad}(s), \tag{15}$$

where $PW_{quad}(s)$ is the pulse width and G, η are constants of muscle activation function.

Figure 8 - Schematic representation of the lower limb with surface electrodes.
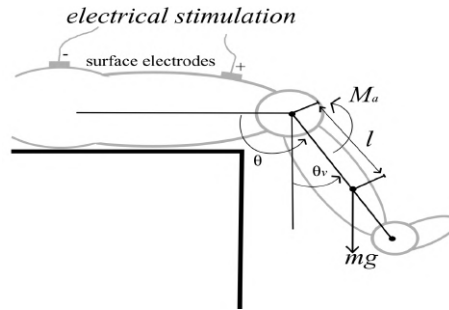
Source: Adapted from Ferrarin and Pedotti (2000)

3.2 MATERIAL AND METHODS

Initially, a Matlab/Simulink® system model that maps stimulation PW and quadriceps torque, using the nonlinear second-order dynamics of the knee and lower leg described in Section 3.1, was developed. Additionally, to perform a more realistic simulation process including muscle fatigue, tremors and spasms, the "non-idealities" block from Lynch, Graham and Popovic (2011) was reproduced and implemented. Figure 9 illustrates waveforms of all non-idealities included at the same time $t = 15s$ as smooth, moderate and critical to the normalized nominal torque. A saturation block is attached to the system model to comply with real

applications of NMES to individuals, bounding control signal from $0 \, \mu s$ to $500 \, \mu s$.

Figure 9 - Normalized nominal torque with smooth, moderate and critical non-idealities.
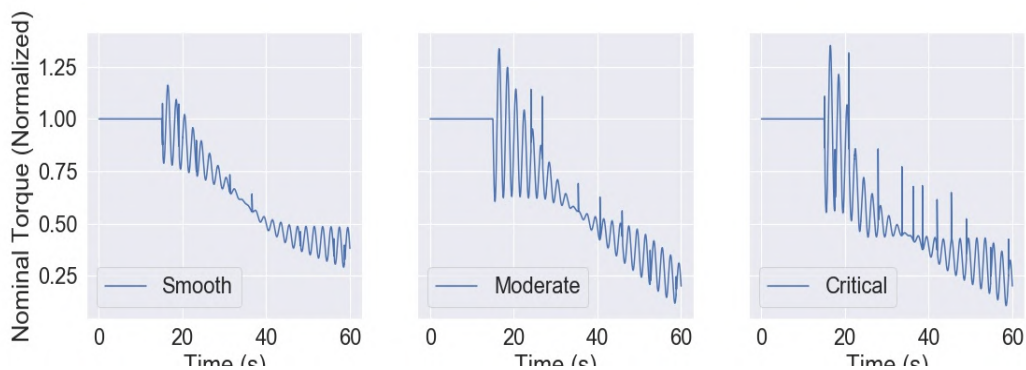
Source: Developed by the author

In this research, the performance of the RISE controller was evaluated considering both time transient and stationary responses, owing to the fact that it will be future tested on real subjects, is important to take into account information about transient response. Three paraplegics (P1-P3) and five healthy (H1-H5) identified individuals from Ferrarin and Pedotti (2000), were used to simulations considering two references trajectories. The first one is a sinusoidal trajectory ranging from $12.5°$ to $45°$ to simulate an isotonic contraction with a repetitive pattern that starts on $20°$, and the second one is a $45°$ step trajectory replicating an isometric contraction.

Initial parameters of IGA used in simulations were size of population equal 10, size of RIP equal to 50, crossover rate equal 1, mutation rate equal 0.3, number of generations equal 50 and k equal 1 iteration. Algorithm performed 30 trials given probabilistic properties of GA to ensure convergence pattern to global minimal.

Initially, simulations will try to tune the controller to the worst case scenario, i.e., with all non-idealities (fatigue, tremors and spasms) included to the model as critical to find the best gain parameters. Afterwards, with these 'best' parameters it will also be tested to the other cases, which combines non-idealities as smooth, moderate and the ideal case with none of them. In addition, simulation results for empirical tuning are presented to compare effectiveness, and all results are presented without penalizing transient response as it is during the optimization process.

In view that SCI population generally presents diagnostics with some aforementioned non-idealities, it motivated us to follow this methodology, which would allow examining if and how the RISE controller could compensate in real-world experiments, in contrary to just ideal cases. Thus, our hypothesis is that by previously including critical external disturbances in simulation procedures, which performs several combinations of gains to better fit on a particular individual, will imply on a more robust controller prepared for extreme cases, and good performances in

smoother situations will be less difficult to achieve.

Further, different metrics for ideal and nonideal conditions were considered to both tracking and regulation problems. To the sinusoidal trajectory and with ideal conditions, metrics were the lag to the desired and actual knee angles $lag(t)$; and the RMSE $E_{rmse}(deg)$ between the desired and actual knee angles. Considering nonideal conditions, these metrics were the exact time where the controller could not compensate tracking anymore for at least 5 seconds $uncT(t)$, and the E_{rms}.

For the step trajectory along ideal conditions, these metrics were calculated as 10%90% rise time $\tau_{rise}(t)$; the steady-state error $e_{ss}(deg)$ between the actual and desired knee angles; the percent overshoot $M.O(\%)$ past the steady-state knee angle; and the 2% settling time $\tau_{settling}(t)$. For non-ideal conditions, these metrics were calculated as the time where the controller could not compensate regulation anymore for at least 5 seconds $uncR$, E_{rms}, peak angular position *PA* (upper or lower the desired knee angle), and the time to peak angular position *PT* respectively.

3.3   RESULTS AND DISCUSSION

Tables 2-6 present metrics performances for control systems, considering an empiric and an IGA tuning approaches for both regulation and tracking situations respectively. Further, Figure 10 presents results on ideal conditions using empiric and IGA tuning for all patients related to both trajectories. Similarly, Figures 11-13 present results for all patients in both trajectories under nonideal muscle conditions (fatigue, tremor, and spasms) as smooth, moderate and critical respectively, using the IGA tuning approach.

Results for an empirical tuning approach to the RISE controller could also guarantee stability on ideal conditions, but once gains selections are immense, one likely choose combinations that would not guarantee best performance and accuracy during rehabilitation. For instance, see Figure 10 presenting commonly found results on our simulations, which by using empiric gains on clinical procedures, the rehabilitation of SCI patients would not result in good tracking performances. On the other hand, the RISE controller can provide high-quality performance with the right selection of gains, motivating the use of some intelligent tuning approach as the one proposed in this research.

Considering IGA fine-tuned responses on ideal conditions, very good results for tracking control were achieved for paraplegic patients. However, results adding non-idealities to the model showed different muscular behavior. For smooth non-idealities included to the model, healthy patients well compensated the whole period with a low increment of RMSE; P1 presented small variations and compensated much better than P2 and P3, where P2 in the final cycle and P3 in the two final cycles failed on tracking the reference angle. Similarly, in moderate and critical scenarios healthy patients well compensated the whole period with a low increase of

RMSE; P1 full failed on compensating in the last cycle, and patients P2 and P3 full failed in last cycles.

Further, results for the step signal trajectory considering ideal conditions lead to zero steady-state error with good performance. Similarly to tracking situations, responses for smooth non-idealities are well compensated by healthy patients and by P1, while P2 and P3 failed on compensating after 40 and 30 seconds respectively. For moderate and critical scenarios, healthy patients could still compensate for almost the whole period; P1 presented good compensation on moderate and poor one on the critical situation; P2 presented problems on compensating after 30 seconds approximately, and P3 failed compensation just after introducing the non-idealities at 15 seconds.

Table 2 - Empiric ideal response metrics.

Metric	H1	H2	H3	H4	H5	P1	P2	P3
$\tau_{rise}(t)$	0.6138	0.5962	0.3565	0.3294	0.3638	0.7995	3.2453	3.0694
$e_{ss}(deg)$	0	0	0	0	0	0	0	0
$M.O(\%)$	16.687	16.902	24.256	25.799	26.232	24.380	0.0289	0.0206
$\tau_{settling}(t)$	6.2046	6.1488	6.7681	6.6522	6.7461	8.1102	6.5566	6.3417
$lag(t)$	5.4	5.5	5.3	5.5	5.4	6.0	0.8	0.6
$E_{rmse}(deg)$	2.4956	2.7943	3.9087	3.4864	3.4943	2.8409	0.7007	0.6913

Source: Developed by the author

Table 3 - IGA ideal response metrics.

Metric	H1	H2	H3	H4	H5	P1	P2	P3
$\tau_{rise}(t)$	0.3352	0.58487	0.3349	0.5737	0.6076	0.7628	0.6209	0.2638
$e_{ss}(deg)$	0	0	0	0	0	0	0	0
$M.O(\%)$	23.894	18.151	26.610	19.313	17.277	30.414	9.0326	11.678
$\tau_{settling}(t)$	4.97	5.8259	6.6995	7.5461	8.7923	7.4267	6.2543	4.9745
$lag(t)$	4.87	5	4.5	4.69	4.65	5.3	0.55	1.2
$E_{rmse}(deg)$	2.4413	2.5868	3.7808	3.5304	3.3886	3.2284	0.6755	0.7308

Source: Developed by the author

Table 4 - IGA smooth response metrics response.

Metric	H1	H2	H3	H4	H5	P1	P2	P3
$uncR(s)$	60.0	60.0	60.0	60.0	60.0	60.0	44.4	31.4
$E_{rms}(deg)$	3.8453	3.1109	3.7296	3.4173	3.2838	4.7022	5.0076	7.5408
$PA(deg)$	56.8	54.168	57.983	54.720	53.784	59.386	18.208	20.714
$PT(s)$	1.587	1.690	1.682	1.745	1.997	2.455	58.602	58.501
$uncT(s)$	60.0	60.0	60.0	60.0	60.0	57.1	52.5	52.1
$E_{rms}(deg)$	2.4531	2.7576	3.9682	3.6422	3.4596	3.6173	1.6189	2.9452

Source: Developed by the author

Table 5 - IGA moderate response metrics.

Metric	H1	H2	H3	H4	H5	P1	P2	P3
$uncR(s)$	60.0	54.2	54.4	58.2	56.6	50.1	40.3	26.9
$E_{rms}(deg)$	4.1903	3.8210	4.1228	3.7129	3.6487	6.0676	8.3207	10.0580
$PA(deg)$	29.178	25.202	30.432	32.911	31.595	16.555	6.3058	12.741
$PT(s)$	58.71	58.67	58.66	58.73	58.68	58.54	58.5	58.5
$uncT(s)$	60.0	60.0	60.0	60.0	60.0	53.2	52.2	40.0
$E_{rms}(deg)$	2.7362	3.0609	3.9622	3.6388	3.5308	4.4485	3.6215	4.3497

Source: Developed by the author

Table 6 - IGA critical response metrics.

Metric	H1	H2	H3	H4	H5	P1	P2	P3
$uncR(s)$	54.3	54.0	54.5	54.8	34.2	15.45	33.6	15.2
$E_{rms}(deg)$	4.8935	4.5646	4.7113	4.2663	4.8730	7.7100	10.3250	11.8600
$PA(deg)$	24.863	22.284	26.444	29.970	27.652	16.365	3.652	12.049
$PT(s)$	58.69	58.67	58.68	58.75	58.71	56.7	58.5	58.52
$uncT(s)$	60.0	60.0	60.0	60.0	60.0	52.3	40.3	27.25
$E_{rms}(deg)$	3.3695	3.5921	4.3305	3.9430	3.9376	5.6544	4.9096	5.8021

Source: Developed by the author

In all cases, transient response presented interesting results, where it seems that stronger muscles present bigger overshoot. However, strong muscles demonstrate less sensitivity to external disturbances modeled in this research. Also, responses are according to reality where a healthy patient even in spite of non-idealities could track and regulate angular position very well and an SCI patient with strong muscles also compensates (P1), but not as well as a healthy one, and SCI patients with weak muscles do not reach well tracking and regulating results with non-idealities in the model. As commented before, it can be due to numerous factors that some papers did not take into account the existing problems with the SCI population assuming that results would be the same for healthy patients.

It is noteworthy that responses to the step and sine trajectories are very similar to real experiments on SCI patients and healthy ones related in the literature (TEODORO, 2018; RIENER; QUINTERN; SCHMIDT, 1996; SHARMA et al., 2009; OLIVEIRA et al., 2017; STEGATH et al., 2007, 2008; FERRARIN; PEDOTTI, 2000; DOWNEY et al., 2015a) and in Chapter 4 of this research, proving effectiveness of simulating knee-joint and non-idealities that are regularly encountered on real world. Thus, our methodology is based on simulation procedures optimizing a control task by an intelligent technique before implementing a controller on real tests. Moreover, this method will provide a lot of information about human identified system behavior to NMES/FES, permitting to save time and resources.

Figure 10 - Analysis of tracking responses using empiric and IGA tuning on ideal conditions.

(a) Step trajectory for patient H1.
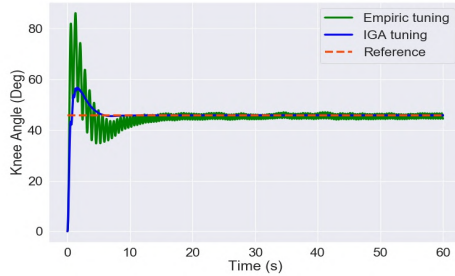
(b) Sine trajectory for patient H2.
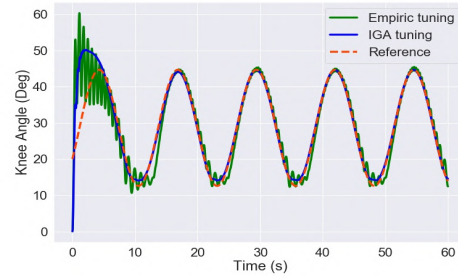
(c) Sine trajectory for patient H3.
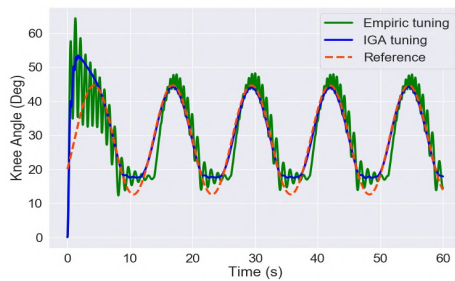
(d) Step trajectory for patient H4.
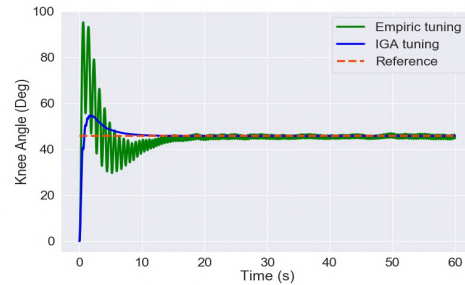
(e) Sine trajectory for patient H5.
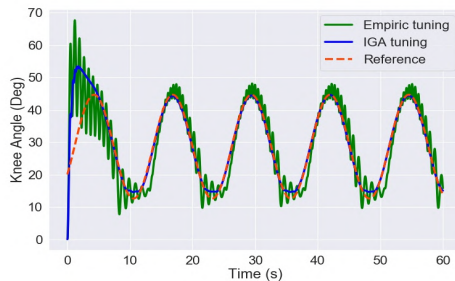
(f) Step trajectory for patient P1.
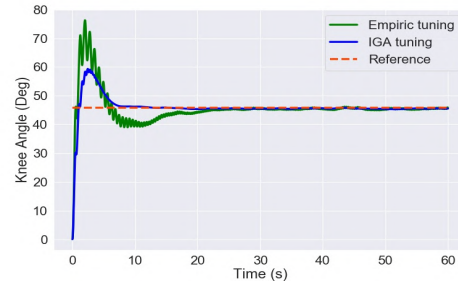
(g) Sine trajectory for patient P2.
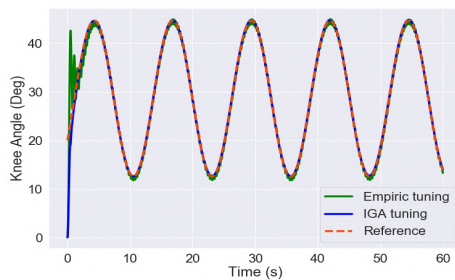
(h) Step trajectory for patient P3.
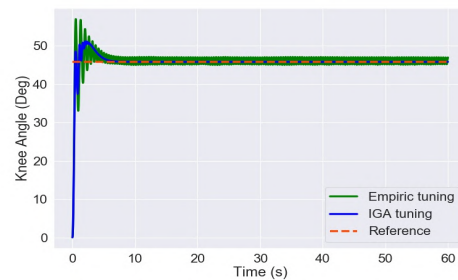
Source: Developed by the author

Figure 11 - Analysis of system responses using IGA tuning considering smooth non-idealities.

(a) Tracking of both trajectories for patient H1.
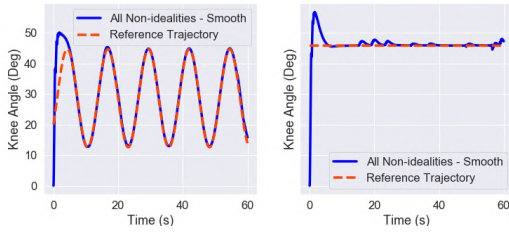
(b) Tracking of both trajectories for patient H2.
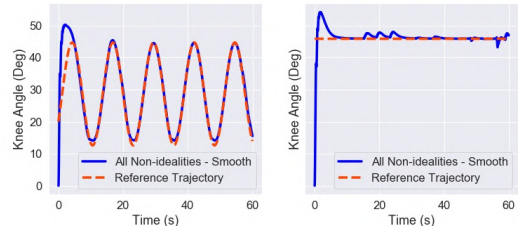
(c) Tracking of both trajectories for patient H3.
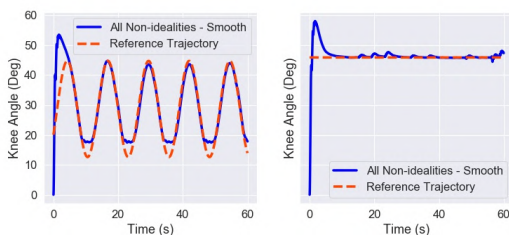
(d) Tracking of both trajectories for patient H4.
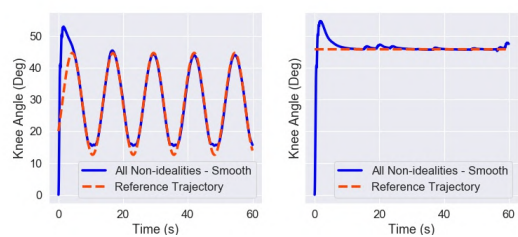
(e) Tracking of both trajectories for patient H5.
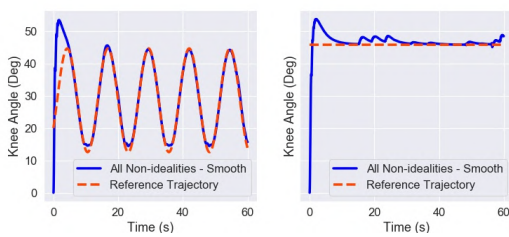
(f) Tracking of both trajectories for patient P1.
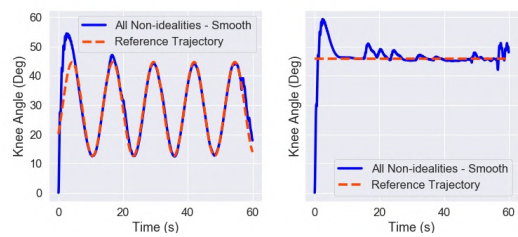
(g) Tracking of both trajectories for patient P2.
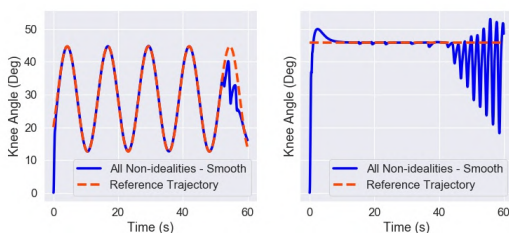
(h) Tracking of both trajectories for patient P3.
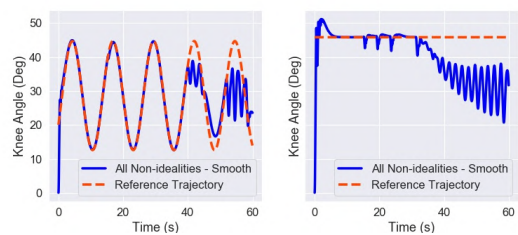
Source: Developed by the author

Figure 12 - Analysis of system responses using IGA tuning considering moderate non-idealities.

(a) Tracking of both trajectories for patient H1.
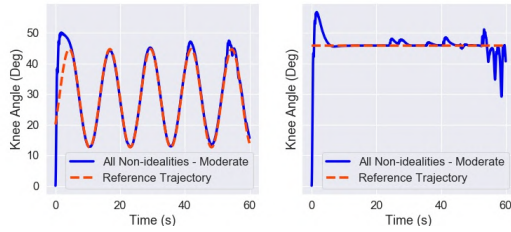
(b) Tracking of both trajectories for patient H2.
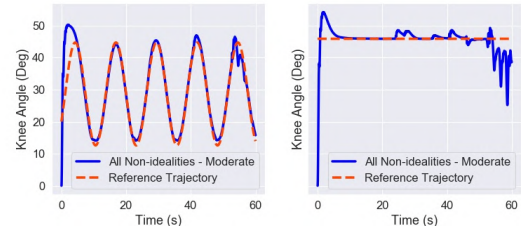
(c) Tracking of both trajectories for patient H3.
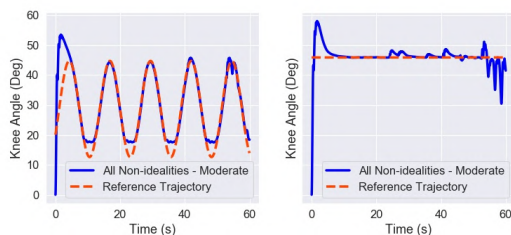
(d) Tracking of both trajectories for patient H4.
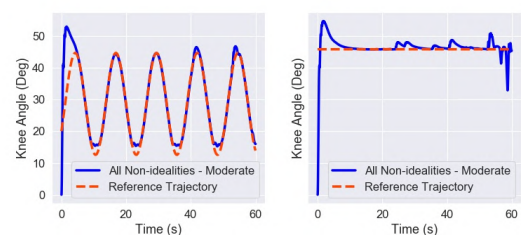
(e) Tracking of both trajectories for patient H5.
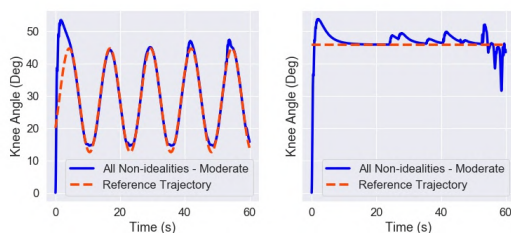
(f) Tracking of both trajectories for patient P1.
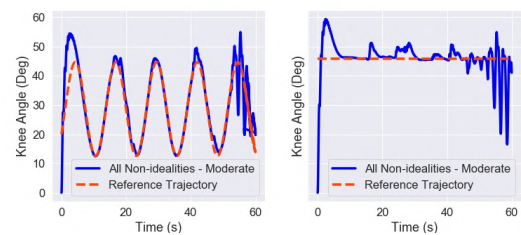
(g) Tracking of both trajectories for patient P2.
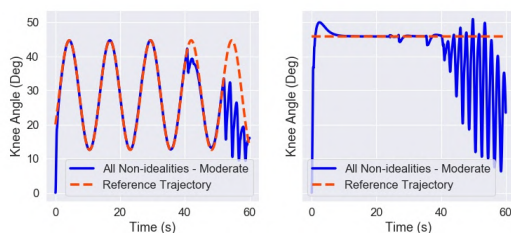
(h) Tracking of both trajectories for patient P3.
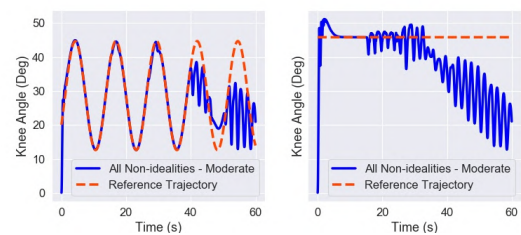
Source: Developed by the author

Figure 13 - Analysis of system responses using IGA tuning considering critical non-idealities.

(a) Tracking of both trajectories for patient H1.　　(b) Tracking of both trajectories for patient H2.
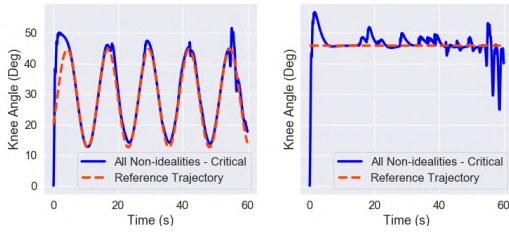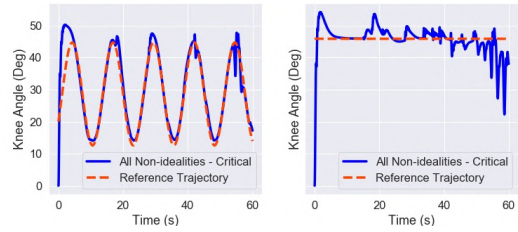
(c) Tracking of both trajectories for patient H3.　　(d) Tracking of both trajectories for patient H4.
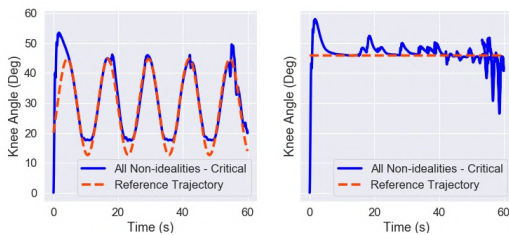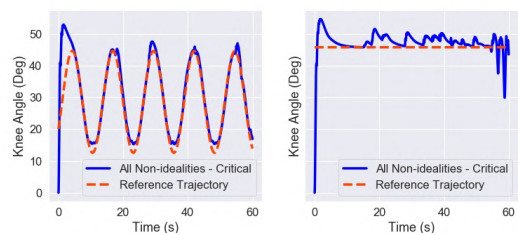
(e) Tracking of both trajectories for patient H5.　　(f) Tracking of both trajectories for patient P1.
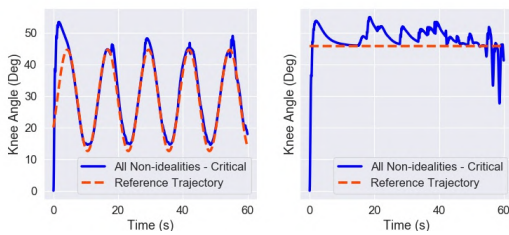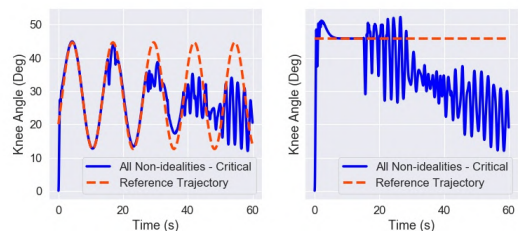
(g) Tracking of both trajectories for patient P2.　　(h) Tracking of both trajectories for patient P3.
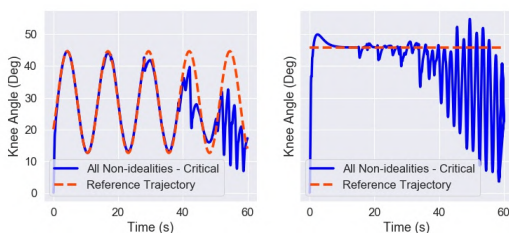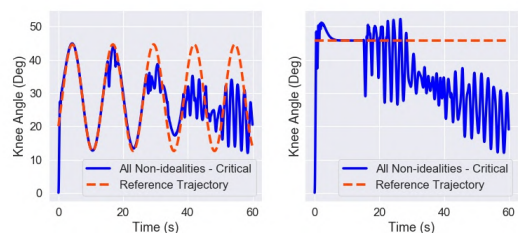
Source: Developed by the author

4 EXPERIMENTAL RESULTS WITH NEURAL NETWORK BLACK-BOX MODELS

On the attempt to substantiate and validate the proposed methodology, experimental results are provided for seven healthy individuals and two paraplegic patients. An identification step based on neural networks black-box models is made using previous rehabilitation data as sessions passed by, aiming to have a better description on the relationship of delivered PW and achieved angular position, where fatigue and other problems as tremors are already implicit in the data.

The following sections of this chapter describe the instrumentation, analyzed individuals, and the procedures used during the real experiments; the results and its analysis; and finally, a conclusion for this chapter is presented.

4.1 INSTRUMENTATION

Figure 14 illustrates the test platform used for conducting the experiments at the Instrumentation and Biomedical Engineering Laboratory ("Laboratório de Instrumentação e Engenharia Biomédica - LIEB") at UNESP - Ilha Solteira. This platform is composed of a NI myRIO controller (National Instruments®) to operate in real time; a current-based neuromuscular electrical stimulator developed by Sanches (2013); an instrumented chair composed by an electrogoniometer (Lynx®), a gyroscope LPR510AL (ST Microelectronics®), two triaxial accelerometers MMA7341 (Freescale®); and two user interfaces developed in the LabVIEW® student version edition, one for identification and the other for controlling.

The neuromuscular electrical stimulator delivers rectangular, biphasic, symmetrical pulses to the individual's muscle, allowing a control adjustment of the pulse width in a range of $0 - 400\mu s$. The stimulation intensity is controlled by setting the pulse amplitude to the quadriceps and controlling the PW. The stimulus frequency was fixed in 50 Hz and the pulse amplitude in 80 mA (healthy subjects) or 120 mA (paraplegic subjects). Further, surface electrodes with rectangular self-adhesive CARCI 50 mm x 90 mm settings are used in this study.

4.2 ANALYZED INDIVIDUALS

The study with volunteers was authorized through a research ethics committee involving human beings (CAAE: 79219317.2.1001.5402) at São Paulo State University (UNESP), and before the participation, written informed consent was obtained from all participants. Table 7

Figure 14 - The complete test platform for electrical stimulation experiments.
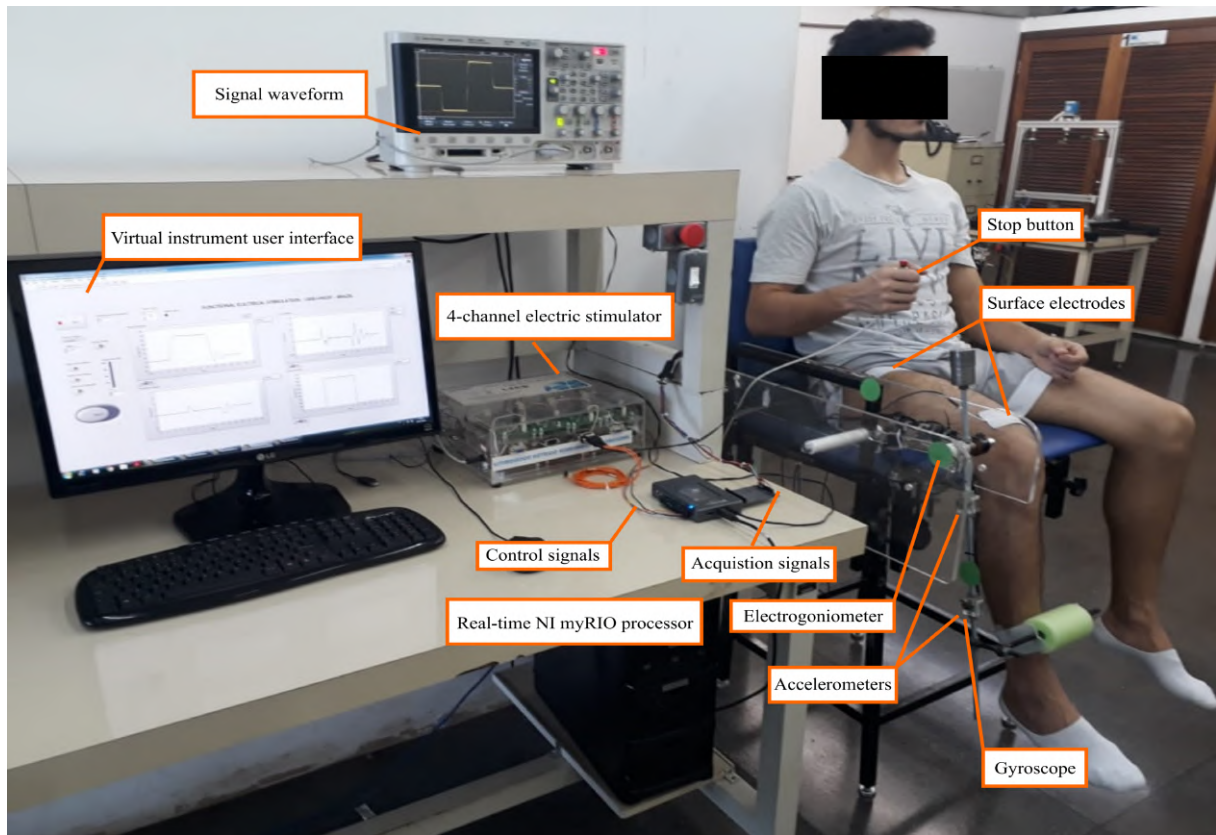
Source: Developed by the author

presents sufficient data on all male individuals that participated in this study.

Table 7 - Specific data on analyzed individuals.

	H1	H2	H3	H4	H5	H6	H7	P1	P2
Age (years)	24	28	27	22	22	28	25	32	43
Weight (kg)	74.1	70.4	75	94.3	73	68.8	78.3	70.0	96.0
Height (cm)	174	167	180	186	175	170	165	170	183
Injury level	-	-	-	-	-	-	-	L4, L5	C5, C6
Injury time	-	-	-	-	-	-	-	9 years	17 years

Source: Developed by the author

The inclusion criteria for individuals were male or female people older or equal than 18 years old. Healthy subjects were expected to have no lesion or congenital disease that could compromise the lower limbs movements, and paraplegic subjects were considered the ones with SCI. As exclusion criteria, pregnant women and people with cardiovascular diseases were not considered to this study. Furthermore, healthy individuals who presented fear or discomfort

during the tests by voluntarily moving or holding the movement of the leg (excessively) were excluded from the analysis. By excessively, it means that as healthy individuals, small voluntary movements is probably present during stimulation and in this level, it is acceptable.

4.3 EXPERIMENTAL SETUP

Initially, the chair backrest and the knee joint position are adjusted for each volunteer to ensure their comfort. A muscle analysis is made to determine the motor point following the methodology described in Teodoro (2018), in order to guarantee proper positioning of the surface electrodes. Therefore, scraping and cleansing procedures are made at the motor point to correctly place the electrodes. After the motor-point identification, a few open loop tests are performed applying a step-type signal during four seconds, in the interest of determining a bounded pulse width band ρ_{min} to ρ_{max} concerning to a desired range of angular position $\theta_{min} = 10°$ and $\theta_{max} = 40°$. Figure 15 illustrates this open-loop stimulation for subject H1. Subsequently, a small time interval for muscle rest is provided.

Figure 15 - Open-loop tests to determine ρ_{min} and ρ_{max}.
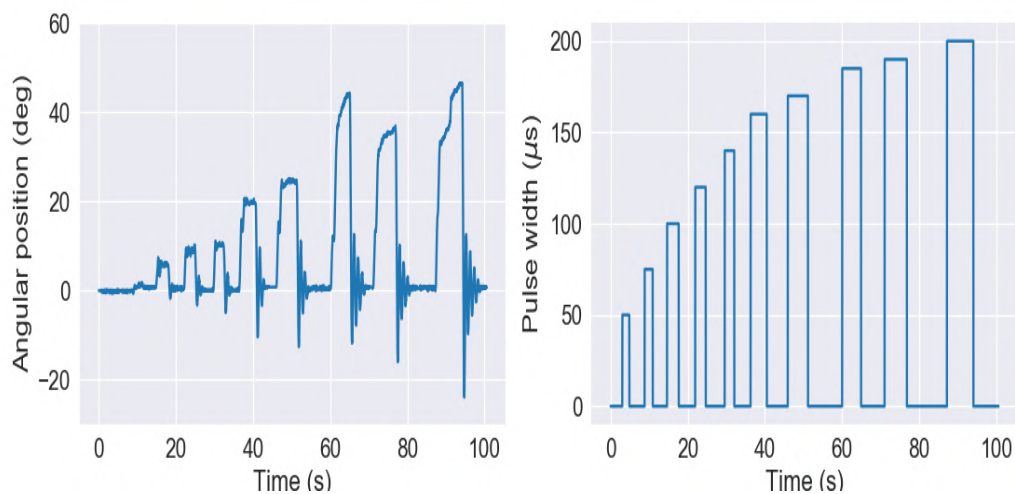
Source: Developed by the author

During the experiments, individuals were instructed to relax, to not influence the leg motion voluntarily and allow the stimulation to control it. Further, during electrical stimulation sessions, the individual could deactivate the stimulation pulses using a stop button, under any displeasure situations.

In the following two subsections, the experimental setup is detailed, where, first, it is assumed a subject for the first time using the proposed methodology, i.e., without any previous data, and then, subjects who participated in two up to five sessions of experimental tests.

4.3.1 First session

Thereafter, a stimulation test is carried out consisting of one minute (less for paraplegic subjects due to premature fatigue problem) of randomly selected PW in the predetermined range (ρ_{min}, ρ_{max}) per individual, being each value applied during minimum four and maximum seven seconds (also random), as Figure 16 illustrates the stimulation test from individual H1. The motivation to follow this methodology is the attempt to map a tracking situation and to recognize the completely nonlinear and time-varying nature of muscles during a high time of electrical stimulation. The pulse width, position, velocity, and angular acceleration data are automatically recorded with 0.02 of time sampling, resulting in a dataset with approximately 3000 samples (60 seconds) at most.

Figure 16 - Randomly selected PW during a random time.
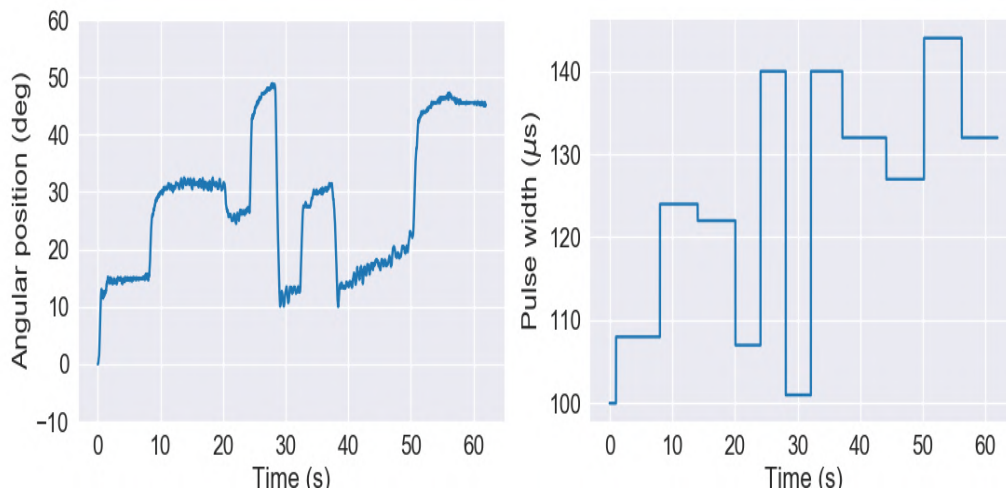
Source: Developed by the author

Afterward, the identification data is read and manipulated for feeding up an MLP feedforward NN with one hidden layer, aiming to map the relationship between the electric stimulus and the achieved angular position. In the literature, one layer has been proved to be sufficient to approximate any continuous function on a compact domain (PREVIDI, 2002; OGUNMOLU et al., 2016). The number of neurons varied from 10 to 1000; hyperbolic tangent activation is used in each neuron from the hidden layer and the output layer is composed of one neuron with linear activation, which gives the estimated output $\hat{y}(k)$.

The time-step value m and the past-step value n were chosen as 1 (for more details, refers to Section 2.3), where Table 8 illustrates an example on 10 samples of how the dataset is arranged, containing the last input value "Pulse_Width$(k-1)$" and the last output value "Angular_Position $(k-1)$" as features, and the actual output value "Angular_Position (k)" as target.

The MLP NN model requires a normal input arranged as [*samples*, *features*], where the observations at previous timesteps are inputted as features to the model, considering that a feedforward NN, as the MLP, can only take a fixed-size input.

Table 8 - Example of how datasets are encoded.

Features		Target
Angular_Position $(k-1)$	**Pulse_Width** $(k-1)$	**Angular_Position** (k)
13.348546°	215μs	13.399383°
13.399383°	215μs	13.382377°
13.382377°	215μs	13.325167°
13.325167°	215μs	13.306247°
13.306247°	215μs	13.347835°
13.347835°	248μs	13.387653°
13.387653°	248μs	13.357460°
13.357460°	248μs	13.256510°
13.256510°	248μs	13.131691°
13.131691°	248μs	13.016152°

Source: Developed by the author

Therefore, using the estimated model, an optimization procedure is performed based on the proposed IGA, introduced in Section 2.2, to find the best gains combination for two reference trajectories. The first trajectory is a sinusoidal wave ranging from 10° to 40° as an isotonic contraction with a repetitive pattern, and the second one is a 40° step wave as an isometric contraction. The motivation to use a smooth range of motion at 40° and a small-time period (sine wave) is the attempt to avoid premature fatigue by diminishing muscles effort.

Considering real-world application of the proposed methodology and by assuming a limited time for a rehabilitation session, the initial parameters of IGA used for simulations were: size of population equal 8, size of RIP equal to 6, crossover rate equal 1, mutation rate equal 0.5, number of generations equal 6 and *k* equal 1 iteration. The algorithm ran a single time, and when the set of solutions was provided and gains combination selected for performing the real experiment, previous simulations to both trajectories were made to check the system's response. Generally, the running time did not exceed 10 minutes of execution.

The simulation system was developed using the Matlab/Simulink® platform, which contains both sine and step trajectories, a saturation block bounding control signal from 0 μs to ρ_{max} μs for each subject, the RISE controller block, and the identified neural network block for each individual.

Lastly, using empiric gains and then the gains encountered in the previous step, the controlling procedure is implemented for both trajectories. Data are recorded with 0.005 of time sampling, generally resulting in a dataset with approximately 12,000 samples (60 seconds) at most.

4.3.2 Two up to five sessions

Differently, for individuals who participated in more sessions with at least 48 hours of difference between two consecutive sessions, the identification step is not considered as it is done when an individual participates for the first time. The data from previous rehabilitation sessions are used for training a neural network model in an offline scheme, where before each next section, all data from a individual is combined to a single dataset and used to better map its relationship with electrical stimulus.

Thus, using each trained identified model, an optimization procedure using the developed IGA is made to find the best gains combination for both sine and step reference trajectories. As this optimization is made in an offline scheme and before the next session, time and computational costs are not too strict as they are for the first session. Therefore, the initial parameters of IGA used for simulations were: size of population equal 10, size of RIP equal to 30, crossover rate equal 1, mutation rate equal 0.3, number of generations equal 30 and k equal 1 iteration. The algorithm ran a single time, and several gains combinations from the set of solutions were simulated to check the system's response and select the best one for both trajectories. Generally, this procedure took at most 1 hour.

For the experimental part, the electrodes are positioned at the motor-point identified in the first session, and similarly, a few open-loop tests applying a step-type signal during four seconds are performed, to determine a bounded pulse width band concerning to $\theta_{min} = 10°$ and $\theta_{max} = 40°$. Afterward, a small-time interval for muscle rest is provided.

Therefore, knowing the fine-tuned gains parameters for each individual, the controlling procedure is applied for both references, and then with an empiric gains combination for comparing results.

4.4 RESULTS AND DISCUSSION

Results and its discussions will be presented in this section divided by nine subsections, one for each individual that participated in the experiments during one up to five sessions at most. For all individuals will be presented:

- a table containing additional technical information about each stimulation session. This table contains data related to initial identification, i.e., the range (ρ_{min}, ρ_{max}) in μs to acquire (θ_{min}, θ_{max}) in degrees. Further, it comprises data for the controlling procedure (empiric and IGA), where $\rho0$ in μs is the initial pulse width for starting the control operation; *sat* in μs is the value to bound control signal preventing possible pain to the individual (as tests are also made with healthy subjects) and quick fatigue due to the

electric stimulus; and empiric and fine-tuned gains used to control-stimulate the lower limb.

The two $\rho 0$ and *sat* values were initially chosen according to the initial identification, i.e., concerning (ρ_{min}, ρ_{max}). As the tests advanced and fatigue was detected, both values were increased but under-estimated to prevent the problems aforementioned (pain, fatigue). Further, the same empiric gains were applied for both sine and step trajectories, and in this table, all unit of measurements is omitted due to page length limitation;

- a table with information on the identified NN model such as the training time (TT), the correlation between input and output data (Corr), and the mean squared error (MSE);

- a table presenting control metrics results for the experiments made. The metrics for evaluating the control system performance on experiments are the RMSE between the desired and actual knee angles considering the whole period of control-stimulation; and the time of effective control (TEC) representing how much time in seconds the lower limb is control-stimulated to track the reference angle. When the lower limb does not track the reference angle, the RMSE metric is represented by NC, meaning "not calculated";

- and to conclude, experimental results are presented in figures comparing both empiric and IGA tuning for all individuals.

4.4.1 Individual P1

Figure 17 illustrates subject P1 who participated in one session. As related by P1, during experiments no discomfort or pain was provoked by stimulation, there is no sensibility under the level of injury (L4, L5), no use of electrical stimulation was made before this session, and currently, none rehabilitation or treatment is being carried out.

Hence, the initial procedure was performed for finding the subject's P1 motor point and the bounded pulse width band (ρ_{min}, ρ_{max}) (just as Figure 15 illustrates), as described in Section 4.3. Thereafter, an stimulation of random PW during 40 seconds was made (similar to Figure 16) and the acquired data were treated and fed into a NN model to map the relationship of PW and angular position.

Using the identified model, the IGA optimization was performed to find the best gains combination for both sine and step trajectories. During this time (about 10 minutes), muscle rested from previous stimulations. Therefore, the controlling procedure using gains encountered by the IGA was made for the sine and step waves, respectively during 30 seconds of stimulation at most. The operation point for the step wave was decreased to $30°$, aiming to avoid premature fatigue. To conclude the session, the same controlling procedure was made using empiric gains.

Figure 17 - Individual P1 in the instrumented chair.

Source: Developed by the author

Therefore, Table 9 describes additional technical information about the stimulation session for subject P1; Table 10 presents information for the identified model, and metrics results on simulations; Table 11 presents control metrics results on experimental results and Figure 18 exhibits control results for subject P1 from the LabVIEW® platform (using IGA tuning only) and one with zoom to the tracking results (empiric and IGA tunings).

As results in Table 11 and Figure 18 show, the proposed methodology could be effectively applied to clinical procedures for treating spinal cord injured patients via NMES/FES. As one will see in the following subsections, the RMSE for the sine wave from P1, was the best result during all experiments made during this research. However, it is notable in the final seconds (about 28 seconds) that the lower limb would start to have more tremors due to the fatigue factor. Similar results were acquired in Chapter 3, where paraplegic subjects presented superior tracking results under ideal conditions, i.e., without non-idealities included such as fatigue, tremors, and spasms.

Using an empirical tuning, the lower limb tracked the sine wave with a lag and presented a slow response to the step wave, but still, tracking results are acceptable with the RISE controller. On the other hand, as previously mentioned, very good tracking results were achieved for both trajectories when the RISE controller was tuned via the proposed methodology.

Table 9 - Technical information on experiments for individual P1.

Identification		Empiric		Sine IGA		Step IGA	
$\rho_{min};\rho_{max}$	$\theta_{min};\theta_{max}$	$\rho 0;sat$	$\alpha_1;\alpha_2;ks;\beta$	$\rho 0;sat$	$\alpha_1;\alpha_2;ks;\beta$	$\rho 0;sat$	$\alpha_1;\alpha_2;ks;\beta$
200;250	18;50	200;350	1;2;30;5	180;300	2.61;3.34;48.94;1.78	180;300	2.72;3.57;47.12;1.54

Source: Developed by the author

Table 10 - Identification results for individual P1.

Session	TT	Corr	MSE
1st	28(s)	0.836	0.0019

Source: Developed by the author

Table 11 - Metrics on experimental results for individual P1.

	Sine				Step			
	Empiric		IGA		Empiric		IGA	
Session	RMSE	TEC	RMSE	TEC	RMSE	TEC	RMSE	TEC
1st	9.1471°	30(s)	2.9842°	30(s)	10.9950°	30(s)	5.9786°	25(s)

Source: Developed by the author

Results from P1 validate and substantiate the first hypothesis made in Section 1.3, whereby using an empirical tuning, the rehabilitation of SCI patients presents inadequate performances while by using the proposed approach control results are improved and fatigue or other problems can be diminished. As SCI population have weak muscles or even atrophied ones due to a total or partial paralysis, the application of empiric gains would not provide good tracking, which would accentuate the fatigue factor, motivating the proposal of this research in the way that when the RISE controller is well-tuned, control performance is improved. Moreover, it is noteworthy that even using a higher pulse amplitude of 120 mA (in contrast with 80 mA for healthy subjects) both $\rho 0$ and *sat* values are higher for paraplegic subjects due to aforementioned problems (weak muscles or even atrophied ones), which allows the control law to switch in a higher range of pulse width to obtain an adequate muscle contraction and control it.

From Table 10 it is notable a high correlation between input and output data. When the data present a high correlation between features and target, the generalization and learning are less difficult, which consequently generated a low MSE for the model. Figure 19 illustrates a comparison between simulation and real experiment for the sine wave. As the correlation between data was high, the model could identify quite well the result in comparison with the real experiment. Both results presented similar tremors in the upper and lower peak value, while the step wave was modeled with a fast response with no stationary error. However, as an approximate model using only the identification data of 40 seconds, this model was not prepared for modeling fatigue and tremors that were present in the real experiment. As we hypothesized in Section 1.3, the modeling of knee joint position under NMES/FES could be improved by taking into advantage the use of past rehabilitation data. However, as P1 did not continue participating in more sessions, we could not validate this second hypothesis.

Figure 18 - Experimental results for individual P1.
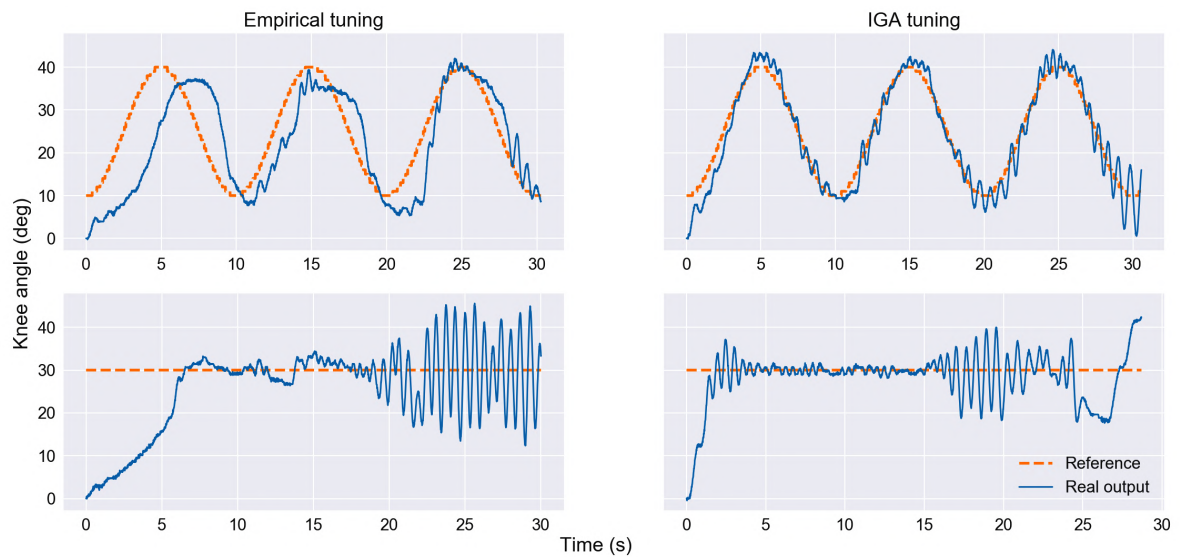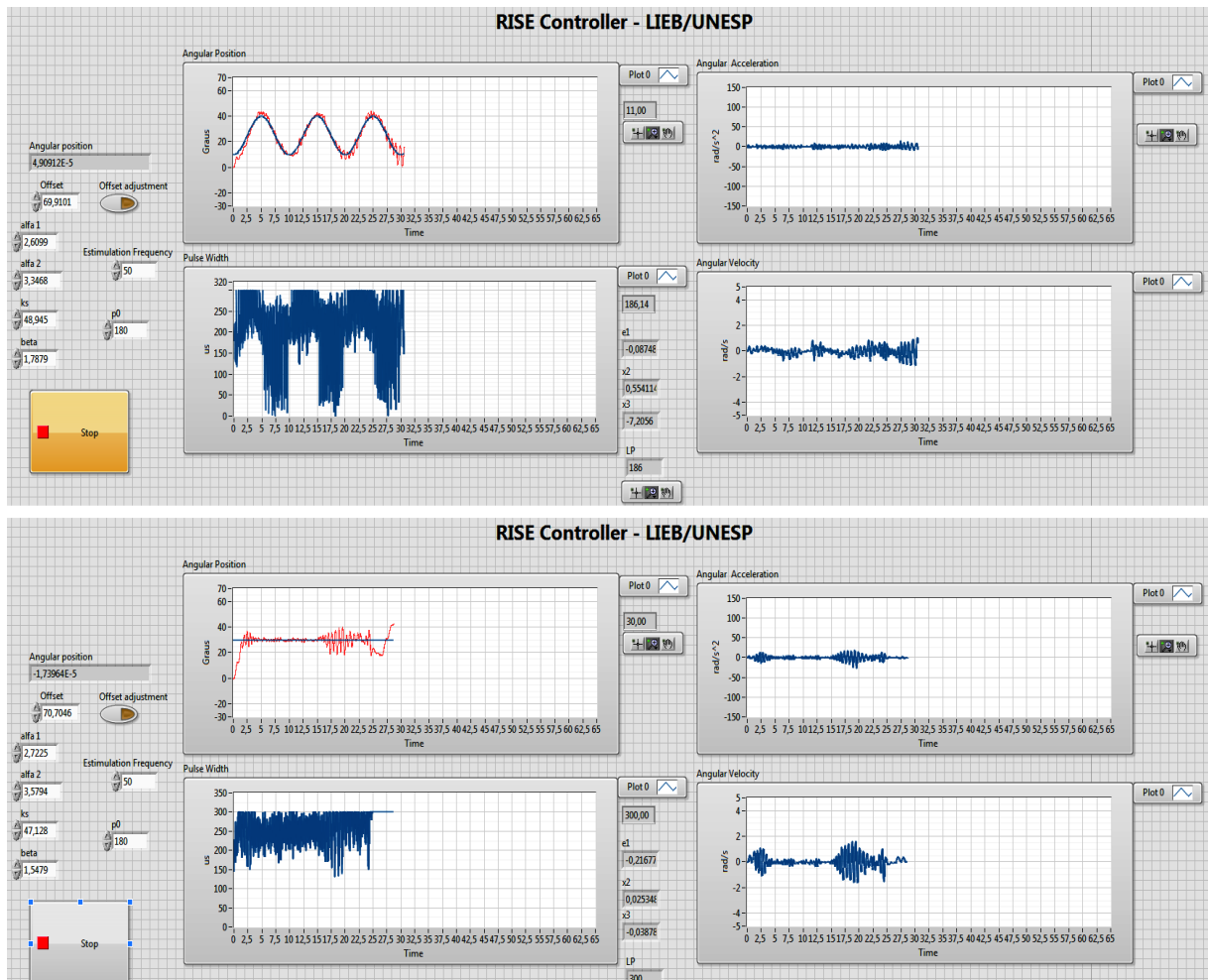
Source: Developed by the author

4.4.2 Individual P2

Just as subject P1, subject P2 illustrated in Figure 20 participated in one session. As related by P2, during experiments no discomfort or pain was provoked by stimulation, there exist pains

Figure 19 - IGA comparison of simulation and real experiment for individual P1.
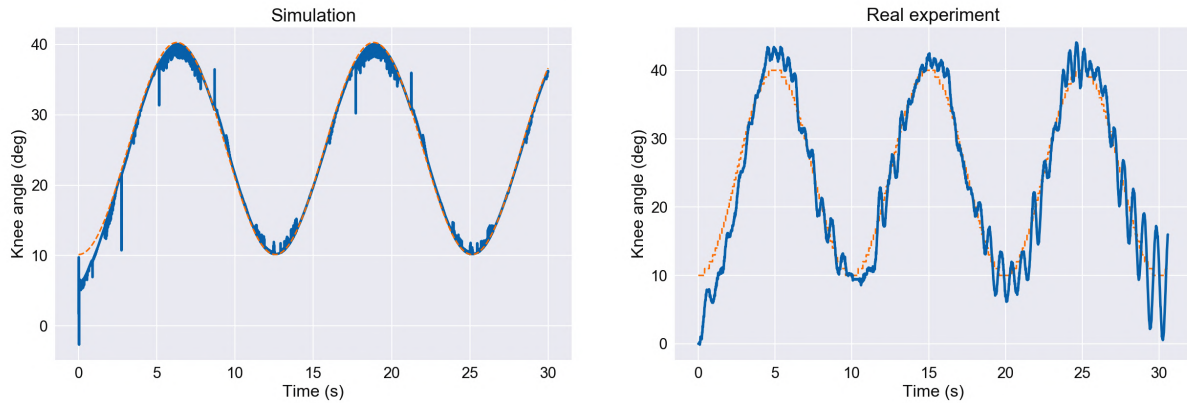
Source: Developed by the author

due to spasms contractions during the day, he feels small sensibility in the lower limbs, he has participated in experiments using Russian current, and currently, none rehabilitation or treatment is being carried out.

Similarly to P1, the same procedure was performed for the stimulation session including identification and control. For more information, the reader is invited to check the previous Subsection 4.4.1. Therefore, Table 12 describes additional technical information about the stimulation session for subject P2; Table 13 presents information for the identified model, and metrics results on simulations; Table 14 presents control metrics results on experimental results and Figure 21 exhibits control results for subject P2 from the LabVIEW® platform (using IGA tuning only) and one with zoom to the tracking results (empiric and IGA tunings).

As one can notice in Figure 21 and Table 14, tracking results for subject P2 were not as good as they were for P1. However, the poor sine wave tracking under IGA tuning could be due to an under-estimation for saturation *sat* that bounds the control signal value, where it seems that a possible good tracking would be acquired if the saturation value had been selected higher. This idea is substantiated by results of the step wave of 30° performed with three minutes interval for muscle rest after the sine wave using the IGA tuning where a very good regulation around the operation point was achieved during 21 seconds approximately.

Table 12 - Technical information on experiments for individual P2.

Identification		Empiric		Sine IGA		Step IGA	
$\rho_{min};\rho_{max}$	$\theta_{min};\theta_{max}$	$\rho 0;sat$	$\alpha_1;\alpha_2;ks;\beta$	$\rho 0;sat$	$\alpha_1;\alpha_2;ks;\beta$	$\rho 0;sat$	$\alpha_1;\alpha_2;ks;\beta$
150;250	8;38	200;370	1;2;30;5	185;310	2.22;3.54;39.50;1.40	190;360	3.01;1.91;48.34;2.65

Source: Developed by the author

Additionally, similar to results from P1, an empirical tuning provided very poor performance for both sine and step trajectories, by not tracking the sine wave and by regulating with

Figure 20 - Individual P2 in the instrumented chair.

Source: Developed by the author

Table 13 - Identification results for individual P2.

Session	TT	Corr	MSE
1st	33(s)	0.796	0.0032

Source: Developed by the author

Table 14 - Metrics on experimental results for individual P2.

	Sine				Step			
	Empiric		**IGA**		**Empiric**		**IGA**	
Session	RMSE	TEC	RMSE	TEC	RMSE	TEC	RMSE	TEC
1st	11.2966°	30(s)	10.7306°	30(s)	10.1067°	23(s)	6.6134°	21(s)

Source: Developed by the author

a stationary error around the operation point from the step wave. In contrast, when using the proposed methodology, even the one with poor performance due to under-estimation value for the saturation value, results are better than using empiric gains. For the step wave, the RMSE metric decreased almost 50%, representing very good tracking results.

From Table 13 it is notable a high correlation between input and output data, which generated a low MSE for the model. As the correlation between data was high, the model identified quite well the real experiment responses. However, due to the under-estimated value of *sat*, fatigue damping and tremors from real-world muscle conditions, the results in real experiments varied from simulations.

Figure 21 - Experimental results for individual P2.
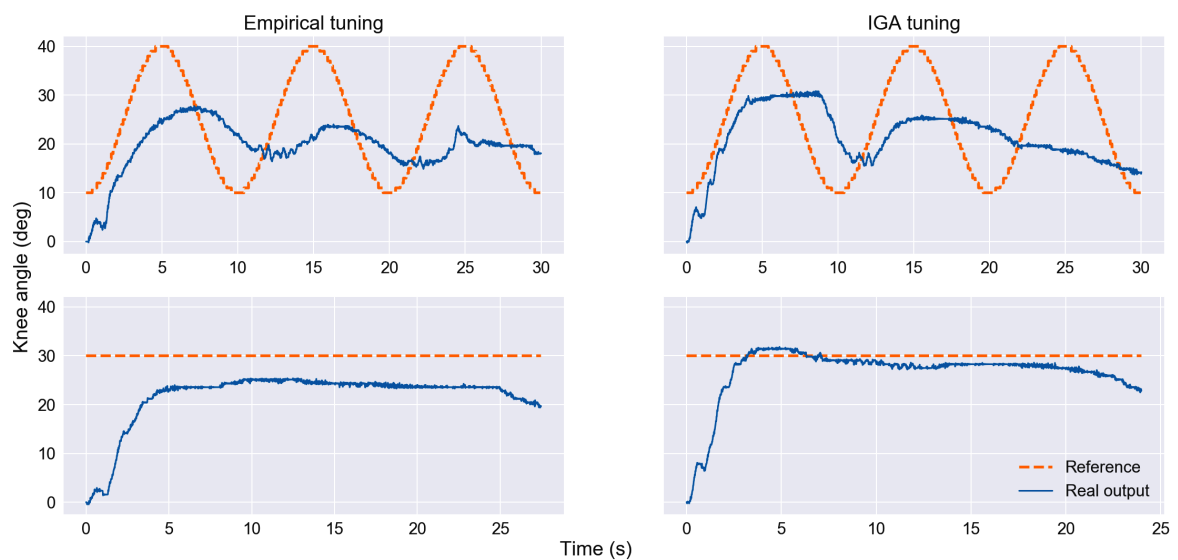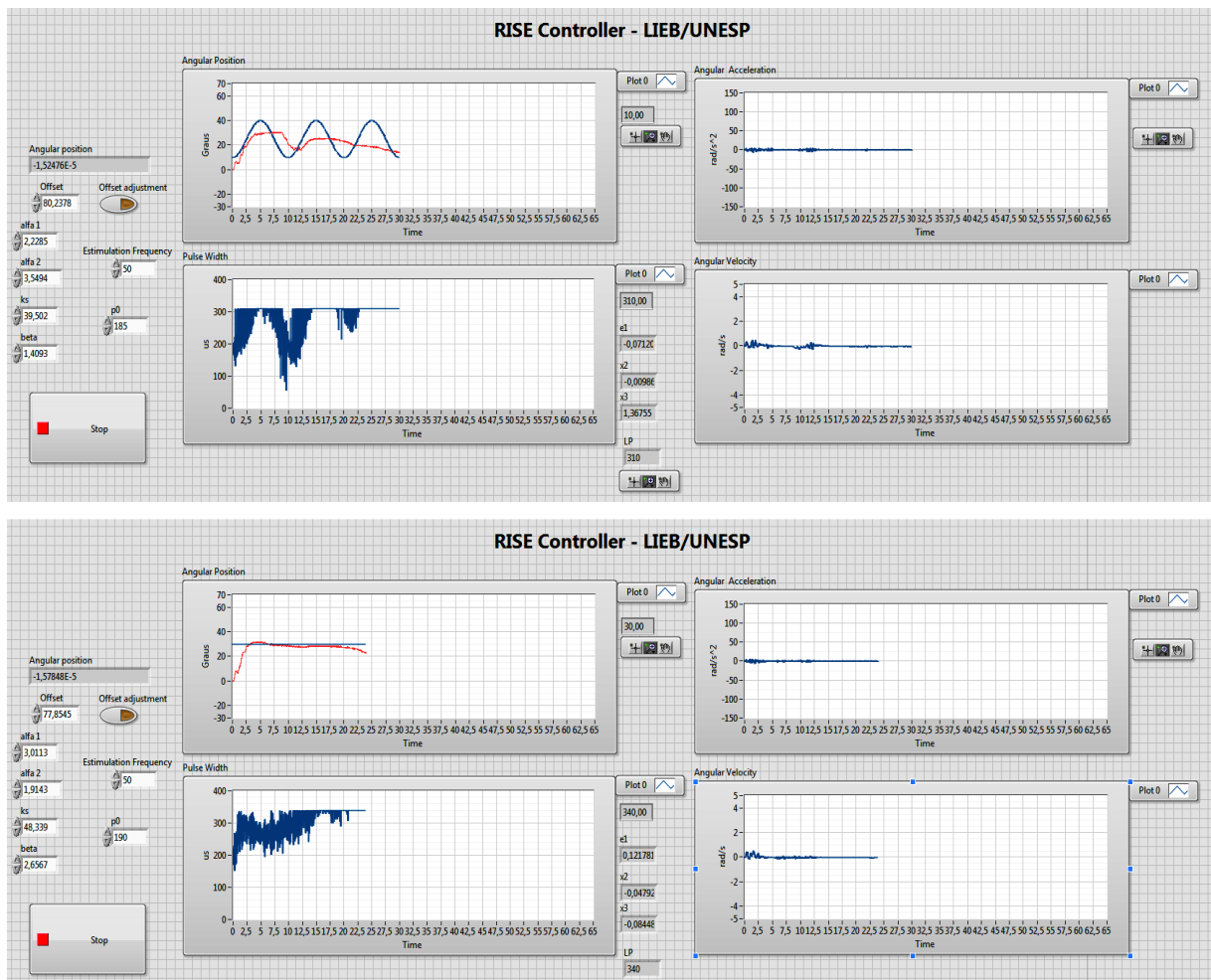
Source: Developed by the author

4.4.3   Individual H1

Individual H1 participated in five sessions, wherein its first session, the initial procedure was carried out for finding its motor point and the bounded pulse width band, as described in

Section 4.3. Thereafter, an stimulation test was implemented (as Figure 16 illustrates) and the acquired data were fed into a NN model to map the relationship of PW and angular position. While the NN was being trained and the IGA optimization later on performed, the controlling procedure with empiric gains was made for both sine and step-signal trajectories respectively. To conclude the session, the same controlling procedure was made with the gains found by the IGA for the identified NN model.

As described in Section 4.3.2, to the second until the fifth session, the initial procedure was carried out and there was no identification step given that the NN model was offline trained with both control and identification previous data. In the second, third and fifth session, at first, the controlling procedure was performed with the gains found by the IGA optimizer, and then with empiric ones, while in the first and fourth sessions, empiric gains were applied first and then the IGA ones. The first session took more time and an additional stimulation than the following others due to the motor-point identification, stimulation test of one minute, and the training/optimization time made to find the best gains combination.

Therefore, Table 15 describes additional technical information about each session, being each line of the table a session day for individual H1; Table 16 presents information for the identified models, and metrics results on simulations; Table 17 presents control metrics results on experimental results and Figures 22 and 23 display control results for subject H1 in all stimulation sessions.

Table 15 - Technical information on experiments for individual H1.

Identification		Empiric		Sine IGA		Step IGA	
$\rho_{min};\rho_{max}$	$\theta_{min};\theta_{max}$	$\rho0;sat$	$\alpha_1;\alpha_2;ks;\beta$	$\rho0;sat$	$\alpha_1;\alpha_2;ks;\beta$	$\rho0;sat$	$\alpha_1;\alpha_2;ks;\beta$
100;150	10;42	100;170	1;2;30;5	100;170	3.23;1.08;24.74;5.50	100;170	1.37;1.63;54.03;2.36
80;175	10;40	100;190	0.5;1;30;1.5	100;190	1.76;2.28;32.30;2.39	100;190	0.64;1.66;52.26;4.00
100;150	12;45	100;185	0.8;1.2;20.5;2.5	100;150	3.23;2.52;27.33;2.29	100;165	2.30;4.24;59.26;3.49
120;160	10;40	100;180	5;2;15;3	100;180	2.40;4.10;27.05;2.18	100;180	3.12;5.80;43.162;1.35
140;190	10;44	120;220	4;7;25;8	120;210	3.07;4.37;21.73;1.56	120;210	2.61;3.54;39.50;1.30

Source: Developed by the author

Table 16 - Identification results for individual H1.

Session	TT	Corr	MSE
1st	34(s)	0.726	0.0022
2nd	48(s)	0.157	0.0386
3rd	106(s)	0.101	0.0428
4th	144(s)	0.159	0.0411
5th	350(s)	0.113	0.0402

Source: Developed by the author

As demonstrated in Figures 22 and 23, an empirical tuning could also guarantee stability, i.e., the lower limb tracked the step wave effectively in sessions one and four, and in most of the sine trajectories, the leg poorly, but tried to follow the reference angle. However, as previously

Table 17 - Metrics on experimental results for individual H1.

	Sine				Step			
	Empiric		IGA		Empiric		IGA	
Session	RMSE	TEC	RMSE	TEC	RMSE	TEC	RMSE	TEC
1st	7.4946°	60(s)	5.8303°	60(s)	5.9209°	60(s)	6.1677°	60(s)
2nd	8.7529°	60(s)	5.9333°	60(s)	12.2910°	60(s)	8.2012°	60(s)
3rd	14.0928°	60(s)	7.3373°	60(s)	7.2664°	60(s)	4.1644°	60(s)
4th	6.3778°	60(s)	3.6292°	60(s)	6.7410°	60(s)	4.4040°	60(s)
5th	6.3835°	60(s)	3.5624°	60(s)	6.8875°	60(s)	4.4251°	60(s)

Source: Developed by the author

Figure 22 - Experimental results for subject H1 on sessions one and two respectively.
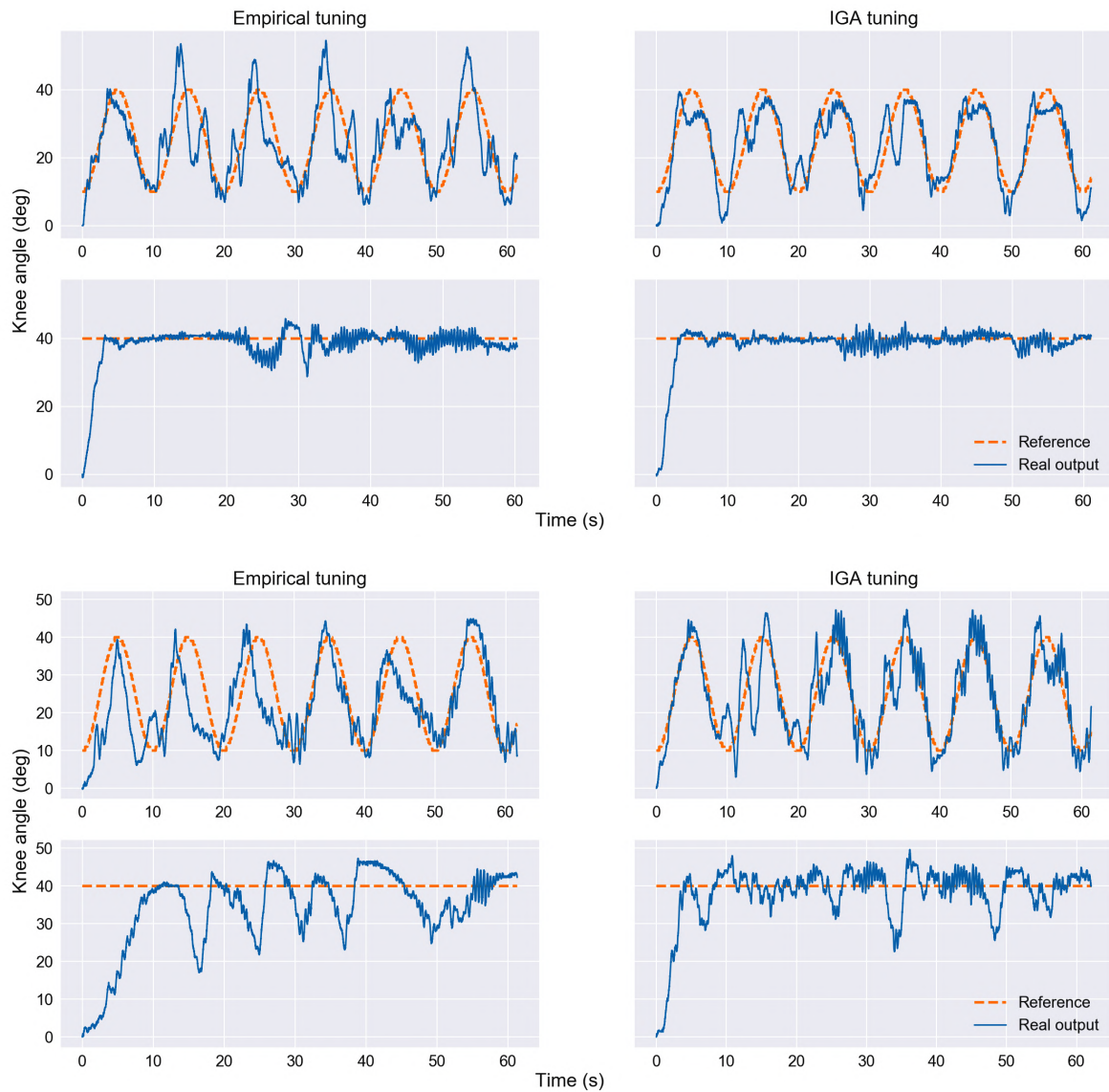
Source: Developed by the author

discussed in Section 3.3, once gains selections are immense, one likely choose combinations that would not guarantee best performance and accuracy during rehabilitation, e.g., compare simulation results from Figure 10 with the result from session five in Figure 23.

As one can notice in Table 17 and in the two previous figures, results for individual H1 using an empirical tuning provided poor tracking performances in most of the sessions, while with an appropriate choice of gains, using the proposed methodology, the lower limb presented better tracking results. Except for session two, results to the step wave presented very efficient regulation around the desired point of operation, and for the sine wave, sessions two and three did not present very positive results, but still, the control law tried to compensate the error between desired and real angle. Furthermore, the RMSE tended to decrease using fine-tuned gains as sessions passed by, showing that the proposed methodology could provide good rehabilitation treatments for SCI patients that continuously go on sessions of NMES/FES.

Additionally, in all stimulation sessions, even the ones with poor performances, the control-stimulated lower limb tried robustly to track the reference angle during 60 seconds, while the RISE controller in the literature presented by Stegath et al. (2007, 2008) demonstrated tracking control on 8 seconds for the stepping trajectory and 20 seconds for a sine wave; Sharma et al. (2009, 2012) presented tracking control on 30 seconds for a step and sine-type signal; and Kushima et al. (2015), Downey et al. (2015b) presented tracking control on 30 and 45 seconds respectively for a sine trajectory.

From Table 16, it is noticed a fast decrement from the first session to the remaining ones in the correlation between input and output data as sessions passed by (given the addition of control data from every new session), which resulted in increments to the MSE metrics for each trained NN model in comparison with the first one. Due to less correlation between data, the generalization and learning procedure of a NN is much harder, however, this model better describes what happens in real experiments, where nonlinearities and the time-varying behavior of muscles are explained by data.

Figure 23 - Experimental results for subject H1 on sessions three, four and five respectively.
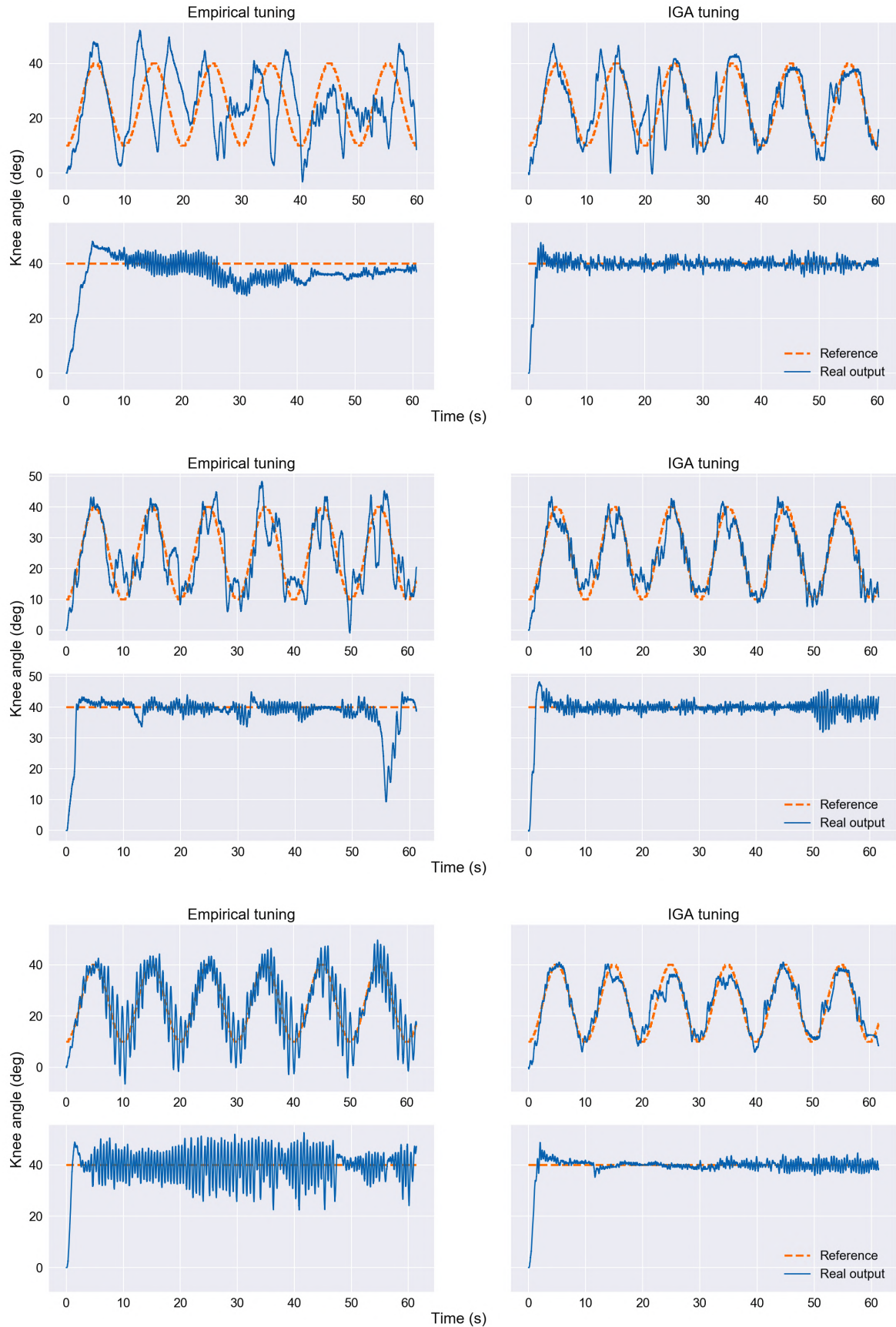
Source: Developed by the author

In this context, Figure 24 illustrates a comparison between results from simulation and real experiments from the individual H1 for sessions one and four using the IGA tuning approach. In the first session, the data were much more correlated and the model could predict quite well what would happen in the real experiment, wherein responses for the step wave are very comparable. Similarly, for the fourth session, the model did also provide a good description of the real experiment, predicting a sine trajectory with tremors in both lower and upper values of the wave and a quick response to the step-signal trajectory with no stationary error. However, as an approximate model, neither of them would be prepared for an exact description of the real system, for instance, considering that voluntary movements, fear or other issues related to thoughts of the individual itself (e.g., social or personal life) that can affect results, could not be predicted by the model.

Figure 24 - IGA comparison of simulation and real experiment for individual H1.
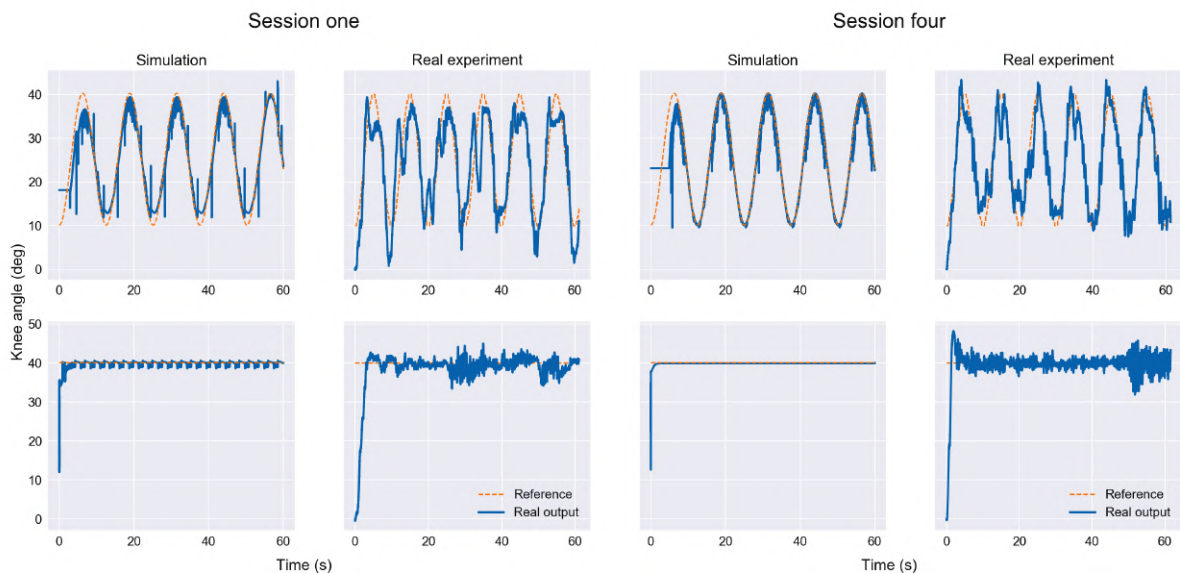
Source: Developed by the author

4.4.4 Individual H2

Individual H2 also participated at five sessions, where the set-up protocol for control-stimulation was similar as it was for H1 (for more details, refers to the previous Subsection 4.4.3 or Section 4.3). Therefore, Table 18 describes additional technical information about each session, being each line of the table a session day for individual H2; Table 19 presents information for the identified models, and metrics results on simulations; Table 20 presents control metrics results on experimental results; and Figures 25 and 26 exhibits control results for subject H2 in all stimulation sessions.

Table 18 - Technical information on experiments for individual H2.

Identification		Empiric		Sine IGA		Step IGA	
$\rho_{min};\rho_{max}$	$\theta_{min};\theta_{max}$	$\rho0;sat$	$\alpha_1;\alpha_2;ks;\beta$	$\rho0;sat$	$\alpha_1;\alpha_2;ks;\beta$	$\rho0;sat$	$\alpha_1;\alpha_2;ks;\beta$
120;150	10;40	100;200	1;2;30;5	100;220	1.90;3.50;48.00;3.00	100;220	1.90;3.50;48.00;3.00
180;220	10;40	200;290	0.8;1.2;20.5;2.5	180;240	1.57;2.37;48.45;1.05	200;260	1.38;1.34;64.41;3.72
150;180	14;41	130;200	0,5;1;30;1,5	150;230	1.47;3.31;30.01;1.87	170;250	3.54;3.83;54.88;1.92
130;150	12;42	150;220	5;2;15;3	110;170	1.42;3.68;35.09;1.99	130;190	2.07;1.75;36.32;1.96
130;160	8;40	120;230	4;7;25;8	120;180	2.03;3.02;36.07;2.23	120;200	2.17;1.76;38.53;1.85

Source: Developed by the author

Table 19 - Identification results for individual H2.

Session	TT	Corr	MSE
1st	94(s)	0.869	0.0064
2nd	132(s)	0.416	0.0397
3rd	148(s)	0.308	0.0390
4th	249(s)	0.282	0.0370
5th	327(s)	0.292	0.0382

Source: Developed by the author

Table 20 - Metrics on experimental results for individual H2.

	Sine				Step			
	Empiric		IGA		Empiric		IGA	
Session	RMSE	TEC	RMSE	TEC	RMSE	TEC	RMSE	TEC
1st	5.2124°	60(s)	5.0555°	44.9(s)	9.7644°	57(s)	6.2122°	37(s)
2nd	8.3179°	60(s)	3.8853°	60(s)	NC	30(s)	7.8566°	25(s)
3rd	11.7414°	35(s)	3.6331°	60(s)	11.8222°	57(s)	5.4572°	37(s)
4th	4.8877°	60(s)	3.5629°	40(s)	6.4240°	34(s)	4.8901°	45(s)
5th	10.7136°	33(s)	4.8582°	23(s)	6.2262°	35(s)	7.2336°	38(s)

Source: Developed by the author

As one can notice in Table 20 and in Figures 25 and 26, the lower limb barely tracked the reference trajectories when control-stimulated using empiric gains constants in most of sessions. In sessions one and five, for the sine trajectory, the lower limb oscillated the whole period of stimulation, being more accentuated in the fifth session, which is very similar to simulation results in Figure 10 and results obtained for individual H1 in Figure 23. Additionally, for the step-signal trajectory, in the first and fourth session, the lower limb tracked the reference angle very well during 30 seconds approximately, and in the last one, it took a while to pass through a very large (20 seconds) transitory period but still presented a good tracking result.

On the other side, by using the proposed methodology to tune the RISE controller, results to the sine wave in all sessions were less or equal to $5°$ with minimum 23 seconds and at most 60 seconds (two of five) of stimulation, representing very satisfactory tracking results. Moreover, for the step-signal trajectory, the control-stimulated lower limb was regulated around

the desired angle, with a poor result in session three where the oscillatory period took 22 seconds approximately, but in most of them, results were very favorable. By comparing results for both empirical and IGA tuning approaches, the difference is discrepant in favor of the proposed methodology with the IGA tuning procedure, which could benefit the SCI population treating with NMES/FES systems.

Figure 25 - Experimental results for subject H2 on sessions one and two respectively.
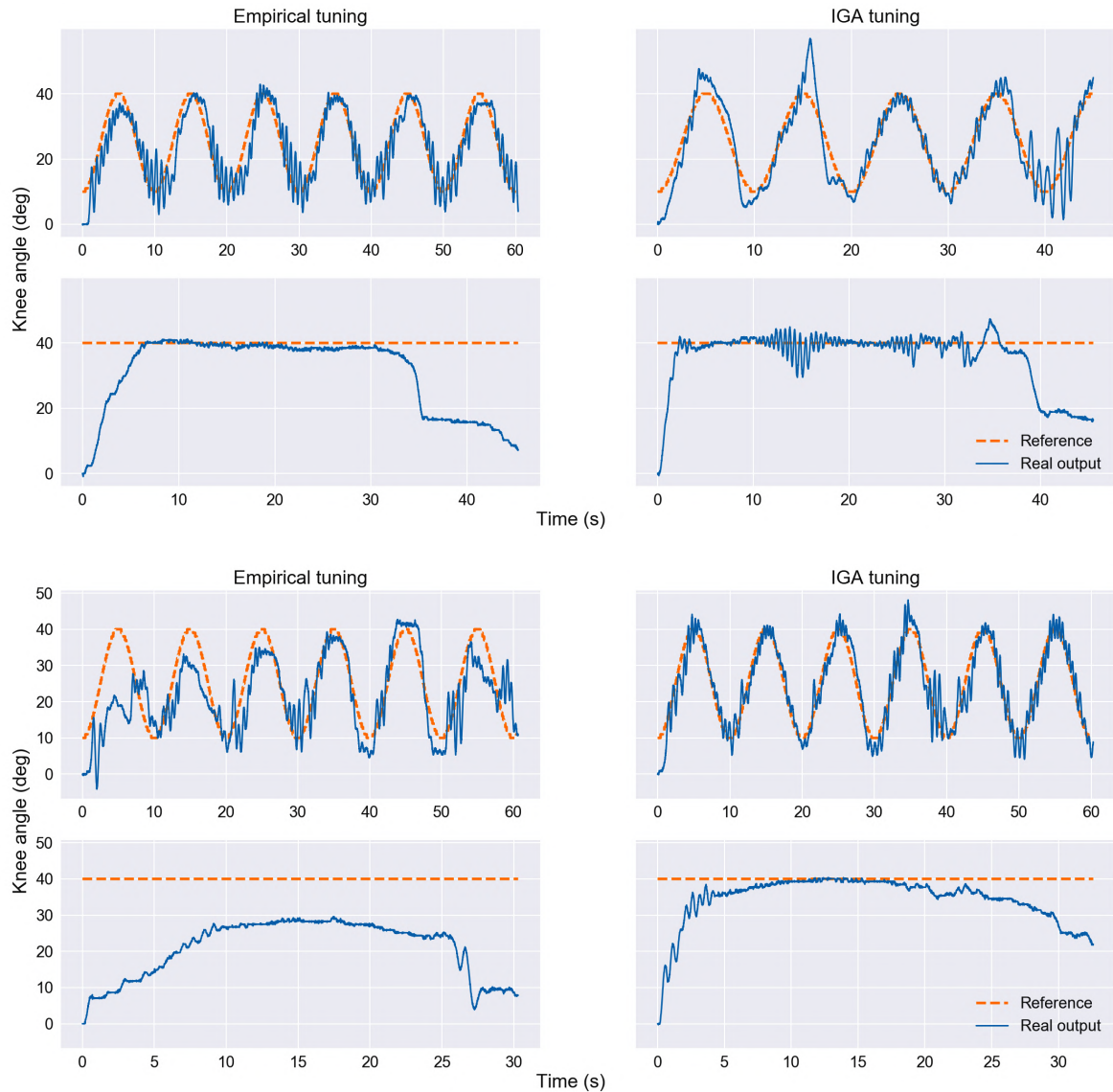
Source: Developed by the author

From Table 19, one can notice the correlation between input and output data dropped to half comparing the two first sessions, and it continued dropping as sessions passed by. For this reason, less correlation between data, the MSE metric increased, but the model fitted better for modeling nonideal conditions such as fatigue and tremors. Nevertheless, for most sessions, the model did not take into account premature fatigue occurring for individual H2.

Figure 26 - Experimental results for subject H2 on sessions three, four and five respectively.
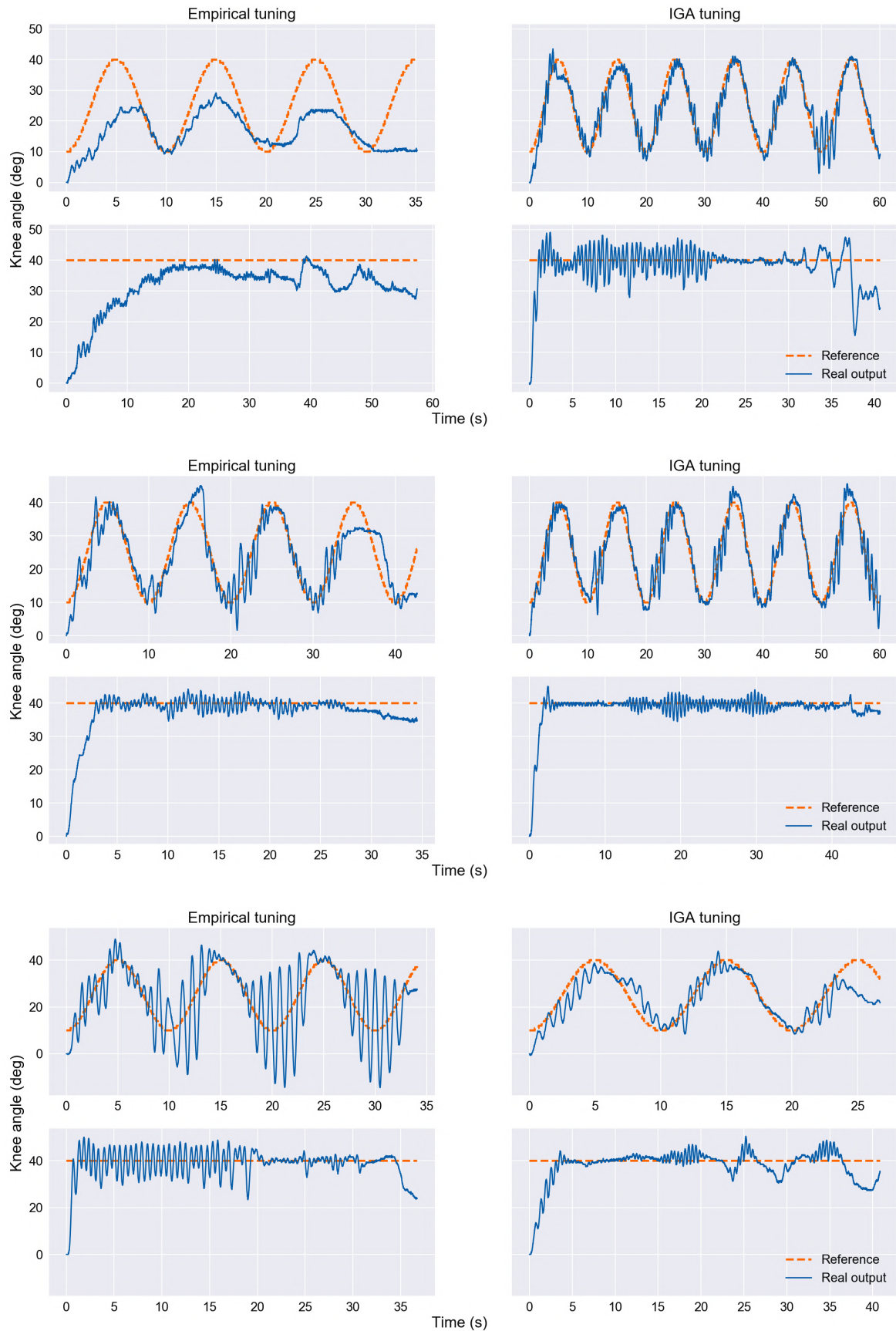
Source: Developed by the author

4.4.5 Individual H3

As well as individuals H1 and H2, the individual H3 did also participated at five sessions, where the set-up protocol for control-stimulation was similarly as for both of H1 and H2 (for more details, refers to Subsection 4.4.3 or Section 4.3).

Therefore, Table 21 describes additional technical information about each session, being each line of the table a session day for individual H3; Table 22 presents information for the identified models, and metrics results on simulations; Table 23 presents control metrics results on experimental results; and Figures 27 and 28 exhibit control results for subject H3 in all stimulation sessions.

Table 21 - Technical information on experiments for individual H3.

Identification		Empiric		Sine IGA		Step IGA	
$\rho_{min};\rho_{max}$	$\theta_{min};\theta_{max}$	$\rho 0;sat$	$\alpha_1;\alpha_2;ks;\beta$	$\rho 0;sat$	$\alpha_1;\alpha_2;ks;\beta$	$\rho 0;sat$	$\alpha_1;\alpha_2;ks;\beta$
110;170	15;40	100;190	0.5;1;30;1.5	100;210	1.4;2.5;60;3.4	100;220	1.47;2.63;57.83;3.36
100;140	18;45	100;190	1;2;30;5	100;140	2.12;2.28;73.74;1.55	100;160	2.77;3.03;57.17;3.47
100;160	14;40	100;185	0.8;1.2;20.5;2.5	100;175	4.75;4.01;19.56;2.73	100;190	1.56;3.95;50.91;3.05
120;150	10;38	100;180	5;2;15;3	120;210	0.93;2.69;28.09;2.45	120;230	3.22;3.99;68.67;1.26
120;150	12;42	100;215	4;7;25;8	100;170	3.25;3.45;22.70;3.23	100;190	2.23;2.85;43.33;2.037

Source: Developed by the author

Table 22 - Identification results for individual H3.

Session	TT	Corr	MSE
1st	102(s)	0.820	0.0038
2nd	136(s)	0.498	0.0238
3rd	230(s)	0.506	0.0231
4th	246(s)	0.510	0.0242
5th	280(s)	0.492	0.0263

Source: Developed by the author

Table 23 - Metrics on experimental results for individual H3.

	Sine				Step			
	Empiric		IGA		Empiric		IGA	
Session	RMSE	TEC	RMSE	TEC	RMSE	TEC	RMSE	TEC
1st	NC	60(s)	6.0192°	30(s)	15.3591°	48(s)	8.1763°	32(s)
2nd	9.2216°	50(s)	7.6157°	50(s)	8.2306°	45(s)	5.5985°	28(s)
3rd	NC	45(s)	4.6164°	33(s)	14.2339°	38(s)	6.2584°	30(s)
4th	3.7757°	33(s)	6.6880°	60(s)	5.4725°	40(s)	6.3576°	55(s)
5th	19.0968°	60(s)	6.5163°	60(s)	7.1020°	60(s)	4.4912°	60(s)

Source: Developed by the author

Figure 27 - Experimental results for subject H3 on sessions one, two and three respectively.
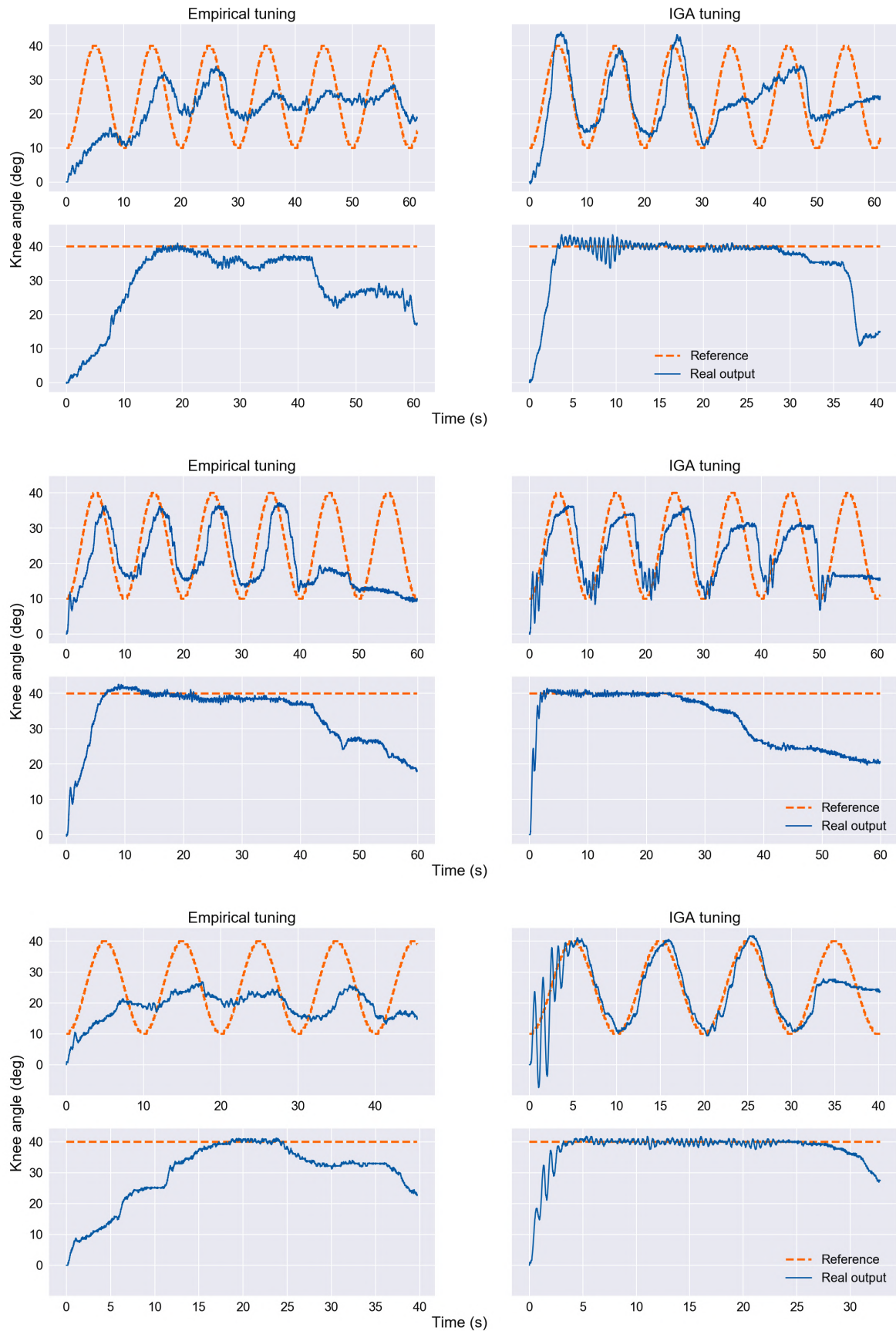
Source: Developed by the author

Figure 28 - Experimental results for subject H3 on sessions four and five respectively.
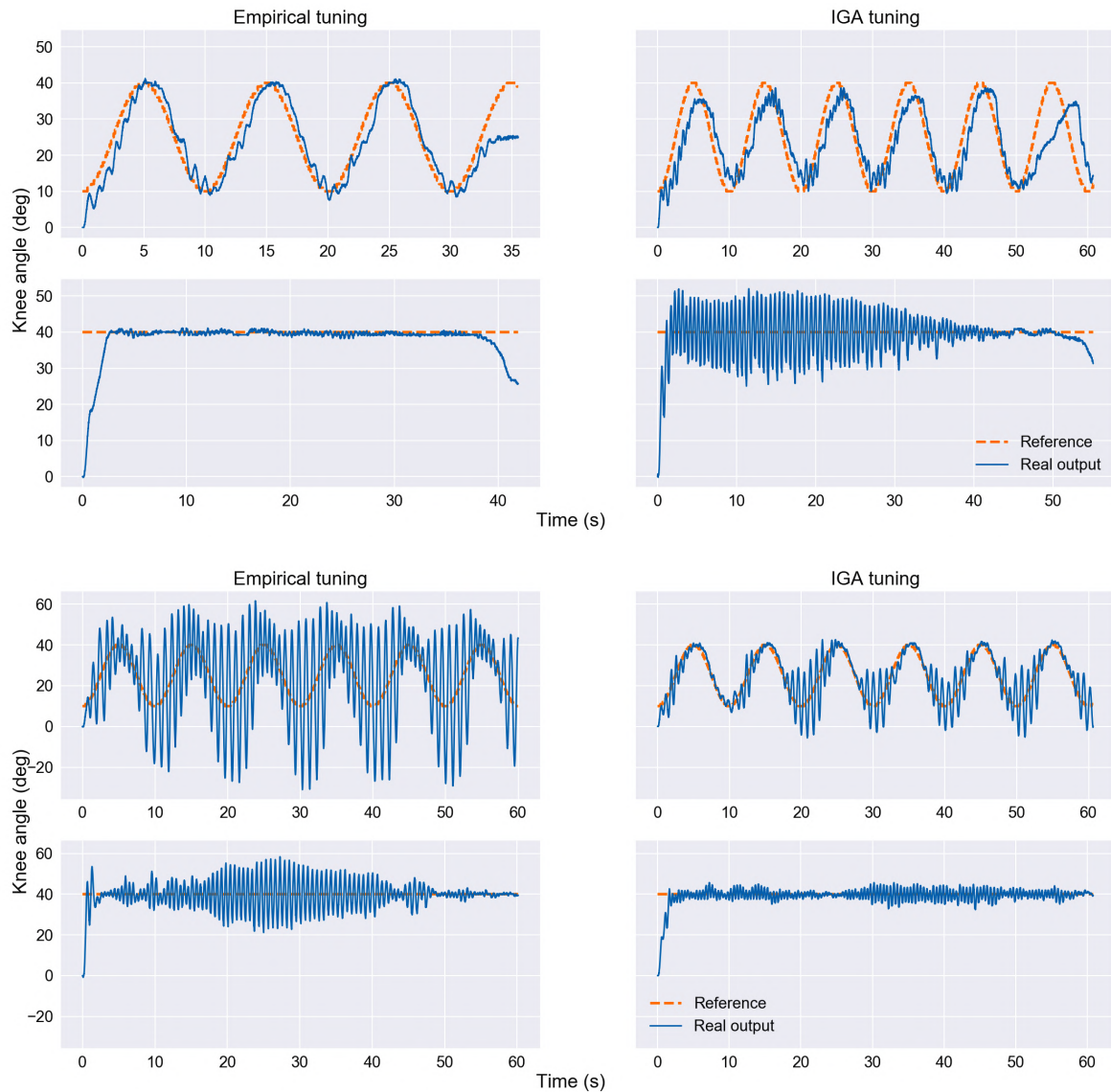
Source: Developed by the author

As one can notice in Table 20 and in Figures 27 and 28, the use of an empirical tuning approach for the RISE controller presented poor performances in almost all of the sessions, where the exception was session four with very good tracking results for both sine and step trajectories. Additionally, in sessions one and three, the control-stimulated lower limb under empirical tuning did not track the reference angle, and as well as for individuals H1 and H2, results from session five in Figure 28, are similar to results presented in Figure 10, substantiating the hypothesis of very poor performances using the empirical tuning approach, which is not ideal for dealing with SCI patients on rehabilitation treatments via NMES/FES.

On the other hand, when the proposed methodology was applied, the control-stimulated lower limb presented superior tracking results. In session one, the lower limb tracked the step

wave with a good performance during almost 38 seconds, and for the sine wave, with some error, but properly tracked the reference angle during 30 seconds. Thereafter, for the rest of the sessions, the lower limb effectively tracked the reference angle for more than 30 seconds, getting to 60 seconds in final sessions, with exception to the step wave in session four that presented long transitory response (almost 40 seconds), and for the sine wave in session five, which presented oscillatory comportment.

In Table 22, the correlation between input and output data decreased as sessions passed by (given the augmentation of control data from every new session), but not as much as for individual H1 and H2. Consequently, the MSE metric increased for each trained NN model comparing to the first session that uses only the identification data.

Therefore, Figure 29 illustrates a comparison between results from simulation and real experiments from the individual H3 for sessions one and five using the IGA tuning approach. In the first session, the data were much more correlated and the model could predict quite well what would happen in the real experiment, e.g., the overshoot response for the step wave and no stationary error. Similarly, for the fifth session, the model did also provide a good description of the real experiment, predicting an oscillatory behavior for the first and fifth cycle of the sine trajectory, and a quick response to the step wave with oscillatory behavior the whole period.

However, as approximate models, for the first session, it did not take into account fatigue behavior after 30 seconds of stimulation, and for the fifth session, it did not predict a very oscillatory behavior during the whole period.

Figure 29 - IGA comparison of simulation and real experiment for individual H3.
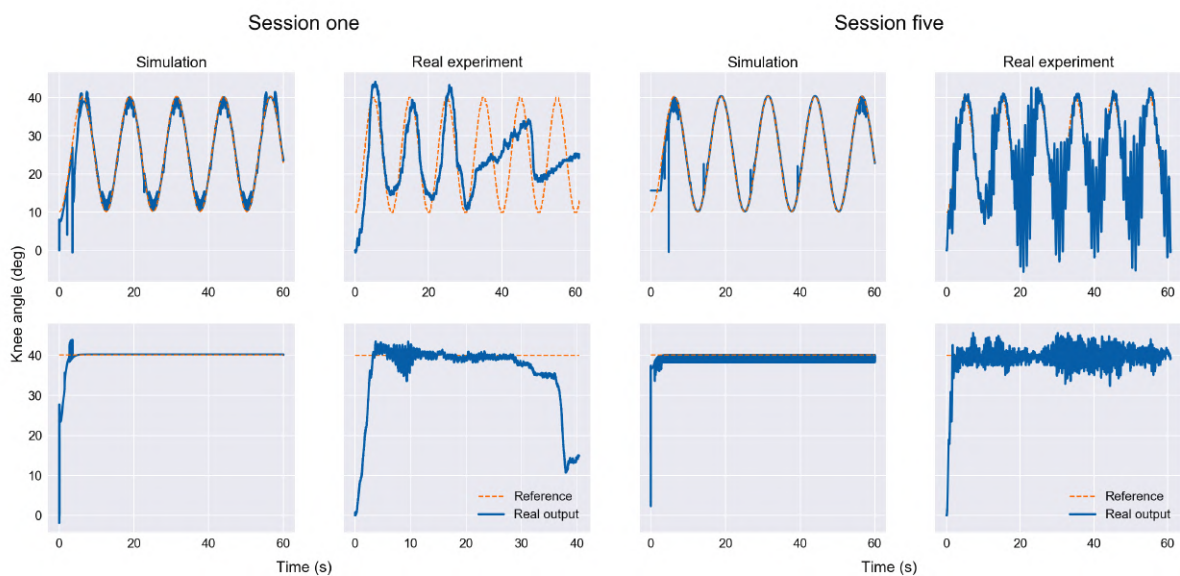
Source: Developed by the author

4.4.6   Individual H4

Individual H4 participated only in two sessions, wherein both sessions, the set-up procedure was carried out similar to the first two sessions of the other individuals (for more details, one can refer to Section 4.3 and Subsection 4.4.3). Thus, in session one, after the identification step, the controlling procedure was applied at first, with empiric gains and then with fine-tuned ones found by the IGA. Inversely, in session two, IGA fine-tuned gains were used at first, and then empiric ones. Therefore, Table 24 describes additional technical information about both sessions, being each line of the table a session day for individual H4; Table 25 presents information for the identified models, and metrics results on simulations; Table 26 presents control metrics results on experimental results; and Figure 30 shows control results for subject H4 in both stimulation sessions.

Table 24 - Technical information on experiments for individual H4.

Identification		Empiric		Sine IGA		Step IGA	
$\rho_{min};\rho_{max}$	$\theta_{min};\theta_{max}$	$\rho0;sat$	$\alpha_1;\alpha_2;ks;\beta$	$\rho0;sat$	$\alpha_1;\alpha_2;ks;\beta$	$\rho0;sat$	$\alpha_1;\alpha_2;ks;\beta$
100;210	10;35	100;250	0.5;1;30;1.5	130;265	1.52;2.50;55.87;1.67	150;265	2.10;1.08;51.24;1.93
120;210	12;36	150;250	1;2;30;5	120;225	4.89;4.89;43.05;2.36	150;235	2.62;5.22;25.55;3.65

Source: Developed by the author

Table 25 - Identification results for individual H4.

Session	TT	Corr	MSE
1st	25(s)	0.815	0.0010
2nd	77(s)	0.476	0.0285

Source: Developed by the author

Table 26 - Metrics on experimental results for individual H4.

	Sine				Step			
	Empiric		IGA		Empiric		IGA	
Session	RMSE	TEC	RMSE	TEC	RMSE	TEC	RMSE	TEC
1st	NC	60(s)	10.1286°	60(s)	12.7898°	60(s)	6.5787°	60(s)
2nd	9.1052°	60(s)	6.5532°	60(s)	7.5069°	60(s)	4.0402°	60(s)

Source: Developed by the author

As clearly seen in Figure 30, the lower limb did not track the sine reference in any of the sessions by using the empirical tuning approach. Similarly, for the step wave, there was a delay (20 seconds) in session one to achieve the operation point angle, where it maintained less than 10 seconds and dropped 10° as a stationary error, and in session two, there were stationary errors above and under the operation point.

Alternatively, by using the proposed methodology one can see in Table 26 that the RMSE error was much lower by comparing with the empirical tuning, wherein session one, the sine

wave was tracked with a lag, but still it is a good result, and for the step wave the lower limb oscillated around the operation point, both with 60 seconds of stimulation. Further, in session two, results to both trajectories were very good during 60 seconds of stimulation, where the first two cycles of the sine wave did not present too much error and the step wave presented smooth behavior around the operation point. Supporting the hypothesis of this research, results to empiric gains present poor tracking performances, while with the proposed methodology, results can be improved by using a model continuously updated with data and an intelligent tuning via IGA.

Figure 30 - Experimental results for subject H4 on sessions one and two respectively.
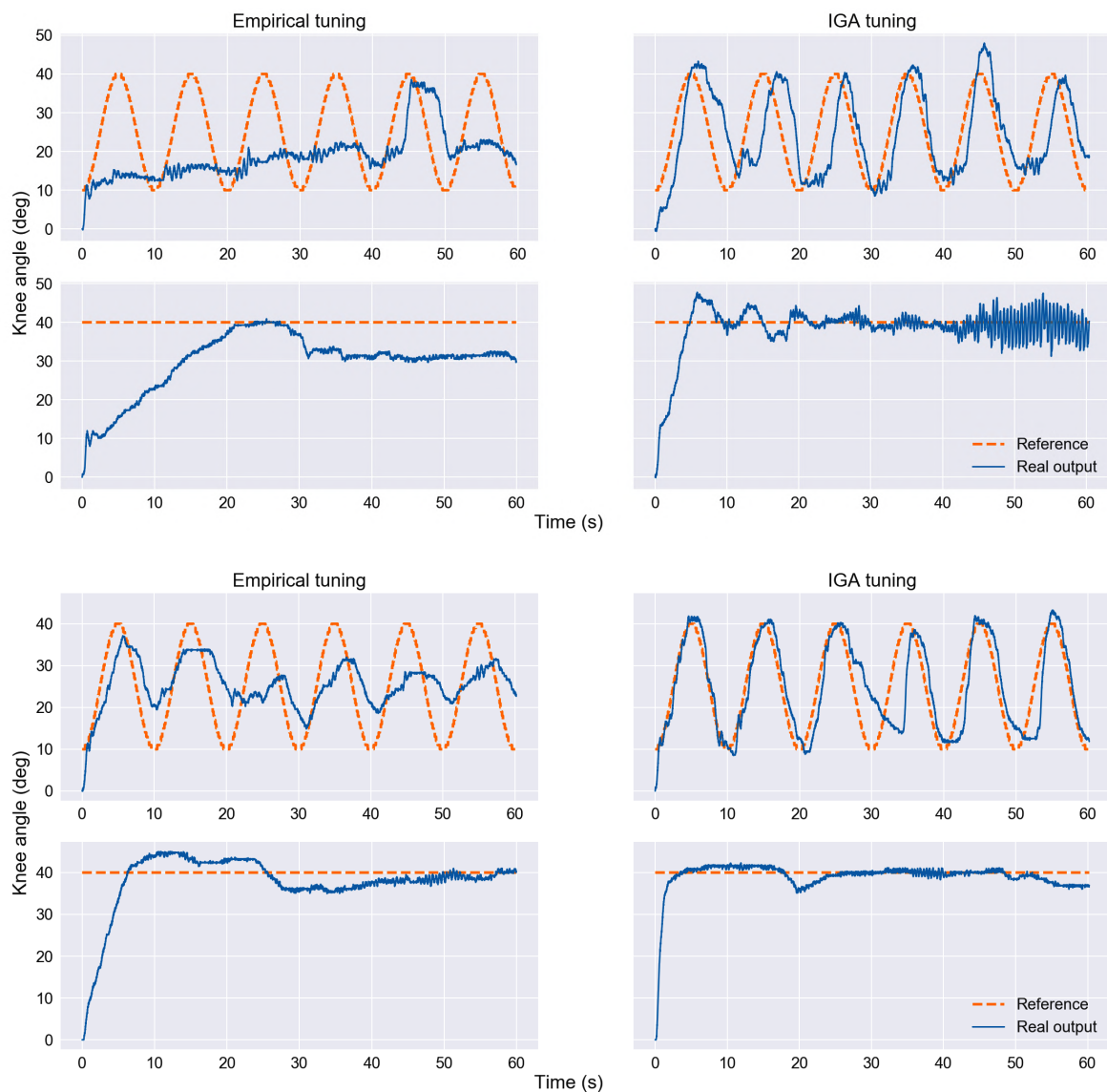
Source: Developed by the author

Moreover, one can observe in Table 25 the correlation between input and output data dropping to half in the second session, where its MSE increased considerably. Therefore, Figures 31

compares the simulation and real experiment in both sessions. As estimated models, in session one was expected fine tracking responses, while in the real experiment, due to several factors aforementioned (e.g., fear or voluntary movement) different behaviors were achieved with tremors and lag. The second model, with less correlation between data, the model predicted a strange behavior at the beginning of the step wave and high tremors for the sine wave, while in the real experiment smoother responses were accomplished.

Figure 31 - IGA comparison of simulation and real experiment for individual H4.
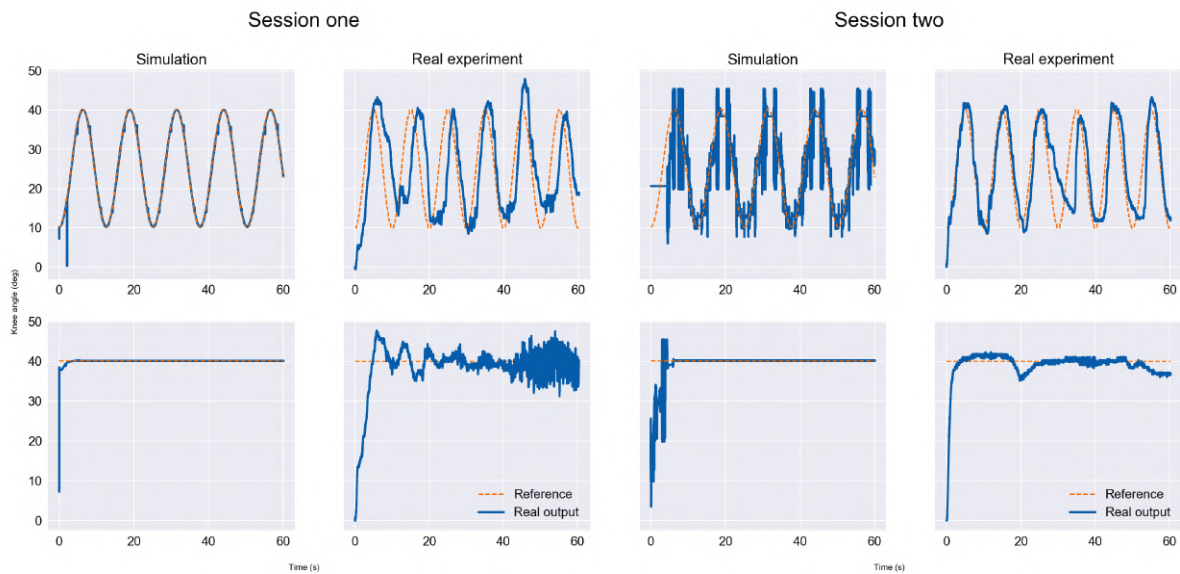
Source: Developed by the author

4.4.7   Individual H5

The individual H5 participated at three sessions, and, as well as for the other participants of five sessions, the set-up protocol was the same as the three initial sessions (for more details, one can refer to Section 4.3 and Subsection 4.4.3). In session one, after identifying the individual, empiric gains were used for the controlling procedure, and then those founds by the IGA. Differently, in sessions two and three, the IGA gains were applied first and then empiric ones.

Therefore, Table 27 describes additional technical information about both sessions, being each line of the table a session day for individual H5; Table 28 presents information for the identified models; Table 29 presents control metrics results on experimental results; and Figure 32 shows control results for subject H5 in both stimulation sessions.

As one can notice in Table 29 and in Figure 32, tracking results for individual H5 using an empirical tuning were very poor in sessions one and three, while in session two, the control-

Table 27 - Technical information on experiments for individual H5.

Identification		Empiric		Sine IGA		Step IGA	
$\rho_{min};\rho_{max}$	$\theta_{min};\theta_{max}$	$\rho0;sat$	$\alpha_1;\alpha_2;ks;\beta$	$\rho0;sat$	$\alpha_1;\alpha_2;ks;\beta$	$\rho0;sat$	$\alpha_1;\alpha_2;ks;\beta$
120;210	10;40	130;220	0.5;1;30;1.5	170;250	3.36;4.09;53.19;3.30	170;275	3.65;1.56;76.66;2.69
120;200	10;40	150;260	1;2;30;5	120;210	2.68;6.85;24.64;3.13	140;230	2.84;1.51;40.93;2.54
90;190	12;38	140;260	0.8;1.2;20.5;2.5	90;210	3.21;2.43;51.30;3.42	120;230	1.16;2.98;45.15;1.20

Source: Developed by the author

Table 28 - Identification results for individual H5.

Session	TT	Corr	MSE
1st	28(s)	0.881	0.0014
2nd	42(s)	0.682	0.0309
3rd	167(s)	0.599	0.0352

Source: Developed by the author

Table 29 - Metrics on experimental results for individual H5.

	Sine				Step			
	Empiric		IGA		Empiric		IGA	
Session	RMSE	TEC	RMSE	TEC	RMSE	TEC	RMSE	TEC
1st	NC	60(s)	6.0060°	20(s)	NC	45(s)	5.7196°	60(s)
2nd	8.0706°	50(s)	3.0171°	21(s)	8.0762°	52(s)	5.4818°	50(s)
3rd	NC	60(s)	3.8723°	52(s)	13.0323°	45(s)	6.3512°	50(s)

Source: Developed by the author

stimulated lower limb tried to track the sine wave with a delay time, but still a good result, and for the step-signal trajectory, a good regulation around the reference angle was acquired.

Notwithstanding, when using the proposed methodology for finding gains constant of the RISE controller, the lower limb presented very good tracking results for both trajectories, in which the RMSE dropped to half comparing the sine wave for the two final sessions with the first one. In sessions one and two, the time of effective control was very low (around 20 seconds only) for the sine wave, i.e., the lower limb tracked two sine cycles before the controller saturate. However, for the step wave, the time of stimulation was bigger than 50 seconds in all three sessions with good tracking results, where the worst regulation was at the first session. In the last session, using IGA fine-tuned gains, both trajectories were tracked during 50 seconds with low RMSE.

In Table 28 one can notice that the correlation between input and output data did not drop as much as for the other individuals, but still, the MSE increased from session one to the others.

Figure 32 - Experimental results for subject H5 on sessions one and two respectively.
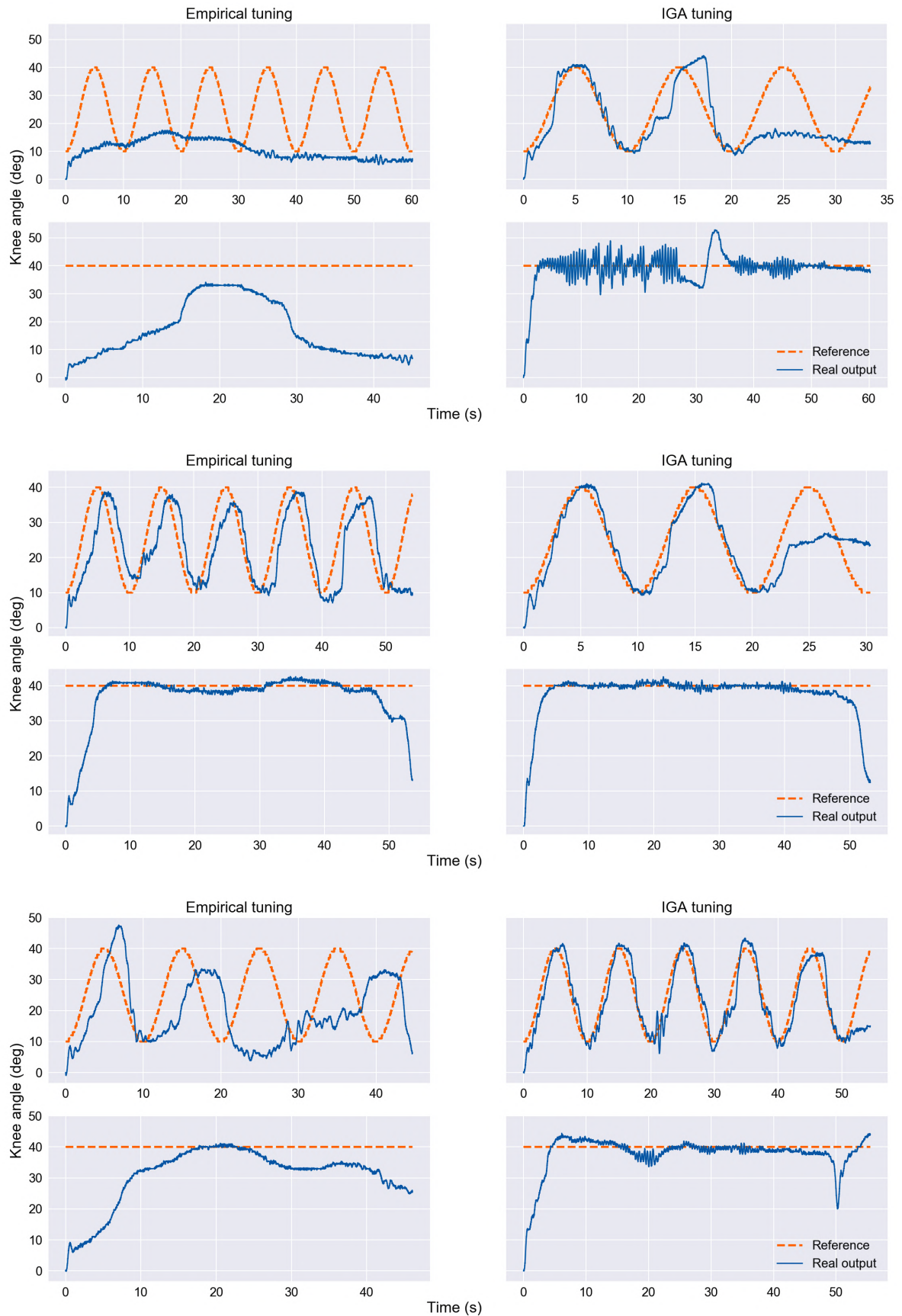
Source: Developed by the author

In this context, Figure 33 exhibits the comparison of simulation and real experiments for sessions one and two. As data were well correlated for both sessions, both models predicted quite well what would happen in the real experiment where the first modeled a difficulty at the beginning of the sine wave, and a small overshoot with no stationary error for the step wave. Similarly, the second model identified some small tremors during the sine trajectory and a fast response with no overshoot or stationary error for the step wave. However, as approximate models, neither of them could predict the fatigue factor in session one and two for the sine wave.

Figure 33 - IGA comparison of simulation and real experiment for individual H5.
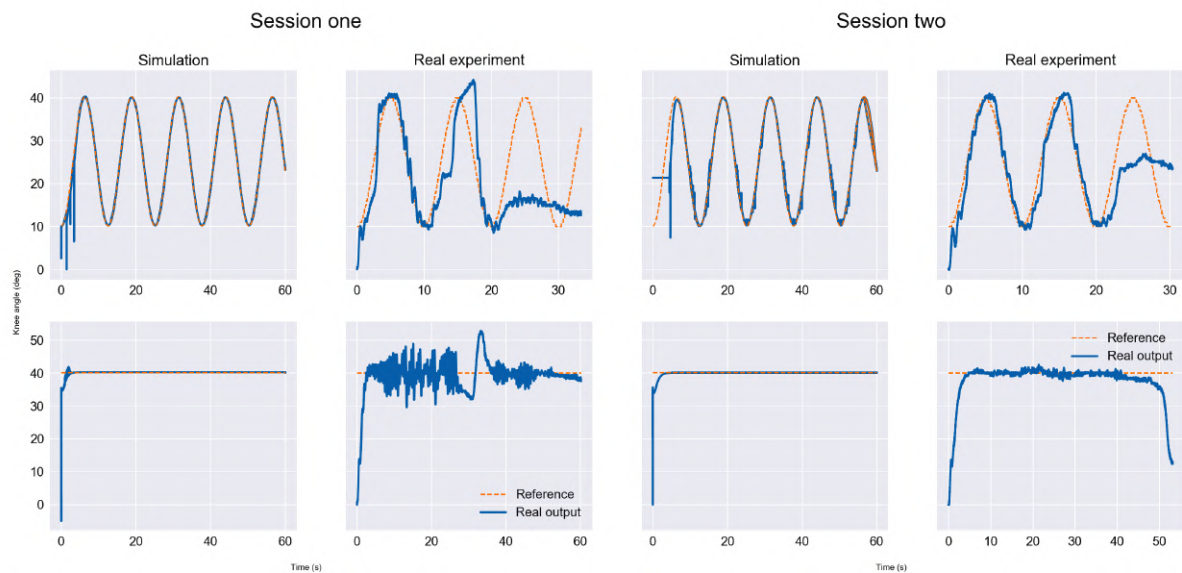
Source: Developed by the author

4.4.8 Individual H6

In the same way as individuals H1, H2, and H3, the individual H6 did also participated in five sessions, where the set-up protocol for control-stimulation was similarly as for those individuals (for more details, refers to Subsection 4.4.3 or Section 4.3). Therefore, Table 30 describes additional technical information about each session, being each line of the table a session day for individual H6; Table 31 presents information for the identified models; Table 32 presents control metrics results on experimental results; and Figures 34 and 35 display control results for subject H6 in all stimulation sessions.

Similar to other individuals, one can see in Figures 34 and 35 and in Table 32 that the proposed methodology is better than an empiric tuning approach for controlling the lower limb via NMES/FES. Using the empiric approach, in both sessions one and two, the control-stimulated

Table 30 - Technical information on experiments for individual H6.

Identification		Empiric		Sine IGA		Step IGA	
$\rho_{min};\rho_{max}$	$\theta_{min};\theta_{max}$	$\rho0;sat$	$\alpha_1;\alpha_2;ks;\beta$	$\rho0;sat$	$\alpha_1;\alpha_2;ks;\beta$	$\rho0;sat$	$\alpha_1;\alpha_2;ks;\beta$
100;150	20;44	100;190	0.5;1;30;1.5	100;205	1.92;2.41;69.71;1.69	100;210	1.92;2.41;69.71;1.69
100;160	10;46	110;200	1;2;30;5	100;165	1.92;4.14;44.26;1.50	200;260	1.92;2.41;55.83;1.69
110;130	12;48	100;180	0.8;1.2;20.5;2.5	100;140	3.85;4.00;21.51;2.85	100;160	1.22;1.64;30.44;3.50
120;140	22;50	110;160	5;2;15;3	120;190	1.63;4.26;23.74;1.70	120;210	1.03;6.16;66.38;1.14
100;150	18;42	110;185	4;7;25;8	100;140	2.24;2.22;28.37;2.06	100;160	2.12;2.35;46.93;1.67

Source: Developed by the author

Table 31 - Identification results for individual H6.

Session	TT	Corr	MSE
1st	48(s)	0.974	0.0006
2nd	229(s)	0.377	0.0593
3rd	371(s)	0.323	0.0543
4th	203(s)	0.294	0.0522
5th	241(s)	0.281	0.0495

Source: Developed by the author

Table 32 - Metrics on experimental results for individual H6.

	Sine				Step			
	Empiric		IGA		Empiric		IGA	
Session	RMSE	TEC	RMSE	TEC	RMSE	TEC	RMSE	TEC
1st	NC	45(s)	9.3820°	60(s)	13.9144°	60(s)	5.9438°	60(s)
2nd	12.7944°	60(s)	4.8235°	60(s)	8.3549°	60(s)	4.6948°	60(s)
3rd	8.2469°	60(s)	4.6400°	30(s)	8.8306°	60(s)	7.2866°	60(s)
4th	3.5344°	31(s)	4.5616°	60(s)	4.5510°	60(s)	6.7779°	60(s)
5th	16.4833°	60(s)	3.7170°	42(s)	7.8716°	60(s)	4.8954°	60(s)

Source: Developed by the author

lower limb barely tracked the reference angle.

Additionally, by comparing empiric responses from H6 with H1-H3, similar behaviors are detected for sessions four, which provided very good tracking for both sine and step waves, and for session five a very poor tracking for both trajectories with big oscillation (as discussed in Chapter 3 and seen in Figure 10).

On the other side, using the proposed methodology, the RMSE of the sine wave dropped to half comparing the first two sessions and continued decreasing until session five. With four exceptions of ten stimulations, the individual H6 presented results for 60 seconds, almost as well as it was for individual H1 in comparison with the literature that presents results in the range of 8 to 45 seconds of stimulation. The best result for the sine wave was achieved in session five, with very low RMSE of 3.717° and in for the step wave in session two also with very low RMSE of 4.6948°.

Figure 34 - Experimental results for subject H6 on sessions one, two and three respectively.
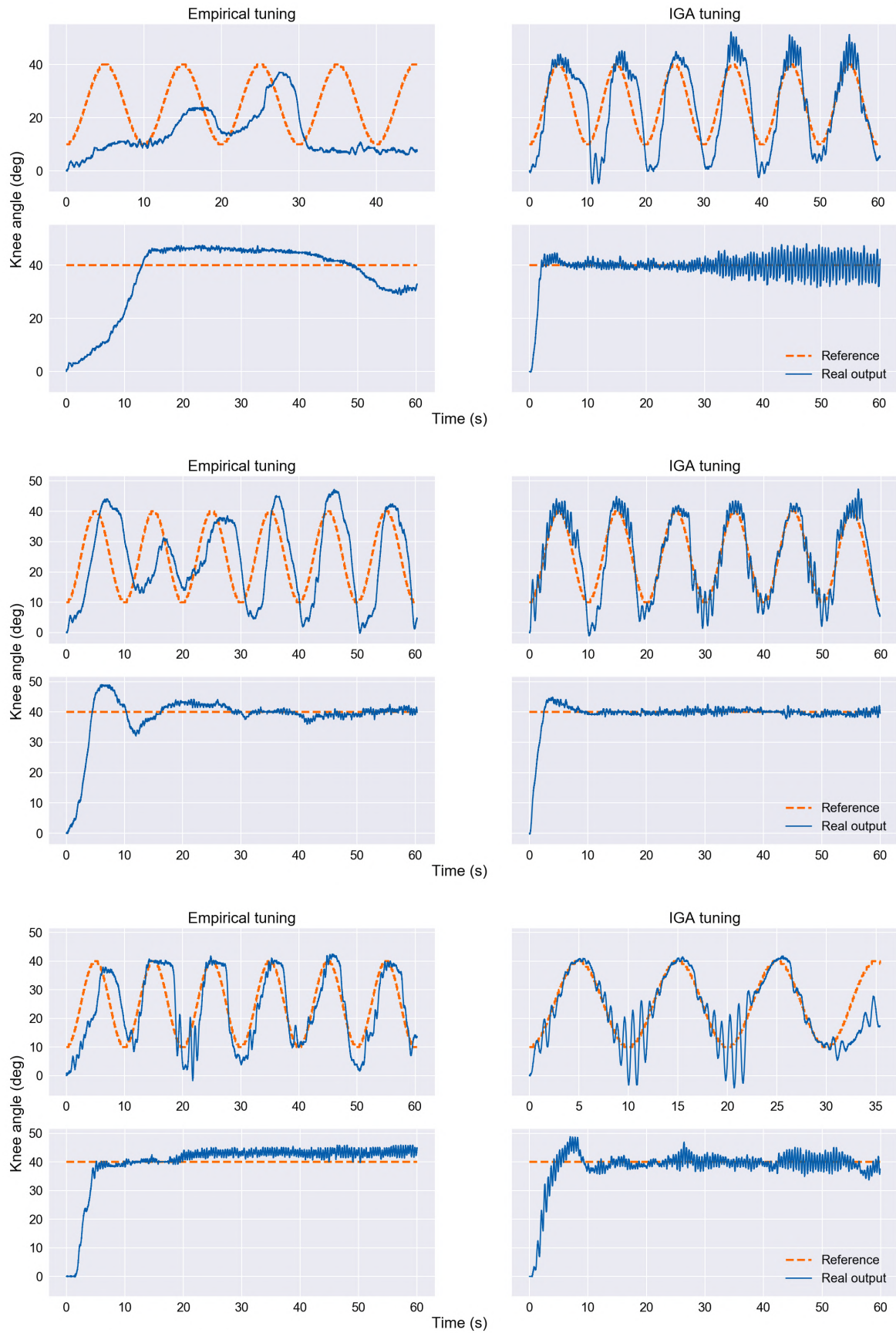
Source: Developed by the author

Figure 35 - Experimental results for subject H6 on sessions four and five respectively.
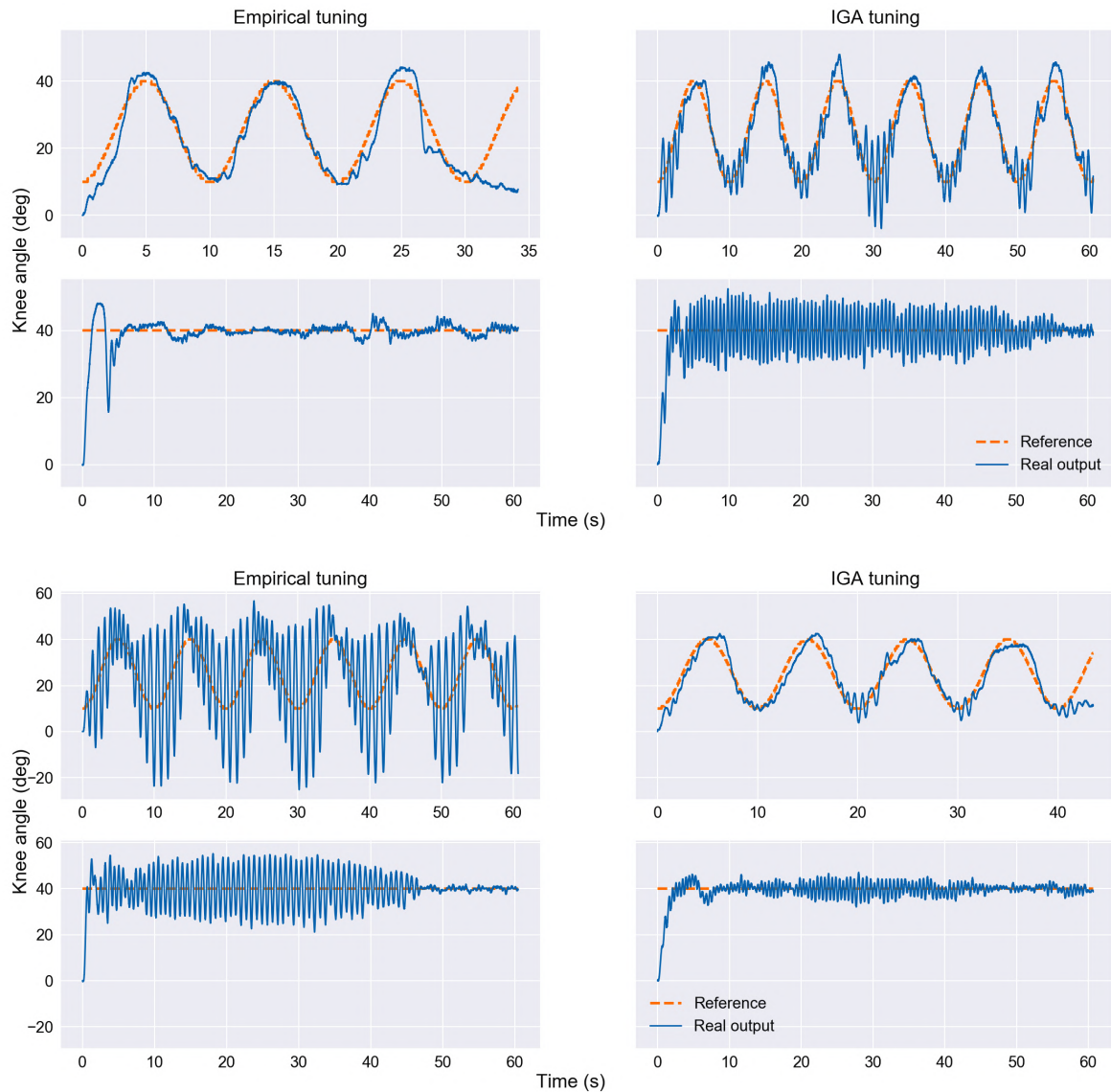
Source: Developed by the author

From Table 31 one can notice a fast decreasing on the correlation between input and output data, where the MSE increased quite much comparing with session one. Therefore, Figures 36 illustrates the comparison of simulation and real experimental results for sessions one and five. As approximate models, the modeling for session one predicted some tremors in some part of the sine wave and fast response with no overshoot or stationary error for the step wave, which would happen in ideal conditions, however, the model did not take into account tremors occasioned by fatigue or even voluntary movements that may be occurred in session one as it was the first time with electrical stimulation. The second model, for session five, predicted pretty well tremors for the sine wave and an oscillatory permanent for the step wave, where as one can see, even that the correlation between data is not high, the model approximates to

real-world experiments with fatigue and tremors implicit on previous data.

Figure 36 - IGA comparison of simulation and real experiment for individual H6.
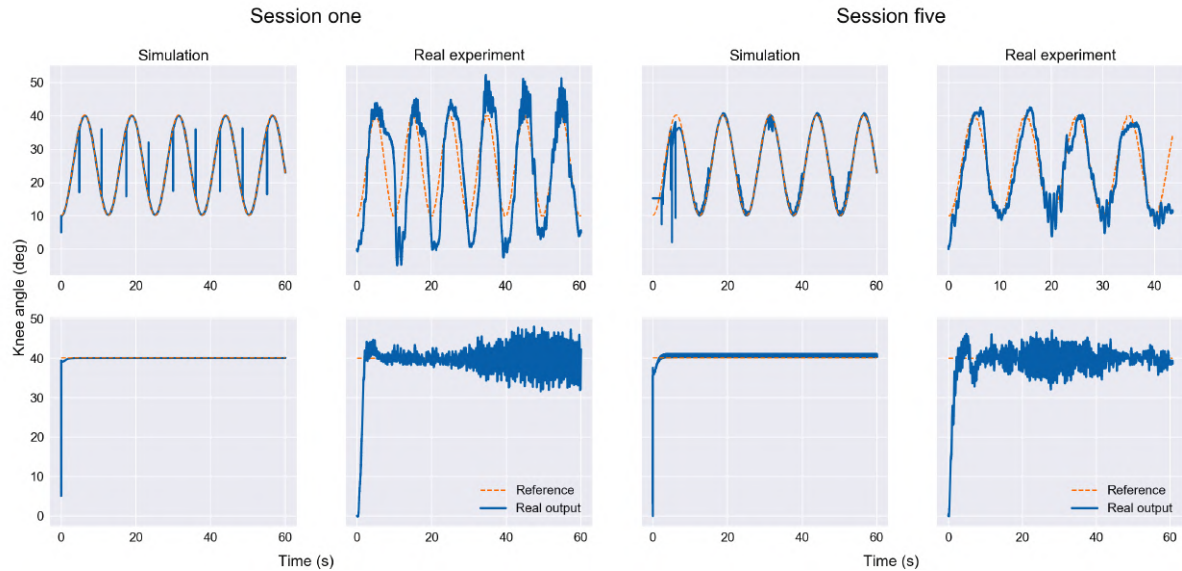
Source: Developed by the author

4.4.9 Individual H7

As well as individual H4, individual H7 participated only in two sessions, wherein both sessions, the set-up procedure was carried out similar to the other individuals (for more details, one can refer to Section 4.3 and Subsection 4.4.3). Thus, in session one, after the identification step, the controlling procedure was applied at first, with empiric gains and then with fine-tuned ones found by the IGA. Inversely, in session two, IGA fine-tuned gains were used at first, and then empiric ones.

Therefore, Table 33 describes additional technical information about both sessions, being each line of the table a session day for individual H7; Table 34 presents information for the identified models; Table 35 presents control metrics results on experimental results; and Figure 37 shows control results for subject H7 in both stimulation sessions.

As one can notice in Figure 37 and Table 35, results using an empiric approach to tune the RISE controller did not present good results at all, where the lower limb did not track either the sine or the step trajectories. Notwithstanding, using the proposed methodology, the first session presented a poor, but still acceptable tracking result, and session two a better result for both trajectories. It is noticed that when the lower limb was higher than the desired angle, the control law dropped the pulse width, where the lower limb presented some dropping behavior

in session two. When comparing both tuning procedures, the proposed one based on an IGA outstands the empirical by far, substantiating the hypothesis made in this research.

Figure 37 - Experimental results for subject H7 on sessions one and two respectively.

Source: Developed by the author

Additionally, one can notice in Table 34 that the correlation between input and output data was kept higher than 0.5 for both sessions, and the MSE increased from session one for two. Nevertheless, Figures 38 illustrates the comparison between simulation and real experiments for both sessions using the IGA tuning approach. Due to high correlation between data, both models could identify quite well what would happen in the real experiment. In session one, the simulation model presented tremors for the sine wave during the whole period and a very similar behavior for the step response. Similarly, for the second sessions, the step responses are very similar in simulation and real experiment while the sine wave presented tremors and an

error every peak value of the trajectory.

Table 33 - Technical information on experiments for individual H7.

Identification		Empiric		Sine IGA		Step IGA	
$\rho_{min};\rho_{max}$	$\theta_{min};\theta_{max}$	$\rho0;sat$	$\alpha_1;\alpha_2;ks;\beta$	$\rho0;sat$	$\alpha_1;\alpha_2;ks;\beta$	$\rho0;sat$	$\alpha_1;\alpha_2;ks;\beta$
80;150	8;40	80;170	1;2;30;5	110;200	3.72;3.85;45.16;1.59	110;220	2.75;3.85;68.51;1.96
100;150	14;36	80;195	0.5;1;30;1.5	80;160	1.15;5.96;44.29;1.20	75;175	2.73;5.79;37.57;2.44

Source: Developed by the author

Table 34 - Identification results for individual H7.

Session	TT	Corr	MSE
1st	33(s)	0.767	0.0038
2nd	73(s)	0.552	0.0173

Source: Developed by the author

Table 35 - Metrics on experimental results for individual H7.

	Sine				Step			
	Empiric		IGA		Empiric		IGA	
Session	RMSE	TEC	RMSE	TEC	RMSE	TEC	RMSE	TEC
1st	NC	60(s)	8.5001°	60(s)	9.5541°	40(s)	7.0442°	21(s)
2nd	NC	60(s)	6.6301°	50(s)	13.1355°	60(s)	5.2125°	60(s)

Source: Developed by the author

Figure 38 - IGA comparison of simulation and real experiment for individual H7.
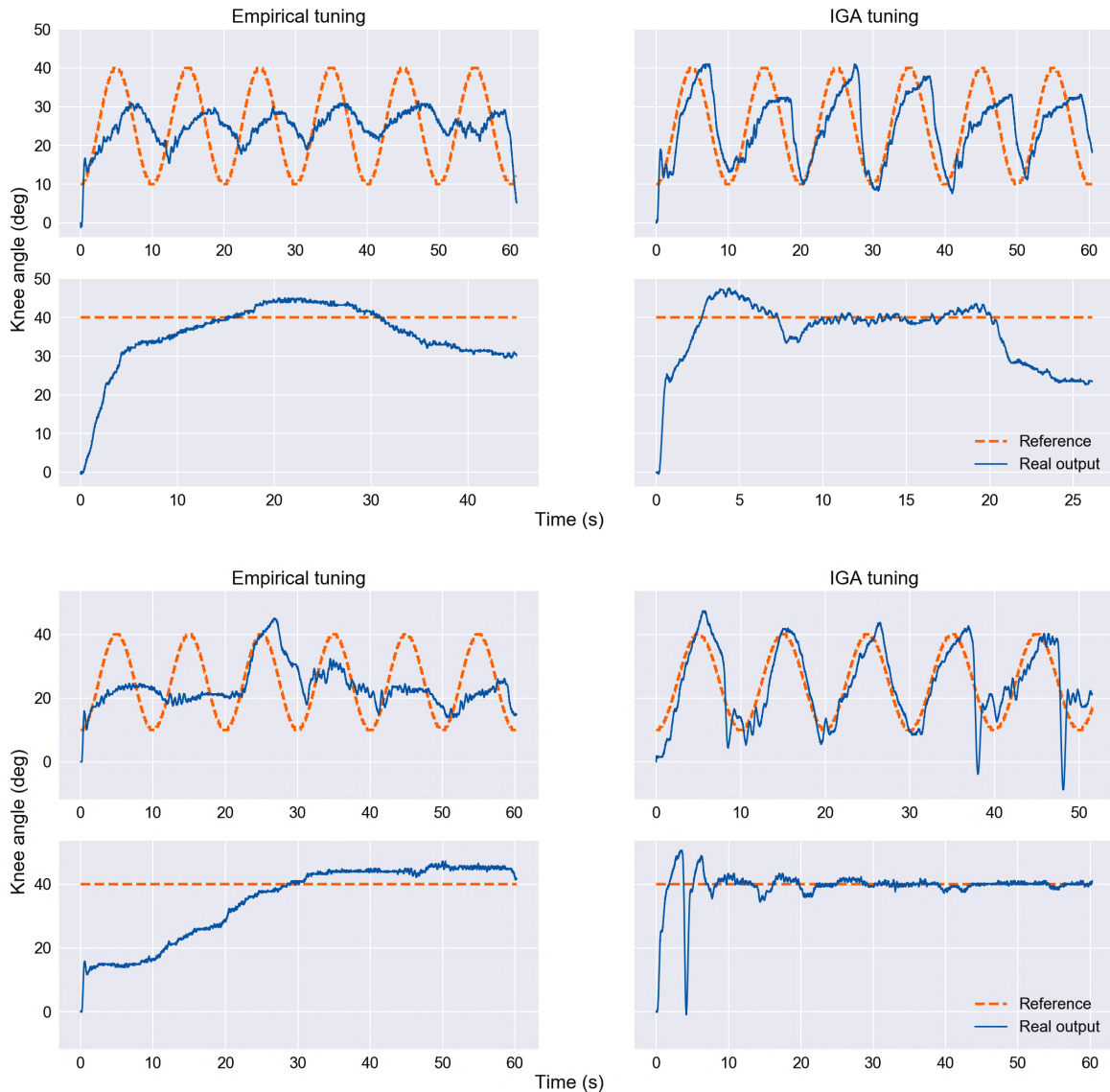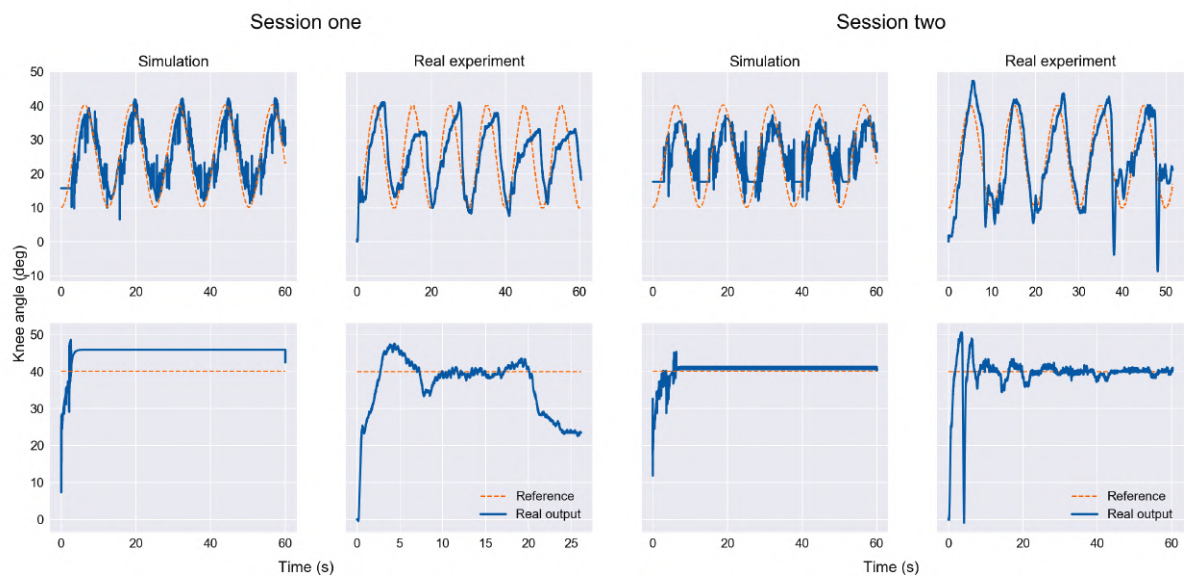

Source: Developed by the author

4.5 CONCLUSION

Aiming to propose improvements to human lower limb tracking control of SCI patients via NMES/FES, this research introduced a novel methodology. In this chapter, the proposed methodology was experimentally implemented with seven healthy individuals and two paraplegic subjects. For the first time, real experiments are made with SCI subjects using the RISE controller, i.e., the literature provides validation just with healthy subjects or via simulations as one can see in Table 1. Moreover, in the experiments made in this research, results are presented for all period of control-stimulation, i.e., when the controller stabilized at the saturation value as an open-loop design, the stimulation was cessed (the TEC metric). Further, for many healthy individuals, the control-stimulated lower limb tried robustly to track the reference angle during more than 45 seconds that is the maximum time presented in the literature for the RISE controller, getting to 60 seconds in many stimulation sessions.

As hypothesized in Section 1.3 and proven in results, the use of an empirical approach on clinical procedures presents several poor performances, wherein most of the tests, the control-stimulated lower limb did not track the reference angle. Alternatively, by using the proposed methodology, for all subjects, satisfactory and suitable tracking results were acquired for both situations, tracking a sine wave via an isotonic contraction and by regulating around an operation point (step wave) as an isometric contraction. Additionally, as sessions passed by (for healthy individuals), it was noticed an improvement of tracking results for some individuals, which between many factors, one could be by the use of past rehabilitation data for identifying the model in an offline scheme before the next session.

As presented in results from Section 4.4, saving real databases of each subject containing detailed information from every rehabilitation session, and by using a single hidden layer on a neural network model, the mapping over the delivered electric stimulus and achieved angular position approximates of real-world models with nonideal conditions (fatigue, tremors, and spasms). Additionally, the simulation system allows liberty of studying the system's response, with the acquired data, before actually going on the real experiment.

Figures 39 and 40 illustrate results from the developed virtual instrument in LabVIEW® for individuals H1 (sine wave) and H6 (step wave) during session five, which presented high oscillatory behavior when empirically tuned and smooth one when appropriately tuned. Focusing on the comparison of the pulse width in both empiric and IGA tuning, as one can notice in these figures, the lower limb responded to the delivered pulse width (i.e., not voluntarily). Using empiric gains, the control signal switches values by going up and down from maximum to minimum values allowed (for H1) maintaining some constant values in a small period, which generated high oscillations, while with IGA gains, this switching was higher but in a small range of pulse width, producing superior control results.

To conclude, Figure 41 summarizes results by illustrating in a bar plot the RMSE metric for both tuning procedures, empiric and IGA, and each trajectory in all sessions and to all individuals. Omitted bars are due to "NC" case where the lower limb did not track the reference angle, or because the individual not participating in the session. It is very noticing the outstanding results using the proposed methodology comparing it with the empirical tuning. Additionally, one can notice that using fine-tuned gains for healthy individuals, in the first sessions results normally presented higher RMSE decreasing its value on the following sessions, which could be due to fear or discomfort to the electrical stimulus or voluntary movements.

Figure 39 - Comparison of pulse width in both empirical and IGA tuning approaches for H1.
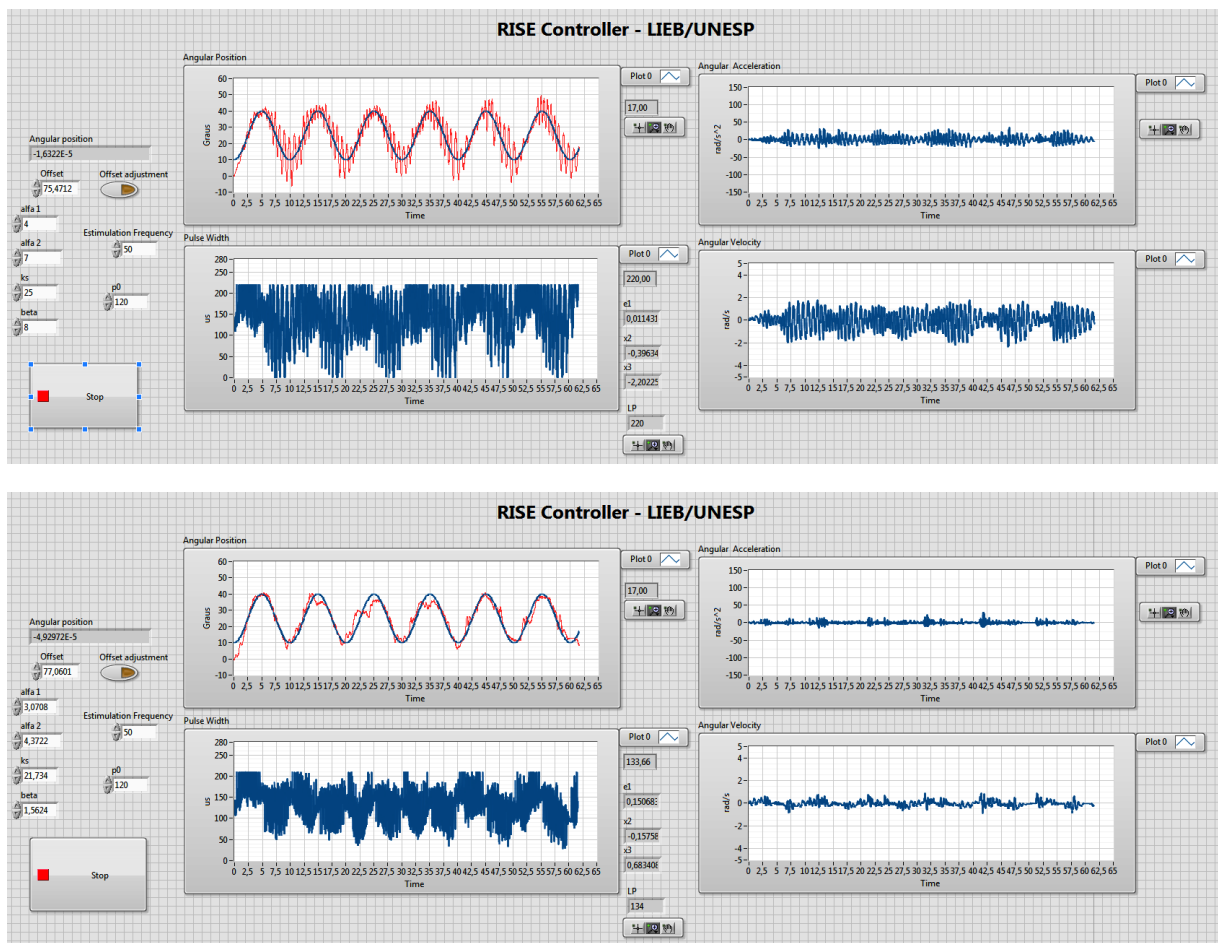
Source: Developed by the author

Figure 40 - Comparison of pulse width in both empirical and IGA tuning approaches for H6.
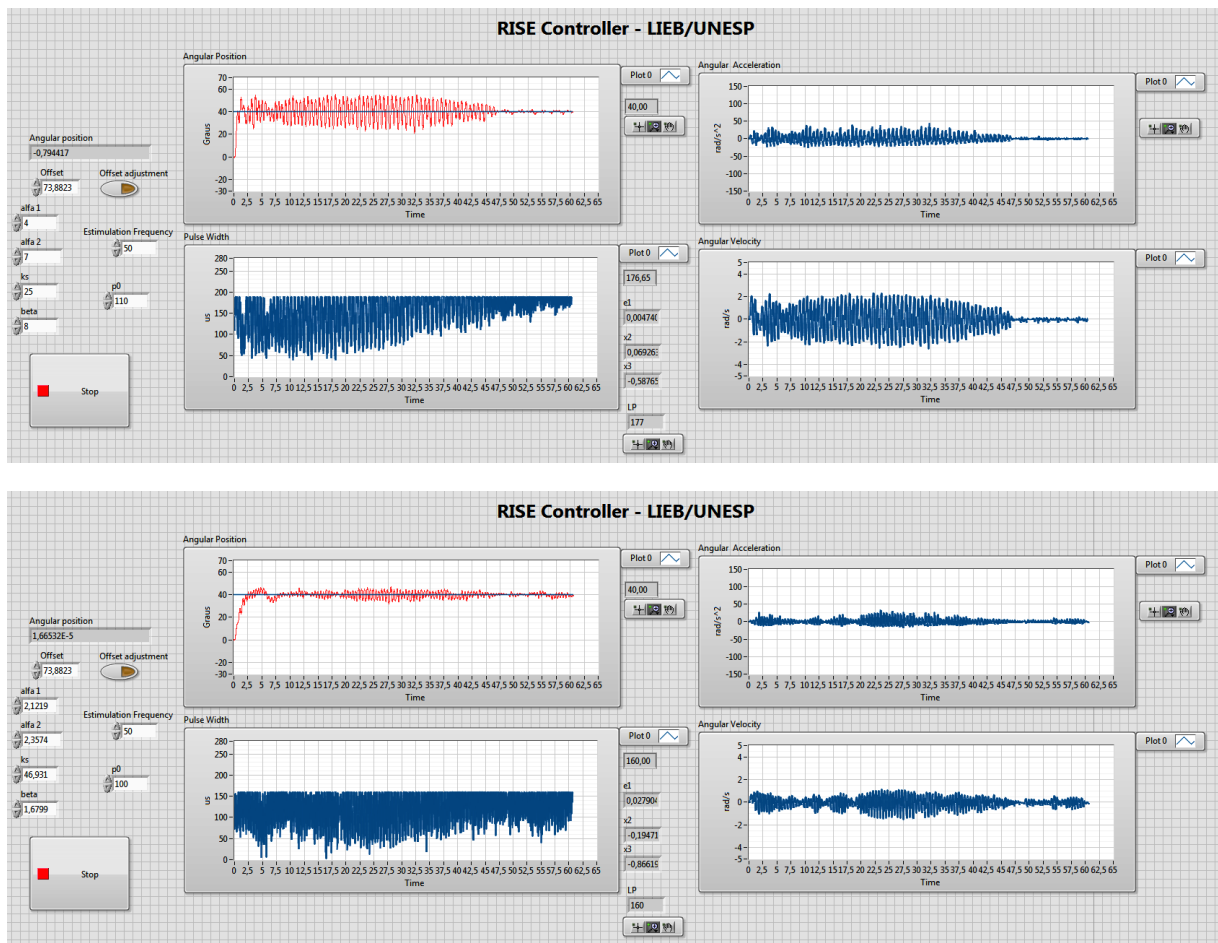
Source: Developed by the author

Figure 41 - RMSE analysis for both empiric and IGA tuning approaches.
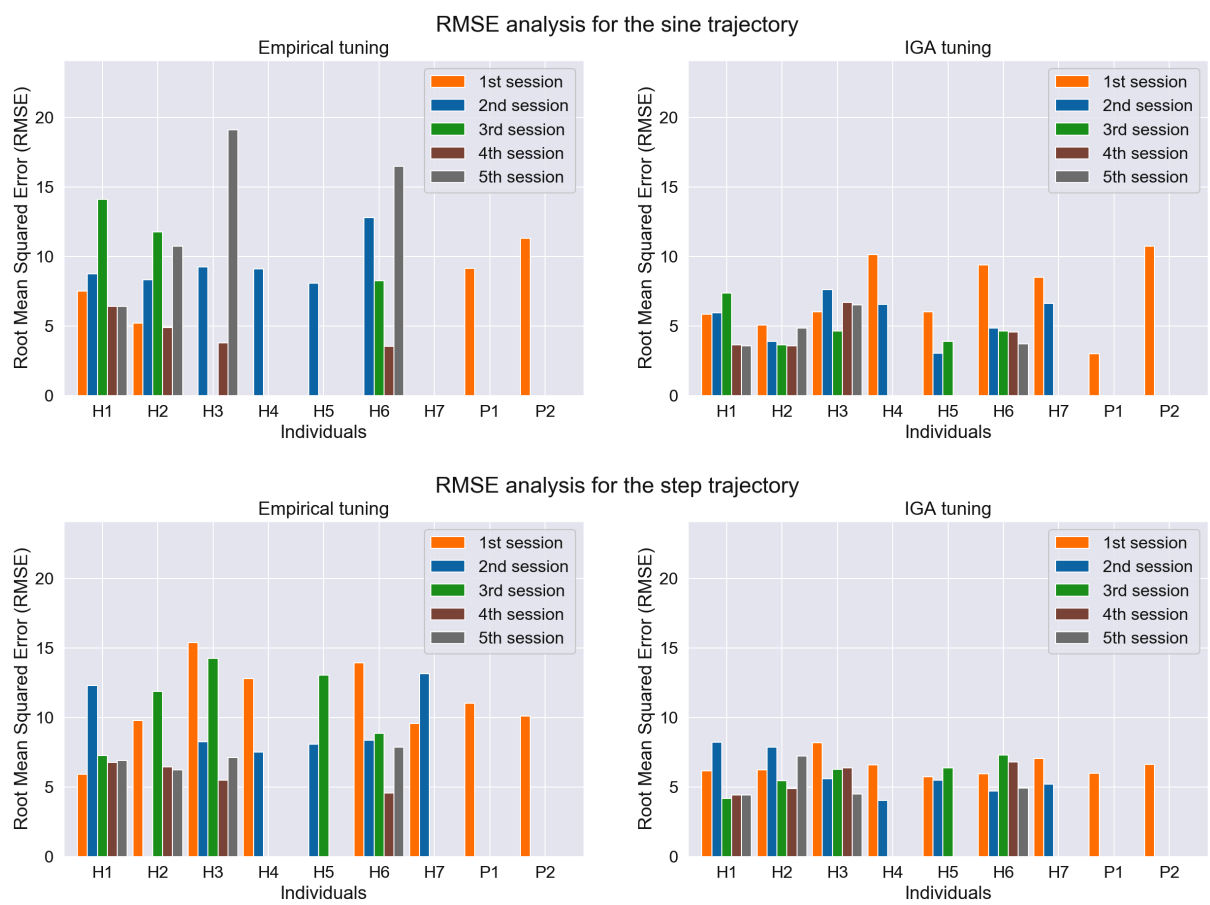
Source: Developed by the author

5 NONLINEAR IDENTIFICATION OF THE KNEE JOINT ANGULAR POSITION UNDER NMES/FES APPLICATION VIA DEEP AND DYNAMIC NEURAL NETWORKS

Several previous investigations for NMES and FES applications to knee joint control in SCI patients have been reported in the literature consisting of two main lines, controlling and modeling. However, an efficient mapping describing the relationship between the muscular model and stimulation parameters is a very strict requirement for developing powerful feedback control techniques, motivating the main focus of this chapter.

In the literature one can find different models of electrically stimulated knee joint mainly divided into two approaches, mathematical models (RIENER; QUINTERN; SCHMIDT, 1996; FERRARIN; PEDOTTI, 2000; LAW; SHIELDS, 2007; LYNCH; GRAHAM; POPOVIC, 2011; BENOUSSAAD et al., 2009), which have a large number of parameters dependent on the physiology of each individual, and black-box models (PREVIDI, 2002; KAMARUDDIN et al., 2016; GHANI et al., 2016), which use no physical insight about the system and will be the approach of this research via deep and dynamic neural networks.

Generally, black-box models are simpler than physical modeling and more appropriate where there is a lack of knowledge of the underlying physiology, or in the case when the physical knowledge is too complex, as it is in this case, where muscular behavior presents time-varying and high nonlinearities properties. Moreover, there is high power for computation and powerful tools to deal with big data nowadays, so, rather than using mathematical models, the use of NNs is driven by these advantages and the ones from the methods itself. Deep neural networks have proven to be very effective tools for solving complex tasks, whereby "deep", it means the stacking of multiple hidden layers for a better abstraction of the problem. The most simple architecture in deep learning applications is the multilayer perceptron (MLP) from the feedforward class referred to as universal function approximators.

On the other hand, Recurrent neural networks (RNNs) offer a promising opportunity for identifying and modeling dynamic nonlinear systems, and currently, it has attracted many interests in most area of sciences and industries by its high and effective power for solving complex tasks. Building black-box identification models for a dynamic system, where its output does not depend only on its current inputs, but on the previous behavior of the system, could be effectively done using dynamic NNs, such as RNNs. Even though RNNs are very compelling dynamic systems for complex tasks, there is the problem of vanishing and exploding gradient, due to the big computation of the gradient over so many time-steps. One of the most popular and applicable RNN is the Long Short-Term Memory (LSTM) architecture, due to its intrinsic

characteristics of maintaining long state memories avoiding the vanish and exploding gradient problem.

This chapter investigates the effectiveness of deep and dynamic neural networks in the specific task of identifying the knee joint angular position under neuromuscular electrical stimulation. Three specific architectures are investigated namely the MLP, a simple RNN, and the LSTM, in which the last one has been recently introduced for nonlinear system identification (WANG et al., 2018; OGUNMOLU et al., 2016; GONZALEZ; YU, 2018; WANG, 2017; HIROSE; TAJIMA, 2017) and has been applied successfully in many tasks in the literature. To the best of the authors' knowledge, the LSTM has never been implemented to this specific application. Hence, in this research, it will be compared the effectiveness of an MLP, a standard RNN, and the LSTM to identify the knee joint angular position under the NMES/FES application using identification and control data from the first session of individuals in Table 7.

In Chapter 4, the use of a single layer MLP provided acceptable models for each individual, however, we aim to study more sophisticated neural network architectures to propose better control-oriented models mapping electrical stimulus and angular position. Therefore, the main objective of investigating these specific neural networks is to propose better modeling for the relationship of delivered stimulus and achieved angular position, such that the developed offline platform using the proposed methodology could take advantage of an improved and more realistic model already in the first session of an SCI patient aiming to rehabilitate via NMES/FES. Assuming a good mapping for an individual using some of the proposed NNs, and taking advantage of all acquired data from previous rehabilitation, the simulation system could better tune the RISE controller and provide better control-stimulation session for an SCI patient.

The following sections of this chapter describe the MLP, RNN and the LSTM; model selection; feature extraction and data encoding; and finally, results and its analysis.

5.1 NEURAL NETWORK METHODS

A description of nonlinear system identification via NNs for dynamic systems is provided in Section 2.3, and in this section, each NN architecture, MLP, RNN, and LSTM, is described.

5.1.1 Multilayer Perceptron (MLP)

The multilayer perceptron is the simplest architecture for deep learning applications from the big class of feedforward NNs, characterized by unidirectional flow of computation. Fig. illustrates a MLP, where $\mathbb{U}$ is the input layer, $\mathbb{H}$ are hidden layers and $\mathbb{Y}$ the output layer, its flow of information is $\mathbb{U} \rightarrow \mathbb{H} \rightarrow \mathbb{Y}$. The training of the NN consists of adjusting each connexion between neurons from one layer to the other, which is composed of weights w_{ij} and biases b_i

values activated by nonlinear functions $f(.)$. During training, a loss function is used to measure the error between desired and actual value outputted from the NN, in which this error is back-propagated through the network in order to update the weights of each module and so 'learn'.

Figure 42 - Multilayer perceptron.
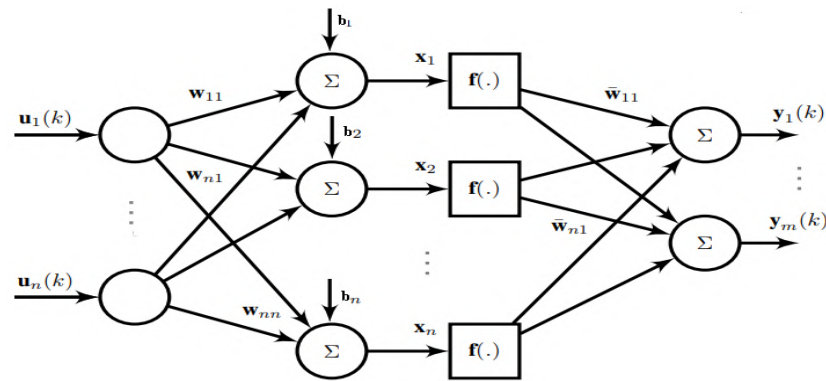
Source: Developed by the author

5.1.2 Recurrent neural network (RNN)

Recurrent neural network is the class of NNs that manipulate sequential data, it has at least one feedback connection that provides the ability to use contextual information when mapping between input and output sequences, i.e., in its topology, any neuron can be connected to any other, and even with itself. Fig 43 illustrates a RNN, where each neuron receives input x, produces an output y, and send it back to itself. At each time step t, a recurrent neuron receives the inputs and its own output from the previous time step (HAYKIN, 2009). Building black-box identification models for a dynamic system, where its output does not depend only on its current inputs, but on the previous behavior of the system, could be effectively done using dynamic NNs, such as RNNs. Even though RNNs are very compelling dynamic systems for complex tasks, there is the problem of vanishing and exploding gradient, due to the big computation of the gradient over so many time-steps. This problem is avoided by other variants of RNNs, e.g., the LSTM detailed in the next subsection.

5.1.3 Long Short-Term Memory (LSTM)

The LSTM NN is a variant of RNNs, which is capable of learning long term dependencies, and it overcame the problem of vanishing and exploding gradient that standard RNNs have. This particular problem make the gradient extremely unstable to deal if a NN runs for a long time, and the LSTM model introduced by (HOCHREITER; SCHMIDHUBER, 1997), can efficiently learn to maintain information over several time intervals without suffering of such problem.

Figure 43 - Recurrent neural network.
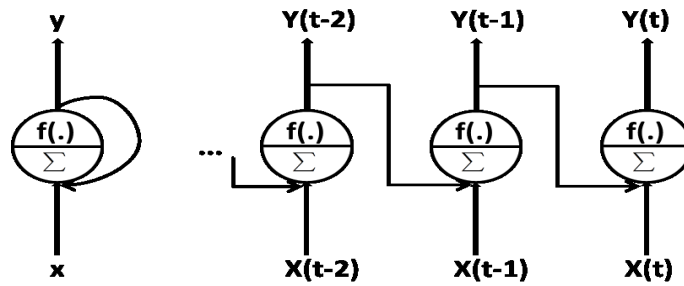
Source: Developed by the author

The essential key behind LSTM success is its memory cell, which divides its states in long-term state $c_{(k)}$ and short-term state $h_{(k)}$. The LSTM cell has three nonlinear gating units attached, the input $i_{(k)}$, forget $f_{(k)}$ and output $o_{(k)}$ gates, which allows to truncate gradients protecting and controlling the long-term state. In a nutshell, an LSTM NN is almost the same as a standard RNN, in which the summation units in the hidden layer(s) are replaced by memory blocks as in Figure 44 that illustrates the inside schematic architecture of LSTM.

Figure 44 - LSTM cell.
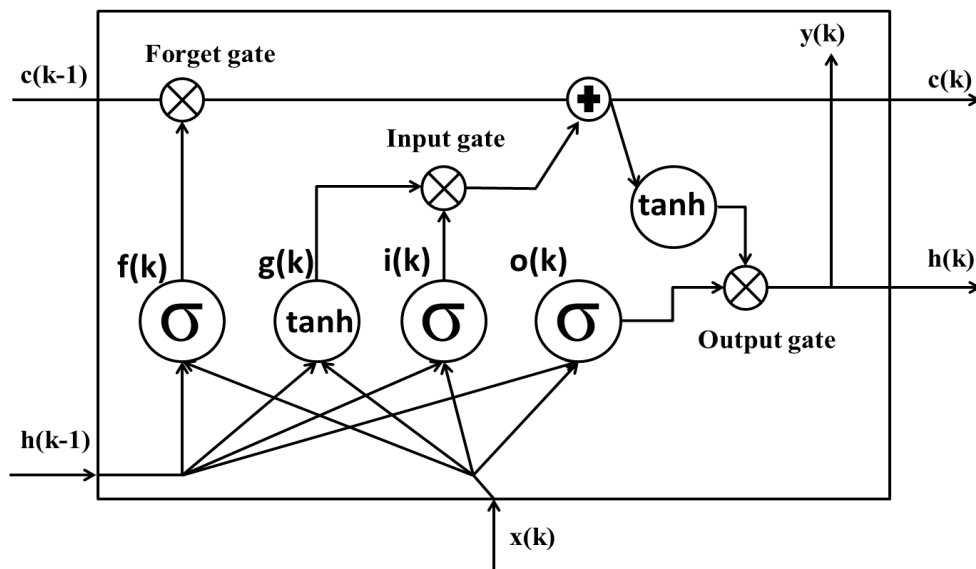
Source: Developed by the author

Initially, both input $x_{(k)}$ and the previous short-term state $h_{(k-1)}$ are fed to four different and fully connected layers. The first layer computes the internal hidden state $g_{(k)}$, using $x_{(k)}$ and $h_{(k-1)}$, and partially store $g_{(k)}$ in the long-term state. The other tree layers are the nonlinear gating units, which use the logistic activation function outputting a Boolean value between 0 for

"close the gate" and 1 for "open the gate". The first one named forget gate is able to preserve long-term states for as long as it is needed, i.e., it controls what to erase from the long-term state. The second one is the input gate, which regulates the flow of new values by recognizing important inputs, i.e., it controls which part of $g_{(k)}$ is able to be added to the long-term state. Lastly, the output gate defines how much of the long-term state should be read and output for both short-term state $h_{(k)}$ and output $y_{(k)}$. The mathematical formulation is as follows (GÉRON, 2017; CERNA et al., 2019; GONZALEZ; YU, 2018)

$$i_{(k)} = \sigma(W_{xi}^T \cdot x_{(k)} + W_{hi}^T \cdot h_{(k-1)} + b_i), \tag{16}$$

$$f_{(k)} = \sigma(W_{xf}^T \cdot x_{(k)} + W_{hf}^T \cdot h_{(k-1)} + b_f), \tag{17}$$

$$o_{(k)} = \sigma(W_{xo}^T \cdot x_{(k)} + W_{ho}^T \cdot h_{(k-1)} + b_o), \tag{18}$$

$$g_{(k)} = \tanh(W_{xg}^T \cdot x_{(k)} + W_{hg}^T \cdot h_{(k-1)} + b_g), \tag{19}$$

$$c_{(k)} = f_{(k)} \otimes c_{(k-1)} + i_{(k)} \otimes g_{(k)}, \tag{20}$$

$$y_{(k)} = h_{(k)} = o_{(k)} \otimes \tanh(c_{(k)}), \tag{21}$$

where $\otimes$ means an element-wise multiplication; W_{xi}, W_{xf}, W_{xo} and W_{xg} are the weight matrices of each four layers (input, forget, output and internal hidden state) for their connection to the input vector $x_{(k)}$; W_{hi}, W_{hf}, W_{ho} and W_{hg} are the weight matrices of the same four layers for their connection to the previous short-term state $h_{(k-1)}$; and b_f, b_g, b_i and b_o are the bias terms of each of the previous four layers. The main objective of nonlinear system modeling with LSTM NN is to update the weights between each layer with the input and the short-term state, such that the output $y_{(k)}$ converges to the system output $y(k)$ in Equation (9).

5.2   MODEL SELECTION

The programming language used in this research was Python and all neural network models were developed using the Keras library (CHOLLET et al., 2015). In the literature, the process of finding the best architecture and tuning its hyperparameters is known as model selection. The NNs architectures used in this research were tuned via a random search procedure, i.e., by randomly selecting the number of stacked layers (one on top of another with a fully connected layer outputting the predicted value) defining an architecture, and then tuning its hyperparameters, such as the number of neurons, batch size and learning rate. The best architectures found for the MLP, simple RNN and LSTM consist of five, one and one hidden layers, respectively.

All models were trained during at most 5000 epochs minimizing the mean squared error loss function via the adaptive moment estimation (Adam) optimizer. Furthermore, to avoid overfitting, two methods of regularization were used in this research, namely Dropout, where

some number of layer outputs are randomly ignored or "dropped out", and an "EarlyStopping" method configured with 15 epochs to monitor the validation loss function decrement recuperating the best weight encountered during training.

5.3 DATA ENCODING

Each acquired dataset during the identification and control operations, described in Section 4.3, contains information about delivered pulse width, angular position, velocity, and acceleration. However, just pulse width and angular position are considered in this study. These data were suitably treated to feed as input to the NNs. Angular position data recorded in radians were transformed into degrees, and due to different scales between pulse width and angular position, the "StandardScaler" method from the scikit-learn library (PEDREGOSA et al., 2011) was applied to re-scale the distribution of values to zero mean and unit variance. When the data is comprised of different scales, most machine learning techniques (as NNs) can benefit from rescaling the attributes to the same distribution.

As explained in Chapter 4, the time-step value m and the past-step value n were chosen as 1, where Table 8 illustrates an example on 10 samples of how the dataset is arranged. Moreover, models receive data in different shapes. The MLP requires a normal input arranged as $[samples, features]$, where the observations at previous timesteps are inputted as features to the model. Differently, both simple RNN and LSTM models require a three-dimensional input configured as $[samples, timesteps, features]$, where one sample is one sequence, a timestep is a point of observation in the sample, a feature is an observation at a timestep, and the sequence is fed in one time step at a time. RNNs can take arbitrary size sequences as the input, which makes them ideal to tackle large sequences of timesteps, for example, bigger m and n values in a nonlinear identification problem, while a feedforward NN, as the MLP, can only take a fixed-size input.

5.4 RESULTS AND DISCUSSION

For each individual in Table 7, identification results and its discussions comparing the effectiveness of deep and dynamic neural networks specifically the MLP, a simple RNN, and the LSTM architecture will be presented in this section. In this research, identifications will be made using the series-parallel structure, which is illustrated in Figure 7 and mathematically described in Equation (11).

Hence, for all individuals, after extracting and encoding the data from the first session (whereby session it means five stimulation tests, the initial identification and four from the controlling operation), data were trained and validated using only the identification data, supposing

the first session of a subject. The testing set was configured as the remaining four datasets acquired from the control operation for both sine and step trajectories using empiric and IGA-tuned gains, which is a more stringent test for evaluating the neural network. That is, as one can see in results from the previous chapter, during control applications there exist several problems such as fatigue, tremors, spasms, and voluntary movements, which will not be detected if a neural network is not properly trained for generalization.

Therefore, Table 36 presents identification results for each individual starting with P1-P2 ending with H1-H7. This table contains information for each NN (MLP, simple RNN, LSTM) about the best architecture found, where $drop(.)$ means a dropout layer, and the RMSE metric for each test set (sine empiric, sine IGA, step empiric, step IGA) and the Total. Moreover, Figures 45-47 illustrate results for the identified models for each individual, comparing the three architectures, separately during the whole period and combined with a zoom on 100 samples, in the specific case of sine IGA, which normally presented more tremors during stimulation tests.

Table 36 - Identification results for all individuals (P1-P2, H1-H7).

Individual	NN model	Architecture	RMSE				
			Sine empiric	Sine IGA	Step empiric	Step IGA	Total
	MLP	6→12→33→69→95	0.0172	0.0248	0.0456	0.0188	0.0290
P1	Simple RNN	97	0.0363	0.0685	0.0537	0.0423	0.0518
	LSTM	1000	0.1656	0.1932	0.1750	0.1610	0.1743
	MLP	8→16→32→66→35	0.0657	0.0616	0.0646	0.0605	0.0632
P2	Simple RNN	108	0.0799	0.0725	0.0717	0.0482	0.0700
	LSTM	262→ drop(0.1)	0.0521	0.0434	0.0561	0.0292	0.0469
	MLP	4→24→48→66→ 64	0.1207	0.1158	0.0624	0.0591	0.0942
H1	Simple RNN	1	0.0483	0.0538	0.0451	0.0400	0.0471
	LSTM	271→ drop(0.1)	0.0470	0.0284	0.0389	0.0202	0.0351
	MLP	6→12→37→57→ 83	0.0479	0.0669	0.03813	0.0387	0.0492
H2	Simple RNN	97	0.1404	0.1301	0.1304	0.1564	0.1398
	LSTM	469→ drop(0.1)	0.0463	0.0586	0.0328	0.0339	0.0443
	MLP	8→19→43→ 69→ 44	0.0247	0.0439	0.0281	0.0323	0.0331
H3	Simple RNN	109	0.0314	0.0816	0.0676	0.0905	0.0694
	LSTM	218→ drop(0.1)	0.0321	0.0729	0.0566	0.0830	0.0620
	MLP	7→29→36→69→59	0.0359	0.0683	0.0639	0.1002	0.0709
H4	Simple RNN	94	0.0307	0.0798	0.0395	0.0574	0.0552
	LSTM	494	0.0486	0.1465	0.1250	0.2478	0.1591
	MLP	5→14→44→67→2	0.01651	0.0314	0.0227	0.0554	0.0360
H5	Simple RNN	72	0.0267	0.0751	0.0692	0.0950	0.0706
	LSTM	433→drop(0.1)	0.013	0.0900	0.0413	0.2064	0.1213
	MLP	5→11→47→63→5	0.0134	0.0149	0.0231	0.0164	0.0176
H6	Simple RNN	94	0.0542	0.0749	0.0301	0.0333	0.0512
	LSTM	207	0.0291	0.1009	0.0775	0.0928	0.0823
	MLP	7→26→42→68→29	0.0694	0.1025	0.0945	0.1009	0.0911
H7	Simple RNN	108	0.0282	0.0370	0.0502	0.0430	0.0390
	LSTM	235	0.0232	0.0372	0.0634	0.0681	0.0466

Source: Developed by the author

Results demonstrated very good identification results for the designed neural networks by following the procedures and models described in previous sections to the series-parallel configuration. The attempt to identify the nonlinear and time-varying relationship of the knee joint under NMES/FES using deep and dynamic neural networks with few data are very promising using the series-parallel configuration, as presented in this research. By few, it means that the identification data used for training/validation contains approximately 3,000 samples while the

testing set is composed of 30,000 samples. Moreover, the identification data have less fuzzy behavior as one can see in Figure 16 while the test data is comprised of PW that switches up and down as the RISE control law decides, i.e., see Figures 39 and 40.

In Table 36 and Figures 45-47, the identified models indicate good fitting to data and very low RMSE metric for all individuals. Even though the data have nonideal conditions such as tremors, fatigue, spasms, and voluntary movements that could be characterized as an ill-defined behavior, the proposed NN models identified the relationship of delivered pulse width and achieved angular position very well. As one can notice, in comparison, all three models achieved the best performance for at least one individual. During training, it was noticed that the MLP took very little time to train (as one can also check it in Section 4.4, where models were trained via a single layer MLP), however, it is noteworthy that this model is not prepared for modeling uncertainties or high disturbances, due to no self-feedback connection such as RNNs have.

Recurrent neural networks, especially the LSTM architecture, are excellent for sequential and time-series data as reported in the literature, which makes them ideal for the identification and modeling of nonlinear systems as our problem. As Table 36 and Figures 45-47 showed, results with just one time-step (low memory) for the series-parallel configuration are very accurately, and we believe that by concentrating more efforts on the tuning procedure trying more architectures and more time steps (adding more memory to the model), results can improve even more.

The use of black-box models such as deep and dynamic neural networks for the identification of the nonlinear relationship of the knee joint dynamics under neuromuscular electrical stimulation is, at first, motivated by advantages of the methods itself, and by a high power for computation and storage of data encountered nowadays. Deep neural network structures are easier to train in comparison with mathematically modeling the knee joint dynamics and executing tests for identifying parameters of each individual. Focusing more efforts on the model selection procedure could provide stronger models for input-output data modeling. Hence, using an appropriate choice of architecture and hyperparameters, the modeling of such dynamics would not be difficult for such deep and dynamic neural networks.

Therefore, as the proposal of this research is based on an offline optimizer for the RISE controller, a proper description of the system (lower limb response to electrical stimulus) via sophisticated methods as the ones introduced in this chapter, would provide a more realistic simulation of the system's response. Consequently, better tuning of the RISE controller for each SCI patient in clinical procedures would be acquired. Moreover, saving every rehabilitation data from a patient, such deep and dynamic NNs can improve the mapping for each patient with the electrical stimulus as sessions pass by.

Figure 45 - Identification results for individuals P1, P2 and H1 respectively.
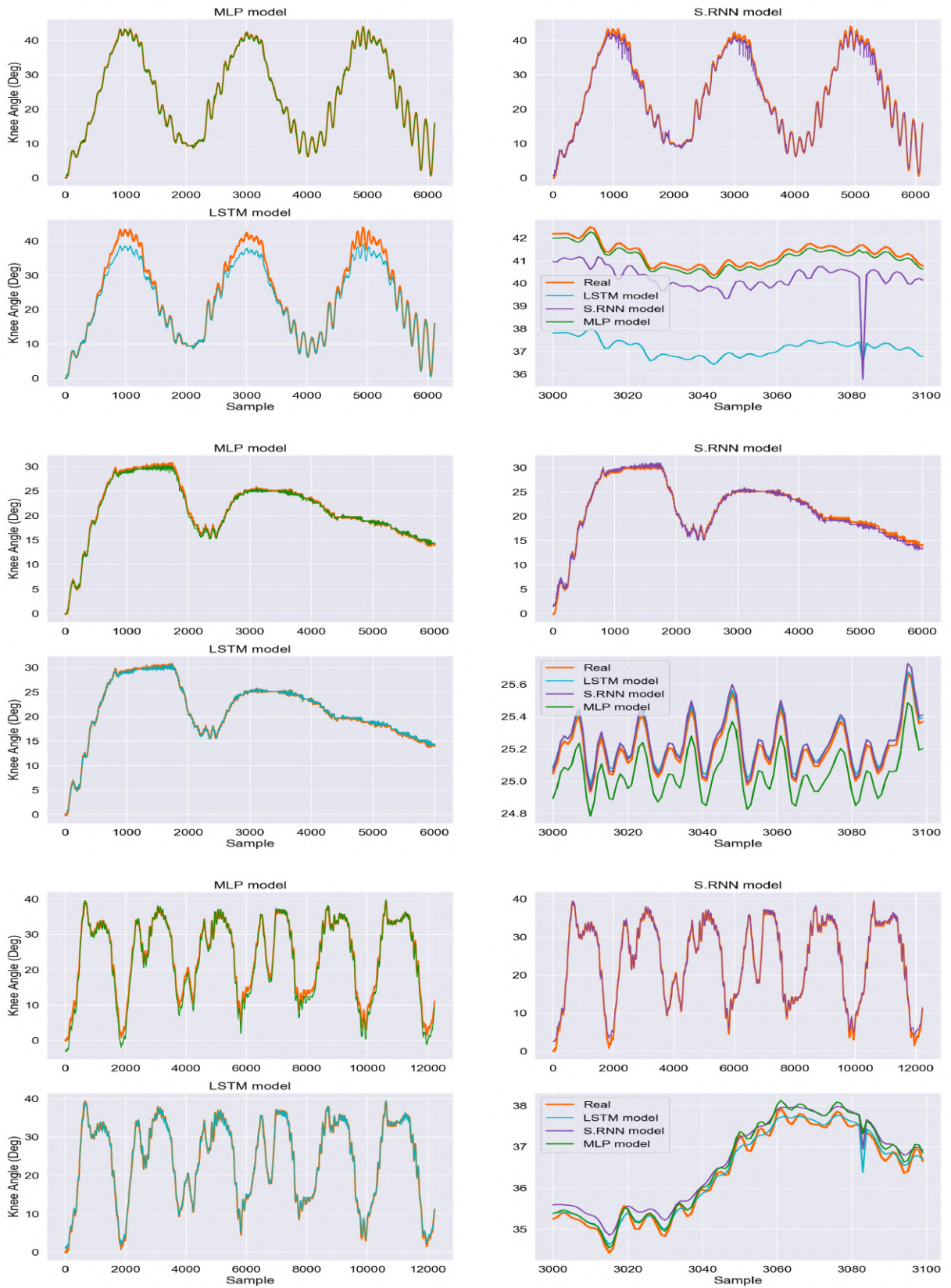
Figure 46 - Identification results for individuals H2, H3 and H4 respectively.
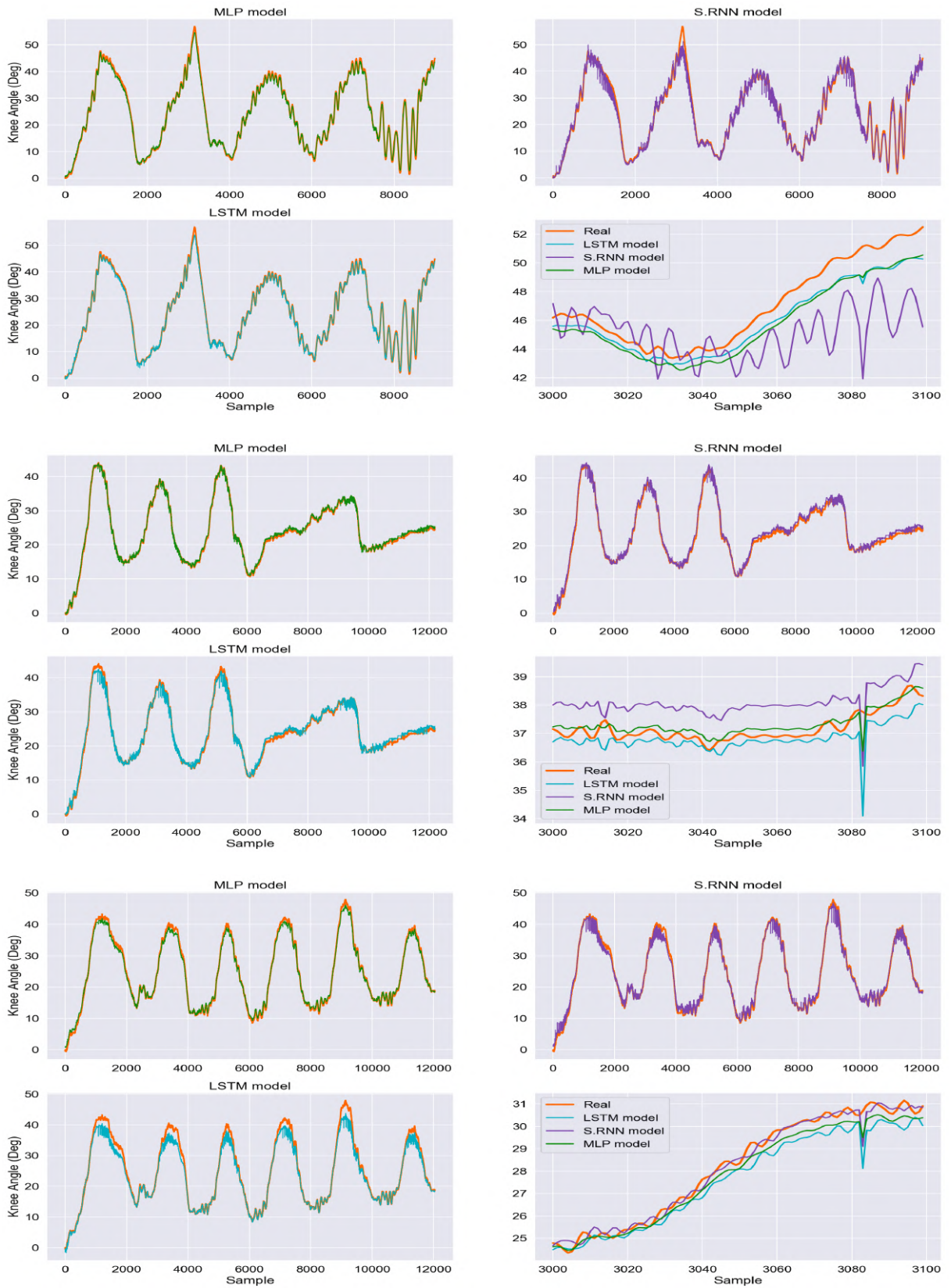
Source: Developed by the author

Figure 47 - Identification results for individuals H5, H6 and H7 respectively.

Source: Developed by the author

6 GENERAL CONCLUSIONS

With the purpose of proposing an improvement to human lower limb tracking control of SCI patients via NMES/FES, this research introduced a novel methodology consisting of an identification step that uses past rehabilitation data, the RISE control method (or fundamentally similar control laws) to guarantee the system's stability and an improved genetic algorithm to tune the controller efficiently.

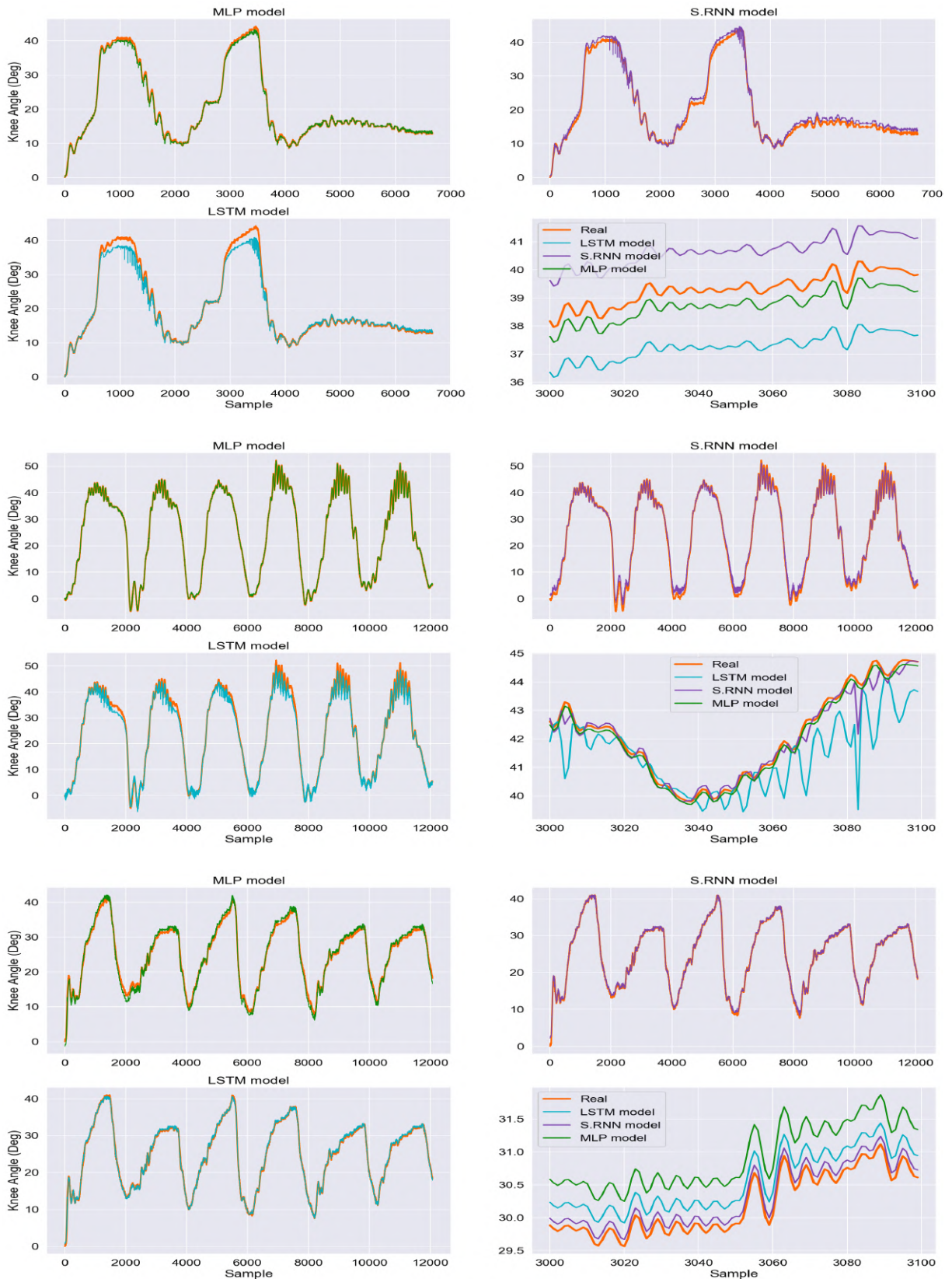Simulation results are presented using a mathematical model, five healthy subjects and three paraplegics identified by (FERRARIN; PEDOTTI, 2000). Furthermore, experiments are made with seven healthy and two paraplegic subjects to substantiate and validate the methodology via real experiments. The proposed methodology for knee joint control would allow people with no technical experience on neural networks, genetic algorithms, or even the control law RISE, to easily use a closed-loop NMES/FES system for SCI rehabilitation.

Additionally, as previously mentioned in Section 1.2 and presented in Table 1, the RISE control method designed for knee joint control present in the literature did not validate this controller for paraplegic subjects. Therefore, for the first time, using the proposed methodology providing an intelligent tuning for each individual, the RISE controller is validated with two spinal cord injured subjects with very good tracking results on both isotonic and isometric contractions, which would not be possible if using a "trial and error" method for tuning the controller by fatigating the muscle before acquiring good tuning.

As hypothesized in Section 1.3 and proven in simulation results in Section 3.3 and in real experiments in Section 4.4, the use of an empirical approach on clinical procedures presents a large number of poor tracking performances trying to stimulate the lower limb via NMES/FES by not taking full advantage of the RISE controller that can better compensate with the right selection of gains. The attempt to improve the rehabilitation procedure directly affects the well-being of SCI patients providing fast recovery in the best performance, in the way that a better tuning will avoid premature fatigue and other problems on SCI patients during rehabilitation.

Moreover, the second hypothesis on the use of past rehabilitation data for system identification was also validated in results, in which as sessions passed by, models lost correlation between input and output data but gained nonlinearities and time-varying properties implicit in data, e.g., tremors and fatigue. Hence, saving real databases of each patient containing detailed information from every rehabilitation session, and by using strong tools, such as neural networks, the mapping over the delivered electric stimulus and achieved angular position will be efficiently addressed.

In this context, as presented in Chapter 5, the use of deep and dynamic neural networks such as the MLP, a simple RNN, and the LSTM architecture, provides very good identification of the knee joint dynamics under NMES/FES, proving to be prospective methods for deeper investigation on nonlinear system identification and modeling. While the MLP takes less time to train, the use of dynamic neural networks such as RNNs is motivated by the self-feedback connection that allows modeling time-series and very complex sequences as the nonlinear identification problem of this research.

Finally, such proposed simulation system running in an offline scheme can take advantage of deep and/or dynamic neural networks, e.g, the ones presented in Chapter 5, for improving the identification step, rather than use a single hidden layer NN as presented in results from Chapter 4. Furthermore, as an NMES-base knee simulation system, using the data saved from each patient, it allows previously testing improvements to the RISE control law and more control techniques before actual implementation in the future, saving time and resources.

6.1 FUTURE WORKS

For future work, a deeper validation using the proposed methodology with spinal cord injured subjects during more sessions is planned. Additionally, for the identification procedure, deeper neural networks will be considered given the simulation system trained in an offline scheme, computational costs could be increased to guarantee a better description of the relationship between knee joint position and electrical stimulation. Therefore, combinations of LSTM with other NN models (e.g., Convolutional NN) is also planned, aiming to implement control-oriented models to the knee joint using NMES. Lastly, fundamentally similar control laws will be considered, as well as improving the simulation system considering other platforms that better suits our problem.

6.2 PUBLICATIONS

During this study, a scientific contribution with simulation results (Chapter 3) was made at the Sixth (6th) International Conference on Control, Decision and Information Technologies (CoDIT 2019) as

ARCOLEZI, H. H.; NUNES, W. R. B. M.; ÑAHUIS, S. L. C.; SANCHES, M. A. A.; TEIX-EIRA, M. C. M.; CARVALHO, A. A. de. A RISE-based Controller Fine-tuned by an Improved Genetic Algorithm for Human Lower Limb Rehabilitation via Neuromuscular Electrical Stimulation. In: 6th International Conference on Control, Decision and Information Technologies. CoDIT, 2019.

Additionally, it is proposed one publication validating the novel proposal with some of the

experimental results (Chapter 4), and other introducing the LSTM NN to identify the nonlinear relationship of knee joint under NMES/FES (Chapter 5) to the XIV Conferência Brasileira de Dinâmica, Controle e Aplicações (DINCON 2019) respectively as

ARCOLEZI, H. H.; NUNES, W. R. B. M.; ARAUJO, R. A. de; CERNA, S.; SANCHES, M. A. A.; TEIXEIRA, M. C. M.; CARVALHO, A. A. de. A Robust and Intelligent RISE-based Control for Human Lower Limb Tracking via Neuromuscular Electrical Stimulation. In: XIV Conferência Brasileira de Dinâmica, Controle e Aplicações. DINCON, 2019.

ARCOLEZI, H. H.; CERNA, S.; NUNES, W. R. B. M.; ARAUJO, R. A. de; SANCHES, M. A. A.; TEIXEIRA, M. C. M.; CARVALHO, A. A. de. On the Ability to Identify the Knee Joint Position Under Neuromuscular Electrical Stimulation Using Long Short-Term Memory Neural Networks. In: XIV Conferência Brasileira de Dinâmica, Controle e Aplicações. DINCON, 2019.

Further, the author participated as a co-author in a scientific contributions made at the aforementioned CoDIT 2019 conference as

CERNA, S. L. Ñ.; GUYEUX, C.; ARCOLEZI, H. H.; COUTURIER, R.; ROYER, G.; LOTUFO, A. D. P. Long Short-Term Memory for Predicting Firemen Interventions. In: 6th International Conference on Control, Decision and Information Technologies. CoDIT, 2019.

REFERENCES

ABLAMEYKO, S. **Neural Networks for Instrumentation, Measurement and Related Industrial Applications**. Amsterdam: IOS Press, 2003.

ARCOLEZI, H. H.; NUNES, W. R. B. M.; NAHUIS, S. L. C.; SANCHES, M. A. A.; TEIXEIRA, M. C. M.; CARVALHO, A. A. de. A RISE-based controller fine-tuned by an improved genetic algorithm for human lower limb rehabilitation via neuromuscular electrical stimulation. In: International Conference on Control, Decision and Information Technologies (CoDIT), 6th., Paris. **Proceedings** [...]. [S.l.]: IEEE, 2019. p. 1197–1202.

BENOUSSAAD, M.; HAYASHIBE, M.; FATTAL, C.; POIGNET, P.; GUIRAUD, D. Identification and validation of FES physiological musculoskeletal model in paraplegic subjects. In: Annual International Conference of the IEEE Engineering in Medicine and Biology Society (EMBC), 31st., 2009, Minneapolis. **Proceedings** [...]. [S.l.]: IEEE, 2009.

CERNA, S. L. N.; GUYEUX, C.; ARCOLEZI, H. H.; COUTURIER, R.; ROYER, G.; LOTUFO, A. D. P. Long short-term memory for predicting firemen interventions. In: International Conference on Control, Decision and Information Technologies (CoDIT), 6th., 2019, Paris. **Proceedings** [...]. [S.l.]: IEEE, 2019.

CHENG, T.-H.; WANG, Q.; KAMALAPURKAR, R.; DINH, H. T.; BELLMAN, M.; DIXON, W. E. Identification-based closed-loop NMES limb tracking with amplitude-modulated control input. **IEEE Transactions on Cybernetics**, Pistacaway, v. 46, n. 7, p. 1679–1690, jul 2016.

CHOLLET, F. et al. **Keras**. 2015. Web. <https://keras.io>.

DOWNEY, R. J.; BELLMAN, M. J.; KAWAI, H.; GREGORY, C. M.; DIXON, W. E. Comparing the induced muscle fatigue between asynchronous and synchronous electrical stimulation in able-bodied and spinal cord injured populations. **IEEE Transactions on Neural Systems and Rehabilitation Engineering**, Pistacaway, v. 23, n. 6, p. 964–972, nov 2015.

DOWNEY, R. J.; CHENG, T.-H.; BELLMAN, M. J.; DIXON, W. E. Closed-loop asynchronous neuromuscular electrical stimulation prolongs functional movements in the lower body. **IEEE Transactions on Neural Systems and Rehabilitation Engineering**, Pistacaway, v. 23, n. 6, p. 1117–1127, nov 2015.

DOWNEY, R. J.; CHENG, T.-H.; DIXON, W. E. Tracking control of a human limb during asynchronous neuromuscular electrical stimulation. In: IEEE Conference on Decision and Control (ACC), 52nd., 2013, Florence. **Proceedings** [...]. [S.l.]: IEEE, 2013.

DURIEZ, T.; BRUNTON, S. L.; NOACK, B. R. **Machine Learning Control – Taming Nonlinear Dynamics and Turbulence**. Switzerland: Springer International Publishing, 2017.

FEO, T. A.; RESENDE, M. G. C. Greedy randomized adaptive search procedures. **Journal of**

Global Optimization, v. 6, n. 2, p. 109–133, mar 1995.

FERRARIN, M.; PALAZZO, F.; RIENER, R.; QUINTERN, J. Model-based control of FES-induced single joint movements. **IEEE Transactions on Neural Systems and Rehabilitation Engineering**, Pistacaway, v. 9, n. 3, p. 245–257, 2001.

FERRARIN, M.; PEDOTTI, A. The relationship between electrical stimulus and joint torque: a dynamic model. **IEEE Transactions on Rehabilitation Engineering**, Pistacaway, v. 8, n. 3, p. 342–352, 2000.

FLEMING, P.; PURSHOUSE, R. Evolutionary algorithms in control systems engineering: a survey. **Control Engineering Practice**, Oxford, v. 10, n. 11, p. 1223–1241, nov 2002.

FONSECA, L. O. da; LOPES, A. C. G.; OCHOA-DIAZ, C.; AZEVEDO-COSTE, C.; FACHIN-MARTINS, E.; BO, A. P. L. Towards transfers in paraplegia assisted by electrical stimulation and inertial system. In: IEEE Life Sciences Conference (LSC), 2017, Sydney. **Proceedings** [...]. [S.l.]: IEEE, 2017.

GÉRON, A. **Hands-On Machine Learning with Scikit-Learn and TensorFlow**. Sebastopol: OReilly Media, 2017.

GHANI, N. A. M.; KAMARUDDIN, S. B. A.; RAMLI, N. M.; NASIR, N. B. M.; KADER, B. S. B. K.; HUQ, M. S. The quadriceps muscle of knee joint modelling using neural network approach: Part 1. In: IEEE Conference on e-Learning, e-Management and e-Services (IC3e), 2016, Langkawi. **Proceedings** [...]. [S.l.]: IEEE, 2016.

GONZALEZ, J.; YU, W. Non-linear system modeling using LSTM neural networks. **IFAC-PapersOnLine**, Oxford, v. 51, n. 13, p. 485–489, 2018.

HAYKIN, S. S. **Neural networks and learning machines**. Third. Upper Saddle River: Pearson Education, 2009.

HIROSE, N.; TAJIMA, R. Modeling of rolling friction by recurrent neural network using LSTM. In: IEEE International Conference on Robotics and Automation (ICRA), 2017, Singapore. **Proceedings** [...]. [S.l.]: IEEE, 2017.

HO, C. H. et al. Functional electrical stimulation and spinal cord injury. **Physical Medicine and Rehabilitation Clinics of North America**, Oxford, v. 25, n. 3, p. 631–654, aug 2014.

HOCHREITER, S.; SCHMIDHUBER, J. Long short-term memory. **Neural Computation**, Cambridge, v. 9, n. 8, p. 1735–1780, nov 1997.

JAIME, R.-P.; MATJACIC, Z.; HUNT, K. Paraplegic standing supported by FES-controlled ankle stiffness. **IEEE Transactions on Neural Systems and Rehabilitation Engineering**, Pistacaway, v. 10, n. 4, p. 239–248, dec 2002.

JEZERNIK, S.; WASSINK, R.; KELLER, T. Sliding mode closed-loop control of FES: Controlling the shank movement. **IEEE Transactions on Biomedical Engineering**, Pistacaway, v. 51, n. 2, p. 263–272, feb 2004.

KAMARUDDIN, S. B. A.; GHANI, N. A. M.; RAMLI, N. M.; NASIR, N. B. M.; KADER,

B. S. B. K.; HUQ, M. S. The quadriceps muscle of knee joint modelling using neural network approach: Part 2. In: IEEE Conference on Open Systems (ICOS), 2016, Langkawi Island. **Proceedings** [...]. [S.l.]: IEEE, 2016.

KAPADIA, N.; ZIVANOVIC, V.; POPOVIC, M. Restoring voluntary grasping function in individuals with incomplete chronic spinal cord injury: Pilot study. **Topics in Spinal Cord Injury Rehabilitation**, Webster Groves, v. 19, n. 4, p. 279–287, oct 2013.

KAWAI, Y.; DOWNEY, R. J.; KAWAI, H.; DIXON, W. E. Co-contraction of antagonist bi-articular muscles for tracking control of human limb. In: American Control Conference (ACC), 2014, Portland. **Proceedings** [...]. [S.l.]: IEEE, 2014.

KUSHIMA, Y.; KAWATAKA, K.; KAWAI, H.; KAWAI, Y.; DIXON, W. E. FES knee bending and stretching system with RISE-based tracking control for human limb. In: IEEE Conference on Control Applications (CCA), 2015, Hawaii. **Proceedings** [...]. [S.l.]: IEEE, 2015.

LAW, L. F.; SHIELDS, R. Mathematical models of human paralyzed muscle after long-term training. **Journal of Biomechanics**, Oxford, v. 40, n. 12, p. 2587–2595, jan 2007.

LEW, B.; ALAVI, N.; RANDHAWA, B. K.; MENON, C. An exploratory investigation on the use of closed-loop electrical stimulation to assist individuals with stroke to perform fine movements with their hemiparetic arm. **Frontiers in Bioengineering and Biotechnology**, Lausanne, v. 4, mar 2016.

LYNCH, C. L.; GRAHAM, G. M.; POPOVIC, M. R. Including Nonideal Behavior in Simulations of Functional Electrical Stimulation Applications. **Artificial Organs**, Hoboken, v. 35, n. 3, p. 267–269, 2011.

LYNCH, C. L.; POPOVIC, M. R. Functional electrical stimulation. **IEEE Control Systems**, Pistacaway, v. 28, n. 2, p. 40–50, apr 2008.

LYNCH, C. L.; POPOVIC, M. R. A comparison of closed-loop control algorithms for regulating electrically stimulated knee movements in individuals with spinal cord injury. **IEEE Transactions on Neural Systems and Rehabilitation Engineering**, Pistacaway, v. 20, n. 4, p. 539–548, jul 2012.

MOHAMMED, S.; POIGNET, P.; FRAISSE, P.; GUIRAUD, D. Toward lower limbs movement restoration with input–output feedback linearization and model predictive control through functional electrical stimulation. **Control Engineering Practice**, Oxford, v. 20, n. 2, p. 182–195, feb 2012.

NARENDRA, K.; PARTHASARATHY, K. Identification and control of dynamical systems using neural networks. **IEEE Transactions on Neural Networks**, Pistacaway, v. 1, n. 1, p. 4–27, mar 1990.

NUNES, W. R. B. M.; TEODORO, R. G.; ARAUJO, R. A. de; SANCHES, M. A. A.; TEIXEIRA, M. C. M.; CARVALHO, A. A. de. Robust and switched control design for electrical stimulation of lower limbs: A linear analysis. In: Congresso Brasileiro de Automática (CBA), 2018, João Pessoa. **Proceedings** [...]. [S.l.]: CBA, 2018.

OGUNMOLU, O. P.; GU, X.; JIANG, S. B.; GANS, N. R. Nonlinear systems identification

using deep dynamic neural networks. 2016.

OLIVEIRA, T. R.; COSTA, L. R.; CATUNDA, J. M. Y.; PINO, A. V.; BARBOSA, W.; SOUZA, M. N. de. Time-scaling based sliding mode control for neuromuscular electrical stimulation under uncertain relative degrees. **Medical Engineering & Physics**, Oxford, v. 44, p. 53–62, jun 2017.

PECKHAM, P. H.; KNUTSON, J. S. Functional electrical stimulation for neuromuscular applications. **Annual Review of Biomedical Engineering**, Palo Alto, v. 7, n. 1, p. 327–360, aug 2005.

PEDREGOSA, F.; VAROQUAUX, G.; GRAMFORT, A.; MICHEL, V.; THIRION, B.; GRISEL, O.; BLONDEL, M.; PRETTENHOFER, P.; WEISS, R.; DUBOURG, V.; VANDERPLAS, J.; PASSOS, A.; COURNAPEAU, D.; BRUCHER, M.; PERROT, M.; DUCHESNAY, E. Scikit-learn: Machine learning in Python. **Journal of Machine Learning Research**, Brookline, v. 12, p. 2825–2830, 2011.

PREVIDI, F. Identification of black-box nonlinear models for lower limb movement control using functional electrical stimulation. **Control Engineering Practice**, Oxford, v. 10, n. 1, p. 91–99, jan 2002.

PREVIDI, F.; CARPANZANO, E. Design of a gain scheduling controller for knee-joint angle control by using functional electrical stimulation. **IEEE Transactions on Control Systems Technology**, Pistacaway, v. 11, n. 3, p. 310–324, may 2003.

RIENER, R.; QUINTERN, J.; SCHMIDT, G. Biomechanical model of the human knee evaluated by neuromuscular stimulation. **Journal of Biomechanics**, Oxford, v. 29, n. 9, p. 1157–1167, sep 1996.

SANCHES, M. A. A. **Sistema Eletrônico para Geração e Avaliação de Movimentos em Paraplégicos**. 2013. 186 p. Tese (Doutorado em Engenharia Elétrica) — Faculdade de Engenharia, Universidade Estadual Paulista, 2013.

SANCHES, M. A. A.; GAINO, R.; KOZAN, R. F.; TEIXEIRA, M. C. M.; CARVALHO, A. A. de; COVACIC, M. R.; ALVES, C. A.; URBAN, M. F. R.; JUNQUEIRA, M. V. N.; CARDIM, R.; ASSUNÇÃO, E.; Gentilho Junior, E. Digital controller design considering hardware constraints: application in a paraplegic patient. **Revista Brasileira de Engenharia Biomédica**, Rio de Janeiro, v. 30, n. 3, p. 232–241, 2014.

SHARMA, N.; GREGORY, C. M.; JOHNSON, M.; DIXON, W. E. Closed-loop neural network-based NMES control for human limb tracking. **IEEE Transactions on Control Systems Technology**, Pistacaway, v. 20, n. 3, p. 712–725, may 2012.

SHARMA, N.; STEGATH, K.; GREGORY, C.; DIXON, W. Nonlinear neuromuscular electrical stimulation tracking control of a human limb. **IEEE Transactions on Neural Systems and Rehabilitation Engineering**, Pistacaway, v. 17, n. 6, p. 576–584, dec 2009.

STEGATH, K.; SHARMA, N.; GREGORY, C. M.; DIXON, W. E. Experimental demonstration of RISE-based NMES of human quadriceps muscle. In: IEEE/NIH Life Science Systems and Applications Workshop (LISA), Bethesda. **Proceedings** [...]. [S.l.]: IEEE, 2007.

STEGATH, K.; SHARMA, N.; GREGORY, C. M.; DIXON, W. E. Nonlinear tracking control of a human limb via neuromuscular electrical stimulation. In: American Control Conference (ACC), Seattle. **Proceedings** [...]. [S.l.]: IEEE, 2008.

TEODORO, R. G. **Controle da posição angular da perna de voluntários hígidos e com lesão medular utilizando estimulação elétrica funcional e técnicas de controle robusto e chaveado**. 2018. 198 p. Tese (Doutorado em Engenharia Elétrica) — Faculdade de Engenharia, Universidade Estadual Paulista, 2018.

WANG, C.; WU, X.; MA, Y.; WU, G.; LUO, Y. A flexible lower extremity exoskeleton robot with deep locomotion mode identification. **Complexity**, London, v. 2018, p. 1–9, oct 2018.

WANG, Y. A new concept using LSTM neural networks for dynamic system identification. In: American Control Conference (ACC), Seattle. **Proceedings** [...]. [S.l.]: IEEE, 2017.

XIAN, B.; DAWSON, D.; QUEIROZ, M. de; CHEN, J. A continuous asymptotic tracking control strategy for uncertain multi-input nonlinear systems. In: IEEE International Symposium on Intelligent Control (ISIC), Houston. **Proceedings** [...]. [S.l.]: IEEE, 2003.

XIAN, B.; QUEIROZ, M. S.; DAWSON, D. M. A continuous control mechanism for uncertain nonlinear systems. **Optimal Control, Stabilization and Nonsmooth Analysis**, Berlin, v. 301, p. 251–264, may 2004.